Neural network activity in the neonatal rat barrel cortex *in vivo*

Dissertation

Zur Erlangung des Grades
Doktor der Naturwissenschaften

Am Fachbereich Biologie
Der Johannes Gutenberg-Universität Mainz

vorgelegt von

Jenq-Wei Yang

geb. am 05.12.1976 in Taiwan

Mainz, 2011

Tag der mündlichen Prüfung: 12. April .2011

Table of Contents

Abbreviations

A1	primary auditory cortex
ACSF	artificial cerebrospinal fluid
CBX	carbenoxolone
CP	cortical plate
CSD	current source density
DC	direct current
DiI	1,1'-dioctadecyl-3,3,3',3'-tetramethyl indocarbocyanine
DTB	diencephalon and telencephalon
FFT	fast fourier transformation
FP	field potential
LIDO	lidocaine hydrochloride monohydrate
IZ	intermediate zone
MEA	multi-electrode array
MUA	multiple unit activity
MZ	marginal zone
(P) 0-7	postnatal day 0 to 7
PP	preplate
PSPB	pallial–subpallial border
S1	primary somatosensory cortex
SD	standard deviation
SP	subplate
SVZ/VZ	subventricular zone/ventricular zone
TCA	thalamocortical afferents
V1	primary visual cortex
VSDI	voltage sensitive dye image
WM	white matter

List of Figures

1 Introduction

1.1 The development of the human brain

Brain development is an extremely dynamic process which involves complex changes in shape and structure over time. In humans, within approximately four weeks (from 26 to 56 days) of postconceptional age, the major subregions of human brain are established and development proceeds from a single neuroepithelial tube to a highly complex three dimensional structure (Ronan R.O'Rahilly, 2006). During the prenatal stage, different populations of neurons send and receive information related to touch, hearing and movement, allowing the development of tactile, visual, auditory and gustative abilities. At birth, the majority of neurons are already in place, but the establishment of connections between them reaches the maximum intensity during early postanatal development and childhood, as reflected by increased synaptic density reported at this age (Huttenlocher, 1979). Myelination of white matter proceeds rapidly after birth and reaches the general pattern of adult myelination by the end of the second year (Sampaio and Truwit, 2001). By the age of 3 years, the brain is about 87% of the adult size (Dekaban, 1978). The normal brain development is controlled by stimuli from the environment and the infant's interaction with its environment helps to sculpt intra- and inter-cortical connections, eventually resulting in the highly specialized adult brain (**Fig. 1**).

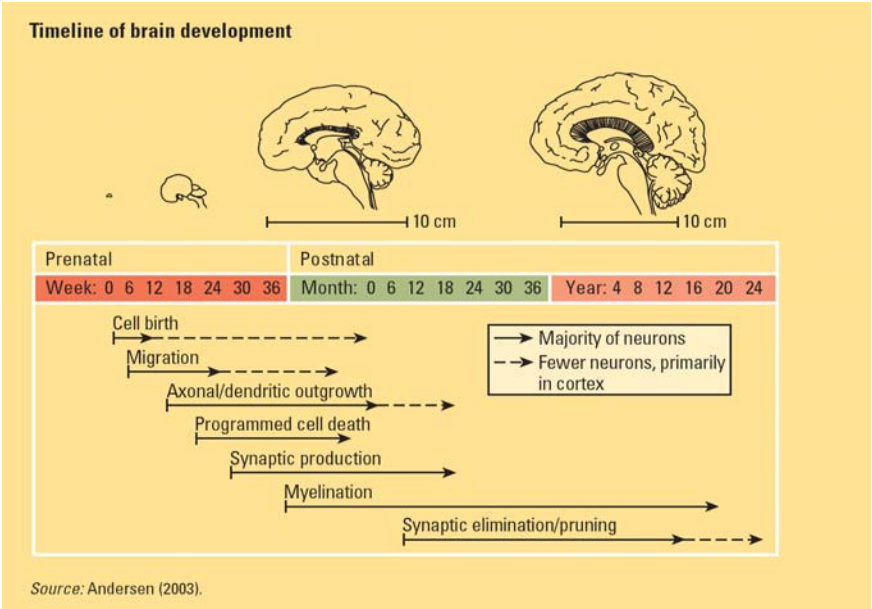

Fig. 1 The stages of human brain development (Andersen, 2003).

1.2 The electrical activity during human brain development

Neurons process and transmit information in the form of electrical signals. This electrical activity can reflect the active condition of neurons in the brain. Electroencephalography (EEG) is the measurement of the electrical activity of the brain. It provides a sensitive, real time, continuous measure of cerebral activity and brain function. For over half of a century EEG recordings have been routinely performed to measure and study brain maturation conditions in premature and full-term infants (Andre et al., 2010;Tharp, 1990;Torres and Anderson, 1985).

At 24 to 27 weeks of postconceptional age the EEG recording from premature babies is dominated by delta waves (0.3-2 Hz). By 28 weeks of postconceptional age, slow delta waves are intermixed with rapid rhythms. The dominant pattern of the rapid activity during this period is a delta-brush pattern (Andre et al., 2010;Khazipov and Luhmann, 2006;Milh et al., 2007) (**Fig. 2**).

A delta-brush consists of 8 to 25 Hz spindle-like, rhythmic activity superimposed on 0.3 to 1.5 Hz delta waves. Delta brushes are predominantly expressed in central areas before 28 weeks and are then recorded in central, temporal, frontal, and occipital areas from 28 weeks to near term (Andre et al., 2010). The sporadic hand and foot movements induce the appearance of delta-brushes in the corresponding areas of the cortex. Direct hand and foot stimulation also reliably evoked delta-brushes in the corresponding brain areas (Milh et al., 2007).

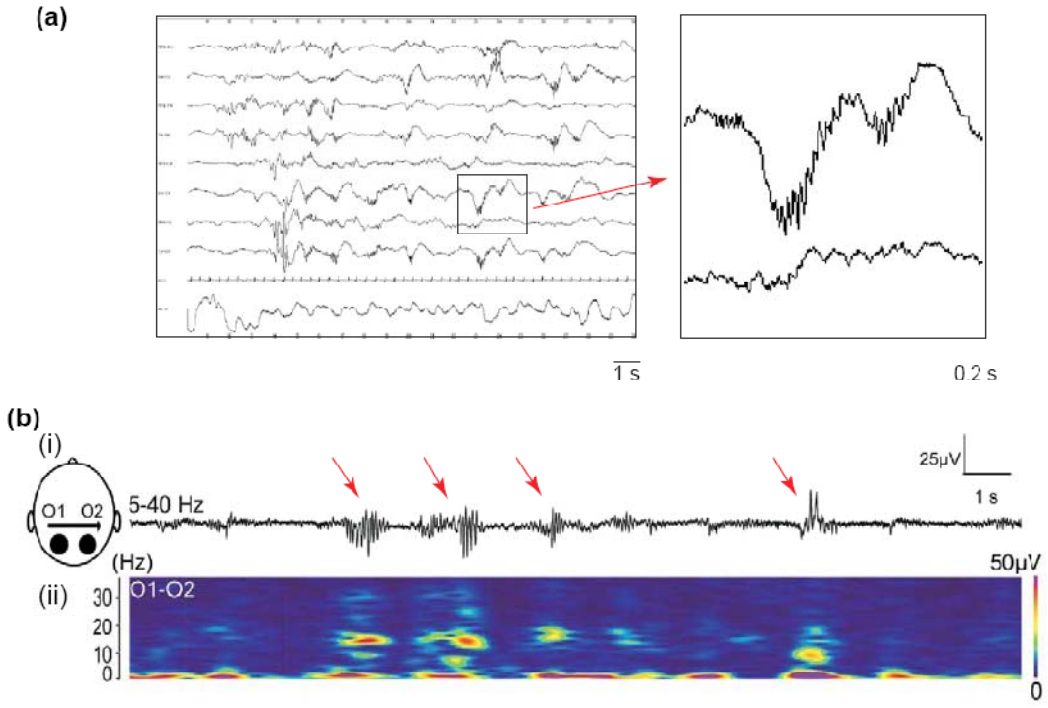

Fig. 2 Hallmarks of the premature human electroencephalogram: tracé discontinu and delta brushes. **(a)** EEG recorded from a premature human neonate aged 33 weeks postconception during quiet sleep. Activity is characterized by discontinuous temporal organization (tracé discontinu), with the episodes of activity separated by the periods of silence. Typical patterns of activity are delta waves (1–3 Hz) in which are often nested high-frequency oscillations: delta brushes (an example delta brush is shown at an expanded timescale on the right). **(b)** (i) Bipolar occipital (O1–O2) recordings from the visual cortex of a premature neonate (filtered at bandpass 5–40 Hz). Note the intermittent rapid oscillations representing the rapid component of delta brushes (marked by red arrows). (ii) Time frequency analysis of the trace in (i). Note that activity at low (delta) frequencies coincides with rapid oscillatory activity during delta brushes. Courtesy of A. Kaminska (a) and M. Milh (b) (Khazipov and Luhmann, 2006).

1.3 Rodents animal models for the investigation of brain development

For obvious reasons, the mechanisms of brain development cannot be addressed in human premature babies and therefore an animal model must be used. Being born at a very immature stage of brain development (altricial species) the rodent is an ideal model (Clancy et al., 2007). Among rodents, rats and mice are the most used species (**Fig. 3**). Rat pups are born after a short gestation (22.5 days), and have long been the general species of choice such that rat macro- and micro-neuroanatomy, neurophysiology, and assessments of behavior are well-mapped. Mice (gestation 19.5 days) are currently considered most amenable to genetic manipulations. They are initially chosen because manipulations were clearly reflected in their physical appearance (Nishioka, 1995). These two species are born at relatively underdeveloped stages and many neurogenic events occur postnatally that can be comparable with premature humans.

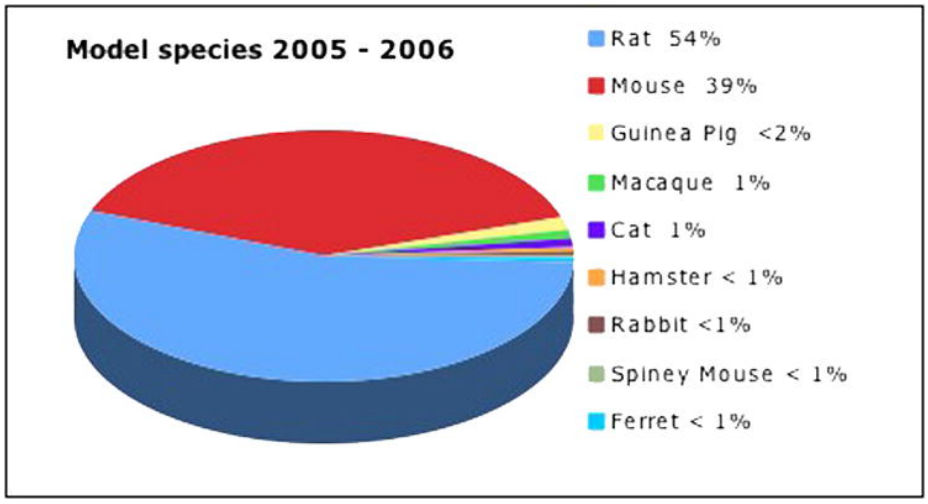

Fig. 3 Proportion of recent studies performed in nine of the most commonly used species (source: Medline)

1.4 Rodent barrel cortex

Similar to humans exploring the environment with the fingers, the rat uses the whiskers for receiving tactile stimuli. The sensory signal perceived by the whiskers is transmitted into the barrel cortex. The barrel cortex of neonatal rodent is an excellent model system for studying early cortical activity during the developmental period corresponding to the premature human neonate stage.

The rodents use their whiskers to explore the world, build spatial representations of their environment, locate objects, and perform fine-grain texture discrimination (Diamond

et al., 2008a;Diamond et al., 2008b). When rodents move their whiskers to touch one object, the tactile information is detected by the mechanoreceptors within the whisker follicles and then transmitted through the infraorbital nerve into the brain stem. This sensory signal is further transferred into the thalamus, finally reaching the barrel cortex (**Fig. 4A**).

The barrel cortex is part of the somatosensory cortex which was firstly characterized in mice by Woolsey and Van der Loos in 1970 (Woolsey and Van der, 1970). The cortex is a six-layered structure where the layer IV receives the main input from the thalamus. The barrels that give the barrel cortex its name are located in layer IV (**Fig. 4C**). If a tangential section is taken through layer IV, the characteristic pattern of the barrels can be seen. The barrel pattern replicates the pattern of whiskers, each whisker corresponding to a single barrel (**Fig. 4B**).

Each barrel is composed of a morphologically and functionally related group of neurons that is vertically arranged across the borders of layers, the so-called cortical column. The cortical columns are an important and fundamental element of the cortical structure (**Fig. 4A**). The well-organized rodent barrel cortex offers a suitable and promising system to study sensory processing in a cortical column, and to correlate whisker-related behavior with neuronal activity in a well-defined cortical map (Lubke and Feldmeyer, 2007;Petersen, 2007;Schubert et al., 2007).

There are many unique advantages of using the rodent barrel cortex as a model to study the neural network mechanisms underlying the structure organization, plasticity and development of the neocortical column. First, the cortical column in barrel cortex can be easily identified *in vivo* (Berger et al., 2007;Ferezou et al., 2007) and in unstained brain slices *in vitro* (Schubert et al., 2006;Feldmeyer et al., 2006). Second, the sensory periphery can be manipulated in various ways and trimmed whiskers can regrow (Feldman and Brecht, 2005). Third, specific neuronal cell types located in a selected cortical layer of a well-defined cortical column of mouse barrel cortex can be targeted by genetic manipulation of specific genes (Aronoff and Petersen, 2008). Fourth, single neuron in a specific barrel column can be monitored and manipulated *in vivo* (Brecht et al., 2004).

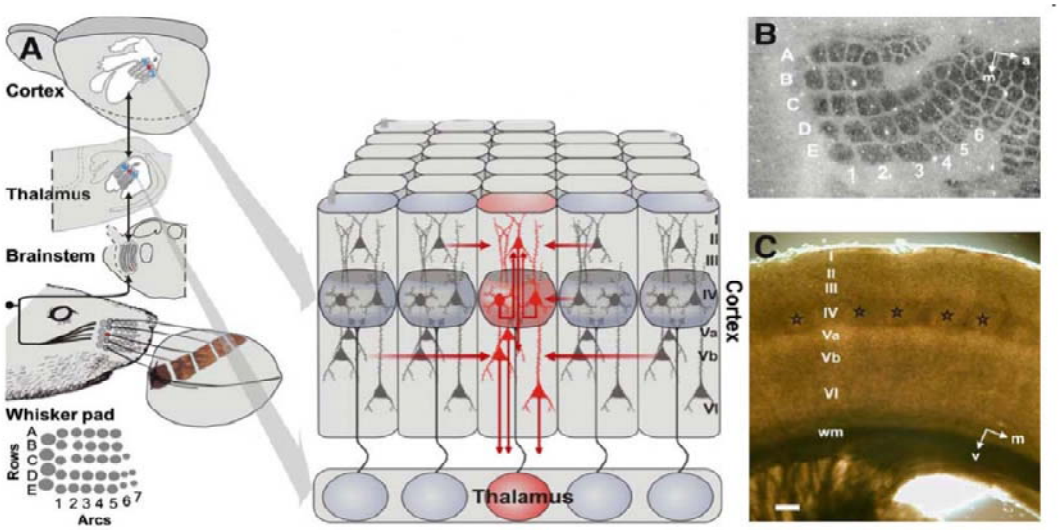

Fig. 4: Anatomical components and hypothetical function of the rodent lemniscal whisker-to-barrel pathway which forms a major part of the trigeminal somatosensory system. A: On the snout, the whisker follicles are indicated by grey circles, except for whisker C1 which is in red (as in all its central representations). Arc 1 whiskers are drawn as black lines touching an object. At each level of the pathway an isomorphic arrangement of neuronal cell groups (Arc 1 in bluish color), reflecting the lay-out of the whiskers on the snout, can be found. These are called *barrelettes* in the primary trigeminal nucleus of the brainstem, *barreloids* in the ventrobasal thalamic nucleus and most prominent *barrels* in the primary somatosensory (barrel) cortex. Included into this scheme is our hypothesis that segregating and integrating cortical circuits (shown as arrows in the cortex) are contained in this pathway which are capable of performing object identification. **B:** Cytochrome oxidase staining of a tangential section through layer IV of the primary somatosensory cortex shows the regular appearance of intensely stained barrels separated by lightly stained septa. Barrels are labeled according to standard nomenclature (Photo provided by courtesy of Pete Land). C: Acute coronal slice through the barrel cortex of a P19 rat. The barrels in layer IV are clearly identifiable (asterisks) as well as all the cortical layers (Roman numerals) that are in vertical register forming a barrel-related column. Scale bar 200 µm; *a* anterior, *m* medial, *v* ventral (Schubert et al., 2007).

1.5 Anatomical development of rat barrel cortex during the first postnatal week

During the first postnatal week the rat barrel cortex rapidly develops and the laminar structure changes dramatically. For the laminar development, layers V and VI have differentiated at birth. Layer IV is clearly apparent in P3 (the day of birth = P0), while layers II and III are clearly present at P4. Cells stop migrating by the end of the first postnatal week in the rat (**Fig. 5**)

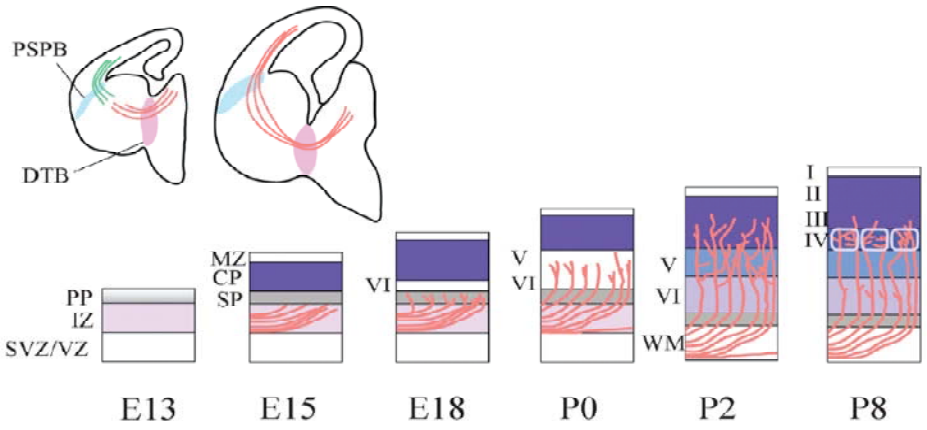

Fig. 5: Schematic diagram illustrating the development of thalamocortical afferents (TCA) from embryonic day 13 (E13) to postnatal day 8 (P8) in rodents. Early growth of TCA from the dorsal thalamus at E13 and E16 (top panels). Detail of thalamocortical axon development in the cortex E13–P8 (lower panels). Thalamocortical axons initially grow through the ventral thalamus, then turn laterally to cross the border between the diencephalon and telencephalon (DTB). Thalamocortical axons and early corticofugal axons arrive in the ventral region of the telencephalon synchronously and are thought to interact. By E16, thalamocortical axons have crossed the pallial–subpallial border (PSPB) and reached the cortex, where they extend tangentially in the intermediate zone (IZ). At this time the lamination of the cortex has begun, the cortical plate (CP) splitting the marginal zone (MZ) and subplate (SP). Between E18 and P2 thalamocortical axons extend side branches into the more superficial regions of the cortex (Naegele et al., 1988), initially interacting with SP, and then growing into layer 4. During this period radial migration of neurons populates the cortex, forming the granular and supragranular layers. By P8 the mature arrangement of thalamocortical axons is virtually established: branches form in layer 6 but the majority of synaptic interaction is in layer 4. Other abbreviations: PP, preplate; SVZ / VZ, subventricular zone / ventricular zone; I, II, III, IV, V, VI, cortical layers 1–6; WM, white matter (Price et al., 2006).

The target of thalamus afferent to the barrel cortex also changes during the first postnatal week in the rat following the development of laminar structure. On the day of birth (P0), thalamocortical axons extend radially through layers VI and V, emit branches within these layers, and thereby some axons reach even the cortical plate (CP). Over the following several days, axons generate more branches within the CP. By P7 individual axons overlap within barrel clusters, spanning the width of a cluster (Catalano et al., 1996). Using DiI labeling (Erzurumlu and Jhaveri, 1990;Catalano et al., 1996) and acetylcholinesterase staining (Schlaggar and O'Leary, 1994), these studies demonstrated that the thalamic afferents show a somatotopic pattern by the end of the first 24 hours after birth (P0/P1) and suggest that the thalamic afferents already carry the pattern information as they arrive in cortex (**Fig. 6**).

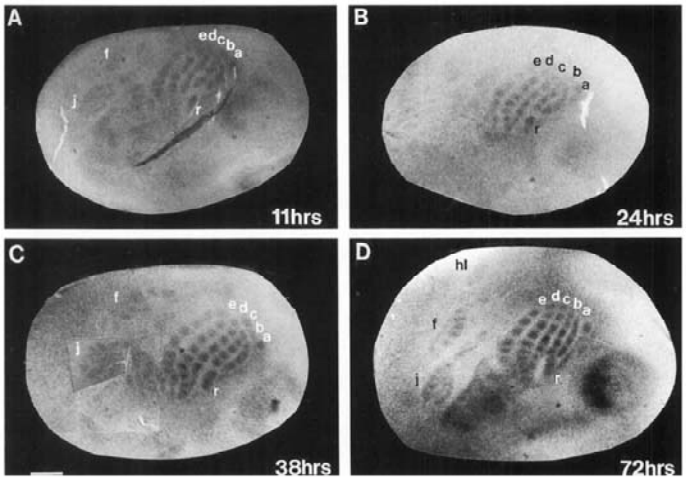

Fig. 6: Tangential distribution of AChE-reactive afferents shows a developmental progression from rows to barrels. A-D: Tangential sections from the flattened cortices of four littermates, processed for AChE. For 11 hours (A), the five rows are marked (a-e), and, in each row, clusters of AChE-reactive afferents are apparent. The jaw (j) representation appears less homogeneous than at an earlier stage. The forelimb (f) representation, though, lacks a disjunctive appearance. Note the sharpening of AChE-reactive patches between 11 and 72 hours. By 38 hours (C), the forelimb representation appears disjunctive. r, rhinal vibrissae; hl, hindlimb. Scale bar = 675 µm (Schlaggar and O'Leary, 1994).

1.6 The rhythmic electrical activity ("oscillations") of rodent barrel cortex during the early postnatal development

The establishment of neural circuits during early postnatal development requires both patterned gene expression and synchronized rhythmic electrical activity. Alteration in the amount or patterning of rhythmic electrical activity affect the normal development of the sensory structures in the cortex (Katz and Shatz, 1996;Spitzer, 2006). This rhythmic electrical activity has been suggested to be instrumental in controlling neuronal differentiation, synaptogenesis, and synaptic plasticity (**Fig. 7**) (Khazipov and Luhmann, 2006).

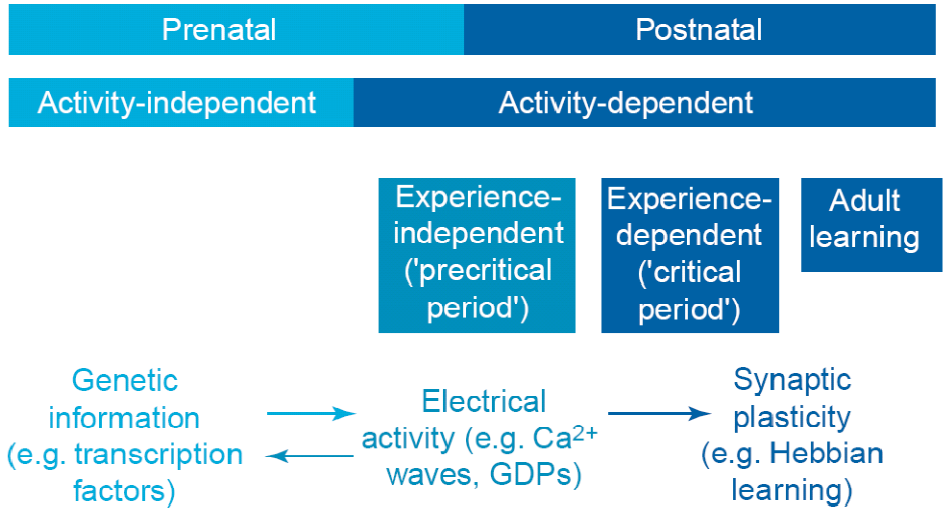

Fig. 7: Formation of early neuronal networks relies on genetic information and on electrical activity. During embryonic development, immature neuronal circuits and crude topographic connections are established on the basis of genetic information. With the emergence of gap-junction coupling, voltage-dependent Ca^{2+} and Na^{+} channels and various neurotransmitter receptors during prenatal and early postnatal stages, neuronal circuits develop highly correlated spontaneous or transmitter-evoked electrical activity patterns, which often propagate over long distances within the network. During perinatal development (e.g. during 'precritical periods'), certain electrical activity patterns induce specific gene expression. During further postnatal development (e.g. during 'critical periods'), the network is modified in an experience-dependent manner based on Hebbian learning rules (Khazipov and Luhmann, 2006).

Rhythmic electrical activity was observed in neonatal mice somatosensory cortex in intact-hemisphere preparations *in vitro* (Dupont et al., 2006). This study indicates that during the first postnatal week, the neonatal rodent cerebral cortex uses different neuronal circuits and mechanisms to generate synchronized oscillatory activity, and that it switches from a subplate-driven, gap-junction-coupled network to a NMDA receptor-driven synaptic network.

The spontaneous spindle-shaped oscillations were also recorded in thick (600-1000 µm) mice somatosensory cortical slices using an extracellular 60-channel recording system in control conditions, in absence of any drug that would enhance neuronal excitability (Sun and Luhmann, 2007). Under these conditions, spindle-shaped oscillations were spatially synchronized in a columnar manner (200-400 µm in diameter). These observations indicate that spindle shaped oscillations are a self-organized activity pattern, generated by mechanisms that are intrinsic to the immature cerebral cortex.

The dominant pattern of electrical activity in the neonatal rat neocortex *in vivo* is spindle bursts (Hanganu et al., 2006;Khazipov et al., 2004). Spindle bursts are spatially confined spindle-shape field potentials composed of rapid oscillations in the alpha-beta

frequency (8-25 Hz) and nested in an envelope of delta waves (1-4 Hz). They have been associated with phase-locked neuronal firing and activation of glutamatergic and GABAergic synapses. In the intact animal, compartmentalized spindle bursts in somatosensory cortex are triggered by sensory feedback resulting from spontaneous movements in a somatotopic manner (**Fig. 8a**) (Khazipov et al., 2004).

Spindle bursts are also the principal pattern of activity in the barrel cortex during the first postnatal week. Like spindle bursts in the body representation areas, spindle bursts in the barrel cortex can be evoked by sensory stimulation. Generation of spindle burst oscillations requires AMPA/kainate receptor activity at glutamatergic synapses. NMDA receptors and gap junctions are also slightly involved in the generation of spindle bursts. GABAergic synapses importantly contribute to the compartmentalization of spindle bursts by surround inhibition (Minlebaev et al., 2007).

Besides the rapid alpha-beta component, the spindle bursts also contain a slow depolarization at delta frequency (‘‘delta wave’’). The delta component of spindle bursts is generated primarily by NMDA and AMPA receptor mediated currents (Minlebaev et al., 2009).

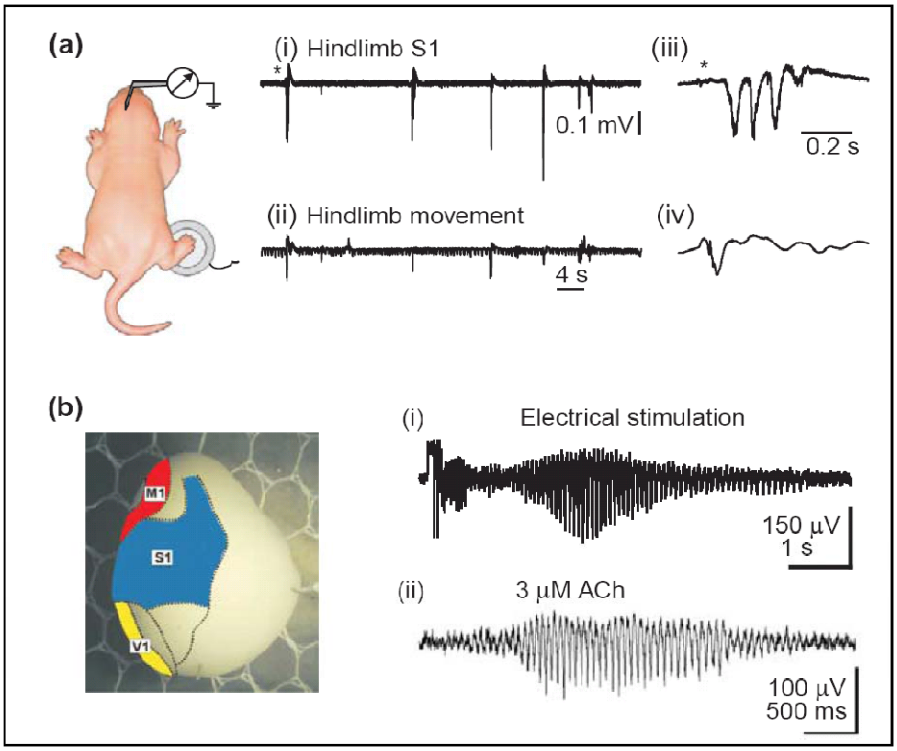

Fig. 8: Tracé discontinu and early patterns of activity in the rat neocortex in vivo and in vitro. A: Simultaneous recordings of (i) the intracortical field potential in the area representing the right foot in the P2 rat somatosensory (S1) cortex and (ii) the actual right-foot movements. Note discontinuous organization of the cortical activity and spindle bursts that are correlated with the movements. (iii) An example of a spindle burst marked by an asterisk in panel (i) that follows the foot movement. Note that the cortical event starts after the movement (iv). **B:** A neonatal rat intact cortex preparation *in vitro*, with the S1, primary auditory (A1) and primary visual (V1) cortical areas indicated. Field-potential recordings from the neocortex reveal oscillations in response to (i) electrical stimulation and (ii) application of 3 *m*M Ach (Khazipov and Luhmann, 2006).

1.7 Aims of the thesis

According to the studies mentioned above, we know that the spindle burst is the most commonly observed rhythmic electrical activity in rat barrel cortex *in vivo*. It is comparable with the spindle-shaped oscillation *in vitro* and also with the delta-brush recorded in the premature infant. However, the exact nature of the *in vivo* activity patterns, their spatial and temporal properties, and the underlying mechanisms are still not elucidated. Here we address the following questions in two projects:

Project1: Which patterns of oscillatory activity are present in the developing barrel cortex *in vivo*?

We use the multi-electrode recording technique to study the normal activity patterns in the rat primary somatosensory cortex (S1) during the first postnatal week *in vivo*. In contrast to calcium imaging techniques, electrophysiological recordings offer the advantage that the properties of the neuronal activity, e.g., frequency, synchronization, and coherence of oscillations, can be characterized with a higher temporal resolution. In this project we report that three patterns of oscillatory activity with distinct properties and spatiotemporal organization can be observed in the newborn rat somatosensory cortex *in vivo*. These coordinated patterns may contribute to the establishment of early cortical networks. Results of this project were already published (Yang et al., 2009).

Project2: What kind of spatial and temporal organization do the early patterns of oscillatory activity show in the developing barrel cortex?

To answer this question, voltage sensitive dye image (VSDI) and multi-electrode recording techniques were used simultaneously. There are many advantages of using VSDI. First, the time resolution of VSDI can reach several ms range. Second, the spatial resolution can reach a 10 to 50 μm range so that the activity within one barrel can be studied. Third, the activity within the barrel cortex corresponding to the major whisker follicles can be monitored in parallel. Thus, VSDI combined with multi-electrode recording techniques gave us the opportunity to study the spatial and temporal properties of several oscillatory activity patterns in the newborn rat barrel cortex.

In the final part of this project, we addressed the question whether spontaneous activity recorded in the barrel cortex is triggered from the thalamus and from the sensory periphery or whether cortical activity can be also generated independently from the thalamus by intracortical mechanisms.

2 Materials and Methods

2.1 Project1

2.1.1 Surgical preparation

All experiments were conducted in accordance with the national laws and the NIH guidelines for the use of animals in research and approved by the local ethical committee. Extracellular recordings were performed in the primary somatosensory cortex (S1, 0-3 mm posterior to bregma and 1-4.5 mm from the midline) of postnatal day (P) 0 to P7 rats (Paxinos et al., 1991) using experimental protocols as described previously (Hanganu et al., 2006;Hanganu et al., 2007). Briefly, under deep ice-cooling anesthesia alone or combined with light intraperitoneal urethane injection (0.5-1 g/kg, Sigma-Aldrich, Taufkirchen, Germany), the head was fixed into the stereotaxic apparatus using two metal bars fixed with dental cement on the nasal and occipital bones, respectively. The bone, but not the dura mater, over S1 was carefully removed by drilling a hole of less than 1 mm in diameter. Afterwards, the body of the animals was surrounded by cotton and kept at a constant temperature of 37° C by placing it on a heating blanket. During recordings, urethane anesthesia (0.1-0.5x of original dose) was given when the pups showed any sign of distress. After 30-60 min recovery, multi-electrode arrays were inserted perpendicularly into S1 to obtain simultaneous recordings of field potential (FP) and multiple unit activity (MUA) at different depths and locations. The electrodes were labeled with DiI (1,1'-dioctadecyl-3,3,3',3'-tetramethyl indocarbocyanine, Molecular probes, Eugene, OR) to enable post-mortem in histological sections the reconstruction of the electrode tracks in S1. One silver wire was inserted into the cerebellum and served as ground electrode (**Fig. 9**).

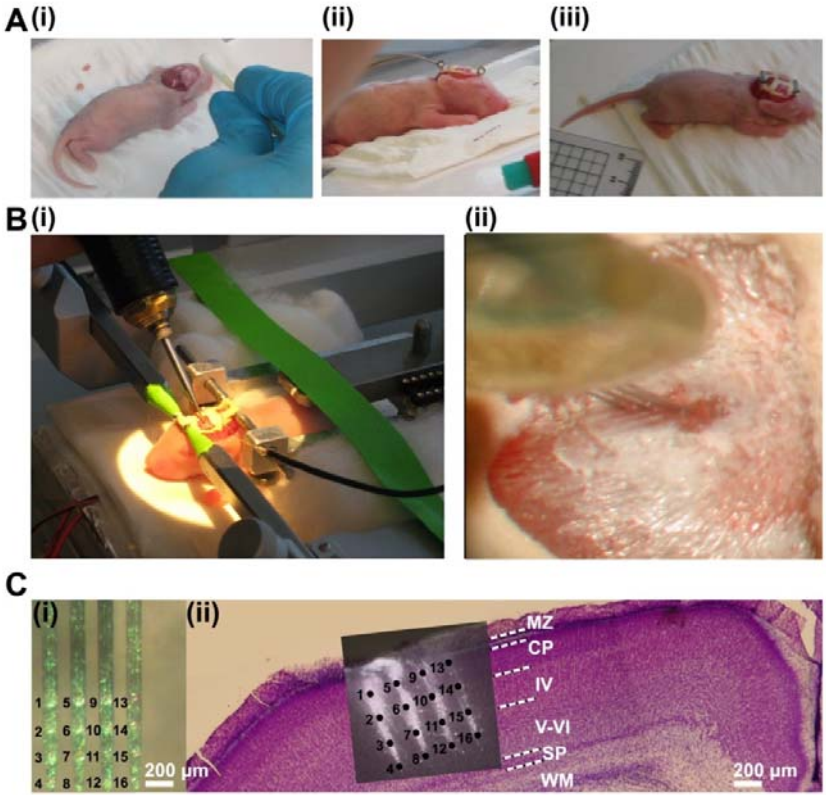

Fig. 9: The experimental procedure for surgery preparation. A: (i) The skin upon the skull was removed. (ii and iii) Dental cement was used to fix two mental bars on the nasal and occipital bones, respectively. **B:** (i) The pup's head was fixed into the stereotaxic apparatus using two metal bars. (ii) The bone, but not the dura mater, over S1 was carefully removed by drilling a hole of less than 1 mm in diameter; afterwards, a 4x4 multi-electrode probe was inserted perpendicularly into cortex. **C:** Multielectrode array used for extracellular recording of the S1 network activity at different cortical depths and locations. (i) Photograph of the 4x4-channel Michigan electrode array covered with DiI crystals. The 16 recording sites are marked by numbers. (ii) Digital photomontage reconstructing the location of the DiI-covered electrode array in S1 of a Nissl-stained 200-µm-thick coronal section from a P3 rat. Black dots and black numbers correspond to those in i and mark the 16 recoding sites in different cortical layers.

2.1.2 Recording and stimulation protocols

FP and MUA recordings were performed using a 1-shank or a 4-shank 16-channel Michigan electrode (1-2 MΩ, NeuroNexus Technologies, Ann Arbor, MI) inserted in dorso-ventral direction in one hemisphere or in both hemispheres at homologous stereotaxic coordinates. The recording sites were separated by 200 µm in vertical and horizontal direction for the 4-shank electrode (**Fig. 9Ci**) and by 50 µm in vertical direction for the 1-shank electrode. Both FP and MUA were recorded for at least 1000 s at a sampling rate of 1, 5 or 20 kHz using a multi-channel extracellular amplifier and the MC_RACK software (Multi Channel Systems MCS, Reutlingen, Germany). Tactile stimulation of all whiskers at a frequency of ~1 Hz was performed by hand.

For electrical stimulation of the whisker pad, electrical pulses (40 V, 100 μs) were applied via a bipolar tungsten electrode (160 μm diameter, California Fine Wire Company, Grover Beach, CA) inserted 1.5–2 mm through the skin into the whisker pad. Low frequency stimulation at 0.1 Hz was used to prevent accommodation.

2.1.3 Pharmacological procedures

Neuropharmacological experiments were performed by the use of a 26GA needle (World Precision Instruments, Sarasota, FL) attached to a microsyringe pump controller (Micro4; World Precision Instruments). The needle was positioned on the cortical surface close to the 1-shank 16-channel Michigan electrode and 200 nl of the drug was applied at a rate of 50 nl/min. The following substances were applied: DL-APV (100 μM) from Tocris (Köln, Germany), carbenoxolone (CBX) (100 μM) from Sigma-Aldrich (Steinheim, Germany) and lidocaine hydrochloride monohydrate (LIDO) (2%) from Sigma-Aldrich. All solutions were prepared on the day of the experiment in artificial cerebrospinal fluid (ACSF) containing (in mM) 124 NaCl, 26 $NaHCO_3$, 1.25 NaH_2PO_4, 1.8 $MgCl_2$, 1.6 $CaCl_2$, 3 KCl and 10 Glucose, pH 7.4. Control experiments with application of ACSF without drug were performed before APV or CBX application. Lidocaine application was performed to certify the diffusion ability of applied solutions into the neocortex at the recording site.

Blockade of neuronal activity from the whiskers to S1 via the trigeminal nerve was achieved by injection of 20 μl lidocaine (2% in saline) subcutaneously into the face just adjacent to the whisker pad.

2.1.4 Data analysis

Data were imported and analyzed off-line using MATLAB software version 6.5 or 7.7 (Mathworks, Natick, MA). To detect the oscillatory events, the raw data were filtered between 5 and 80 Hz using a Butterworth 3-order filter. Oscillatory events were detected as FP deflections exceeding five times the baseline standard deviation (SD). Only events lasting >100 ms and containing more than 3 cycles were considered for analysis. The events were analyzed in their occurrence, duration, amplitude (voltage difference between the maximal positive and negative peak), maximal frequency within each event, and relative frequency fraction corresponding to the theta (4-8 Hz), alpha (8-13 Hz) and beta (13-30 Hz) frequency bands. Time-frequency plots were calculated by transforming the FP events using Morlet continuous wavelet (Sun and Luhmann, 2007).

Minimal and maximal intensities in power were normalized to values between 0 and 1 and were displayed in dark blue and red, respectively. Correlation between oscillatory events recorded at different sites was assessed by cross-correlation and coherence analysis. The maximal cross-correlation and coherence coefficients were calculated by selecting one channel as reference. As spectral measure of correlation between two signals across frequencies, the coherence was calculated from the cross-spectral density between the two signals and normalized by the power spectral density of each (Jerbi et al., 2007). The computation was performed according to the formula

$$C(f) = \frac{\left| \sum_{i=1}^{N} X_i(f) Y_i^*(f) \right|^2}{\sum_{i=1}^{N} |X_i(f)|^2 \sum_{i=1}^{N} |Y_i(f)|^2},$$

where $X_i(f)$ and $Y_i(f)$ are the Fourier transforms of the signals x and y for the i data segment at frequency f, and * indicates the complex conjugate. The computations were carried out by using the magnitude-squared coherence function (MATLAB) based on Welch's averaged periodogram method (non-overlapping 0.5 s time window, frequency resolution 2 Hz). Coherence values ranging from 0 (events are uncorrelated) to 1 (events are perfectly correlated) were encoded from dark blue (0) to red (1) and displayed in coherence maps for all 16 recorded channels. MUA was detected after filtering the traces at 200 Hz high pass filter and setting the detection threshold at 5-fold baseline SD. To measure the phase synchronization between the local FP and MUA, a modified cross-correlation quantification was used (Lu et al., 2005). MUA discharge was detected when the positive value was higher than 7-fold baseline SD. The peaks of the negative trough of the field potential oscillations were used as reference to calculate the cross-correlation histograms with a 2 ms bin width. The values of cross-correlation histograms ranged between 0 (no synchronization) and 1 (perfect synchronization). Current source density analysis (CSD) profiles were calculated from the field potential profiles according to a five point formula described by Freeman and Nicholson (Freeman and Nicholson, 1975). The CSD values $\mathbf{I_m}$ were derived from the second spatial deviation of the extracellular field potentials $\mathbf{\Phi}$ and calculated by the finite-difference formula

$$\mathrm{I_m} = -(1/kh^2) \sum_{m=-n}^{n} a_m \Phi(X + mh),$$

where $\boldsymbol{h}$ is the distance between successive measuring points (50 μm in the present investigation) and $\boldsymbol{X}$ is the coordinate perpendicular to the cortical layer. The remaining constants are as follows: $n = 2$, $k = 4$, $a_0 = -2$, $a_{\pm 1} = 0$ and $a_{\pm 2} = 1$. In the CSD profiles, current sinks are indicated by downward deflections and sources by upward deflections. To facilitate visualization of CSD profiles, we generated color image plots by linear interpolation along the depth axis. The blue color represented current sinks and red color represented current sources.

The stereotaxic coordinates of the barrel cortex were obtained for each pup by scaling the previously reported stereotaxic coordinates of the adult barrel cortex (Paxinos et al., 1991;Welker, 1976) to the age-dependent changes along the bregma-lambda distance. In 24 pups the resulting coordinates were confirmed by tactile or electrical stimulation of the whiskers. In the graphical reconstructions of the barrel field (light blue landmarks in Figs. 19, 21, 23) age-dependent topographic changes within S1 were taken into account and the calculated stereotaxic coordinates were normalized to the lateral and posterior borders (100%) of the barrel field. To estimate any relationship between the properties of oscillatory activity and the stereotaxic location in S1, the occurrence, amplitude, duration and frequency of oscillations were averaged, normalized to the maximal value from each animal and displayed in color-codes: red dots for normalized values exceeding 50% of the maximal values, yellow dots for normalized values ranging between 25% and 50% of the maximal values and black dots for normalized values below 25% of the maximal value (see **Figs. 19A, 21A and 23A**).

Cluster analyses of the field potential oscillatory events were performed by the use of the *k*-means algorithm in Matlab 7.7. The Silhouette validation method was used to calculate and identify the best clustering (number of cluster) (Rousseeuw, 1987).

Data in the text are presented as mean ± SD. In the bar diagrams, data are shown as box plots giving the median, percentiles, outliers and skew. Statistical analyses were performed with Systat (SPSS Inc.) using Student's t-test and Mann-Whitney-Wilcoxon test. The significance levels of cross-correlation and coherence values (**Figs. 20Aii, 22Aii, 24Aii, 25B, 26B**) were determined by the use of the Z-test (Sun and Luhmann, 2007)

2.2 Project2

2.2.1 Surgical preparation

All experiments were conducted in accordance with the national laws for the use of animals in research and approved by the local ethical committee (#23177-07/G10-1-010). Voltage-sensitive dye imaging (VSDI) , field potential (FP) and multiple-unit activity (MUA) recordings were performed in the barrel cortex of postnatal day (P) 0 to P7 Wistar rats using experimental protocols as similar described previously (Yang et al., 2009). Briefly, under deep ice-cooling anesthesia combined with light intraperitoneal urethane injection (1 g/kg, Sigma-Aldrich, Taufkirchen, Germany), the animal´s head was fixed into the stereotaxic apparatus using one aluminum holder fixed with dental cement on the occipital bones (**Fig. 10A4 and B1**). Depending on the experimental design, the skull was opened in one of two different ways. (i) For VSDI experiments, a 3x3 mm^2 area of the skull (0-3 mm posterior to bregma and 1.5-4.5 mm from the midline) was thinned on the left hemisphere using a miniature drill until the residual bone, but not the dura mater, above the barrel cortex could be carefully removed with a fine canula. (**Fig. 10A**). (ii) For experiments performing simultaneous multi-channel extracellular electrophysiological recordings in the thalamus and cortex a 2x2 mm^2 area of the skull (P0-P1: 0-2 mm posterior to bregma and 1.5-3.5 mm from the midline; P6-P7: 1-3 mm posterior to bregma and 2-4 mm from the midline) above the barrel cortex of the left hemisphere was exposed. Additionally another rectangular area (P0/1: 1-2.5 mm posterior to bregma and 1-2 mm from the midline; P6-P7: 1.5-3.5 mm posterior to bregma and 1.5-3 mm from the midline) of the skull was removed for perpendicular insertion of the thalamic multi-channel electrode. (**Fig. 10B**). One silver wire was inserted into the cerebellum and served as ground electrode. Animals were kept at a constant temperature of 37° C by placing them on a heating blanket and covering their bodies with cotton. During recordings, urethane anesthesia (0.1-0.5x of original dose) was given when the pups showed any sign of distress.

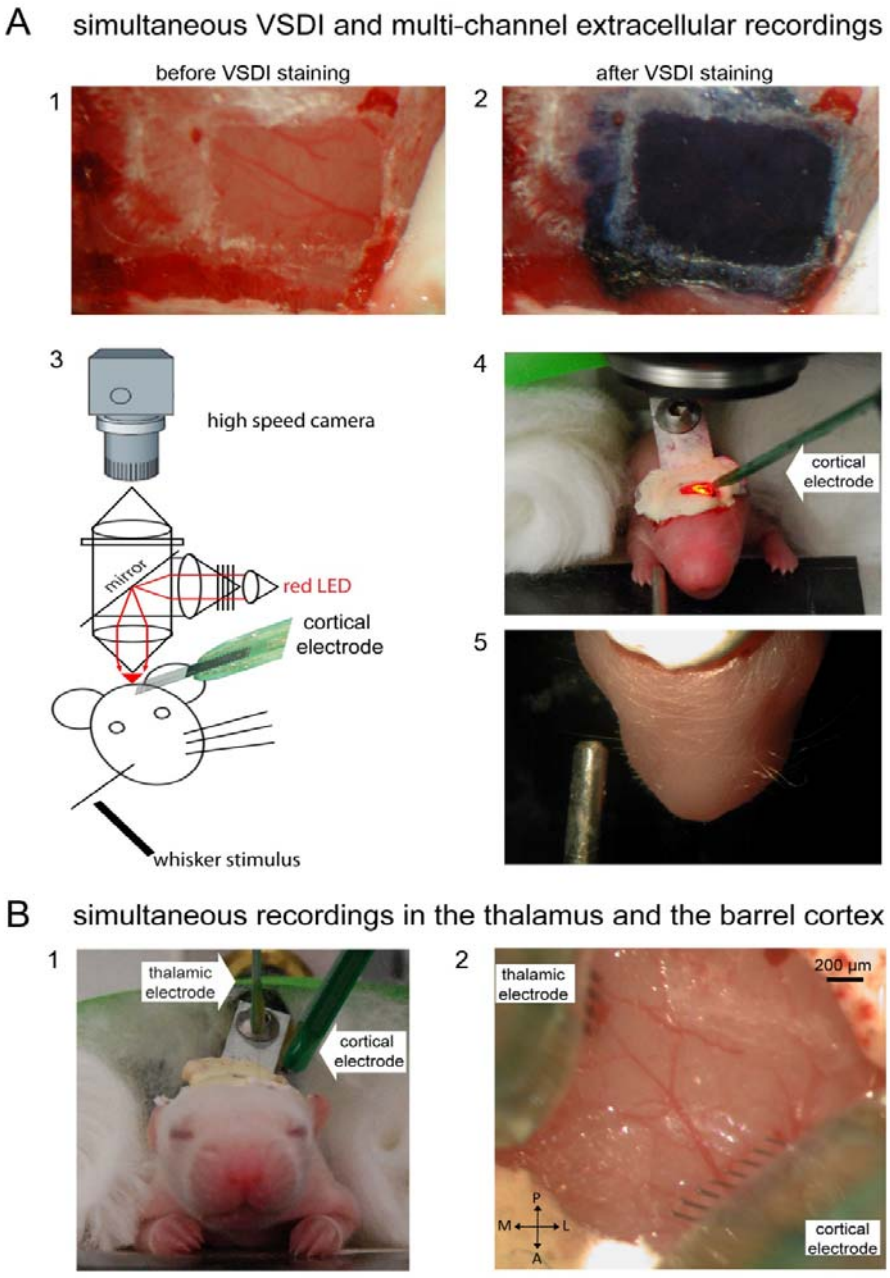

Fig. 10: Experimental set-up. A: Schematic illustration (1) and photograph (2, 3) of experimental set-up combining selective single whisker stimulation, VSDI and cortical 32-channel recordings using an 8-shank electrode. **B:** Photograph of experimental set-up with a 4-shank 32-channel electrode located in the thalamus (left) and an 8-shank 32-channel electrode in the barrel cortex (right) (1). Top view of the recording electrodes inserted into the barrel cortex and thalamus (2).

2.2.2 Whisker stimulation, video recording of whisker movements and recording of body movements

All whiskers except those of arc 2 were trimmed following the surgical preparation. Single whiskers could be stimulated using a protruding device consisting of a miniature-solenoid actuator (Krupa et al., 2001), which was activated by a TTL pulse. The actuator touched the selected whisker nearby its base and deflected it for 10 ms. Stimulus evoked cortical responses were studied with VSDI and multi-electrode extracellular recordings. Whisker movements were recorded with a digital camera (30 frames/s, 640×480 pixels; Nikon Coolpix 995, Tokyo, Japan), mounted on a dissecting microscope (Stemi 1000, Carl Zeiss, Jena, Germany) and stored on a personal computer via CED and Spike2 software (Cambridge Electronic Design, Cambridge, England). Images were analyzed offline using custom-made routines in MATLAB software (version 7.7, Mathworks, Natick, MA). The whisker angle ($\Delta\alpha$) was quantified for each frame (lower traces in **Fig. 37A1-3**) by measuring an in-plane rotation angle of the whisker (**Fig. 37A4**) as described previously by Ferezou et al. (Ferezou et al., 2007). Body movements were detected by the use of a piezoelectric sensor and recorded via a multi-channel extracellular amplifier and the MC_RACK software (Multi Channel Systems, Reutlingen, Germany).

2.2.3 Voltage-sensitive dye imaging

The voltage-sensitive dye RH1691 (Optical Imaging, Rehovot, Israel) was dissolved in a saline solution containing (in mM): 125 NaCl, 2.5 KCl, 10 HEPES (pH 7.3 with NaOH). The voltage-sensitive dye was topically applied to the brain surface and allowed to diffuse into the cortex for 15 to 30 min. Subsequently, unbound dye was carefully washed away with saline solution. This procedure resulted in a complete staining of all cortical layers from the subplate to the marginal zone / layer I in P0-P1 rats (**Fig. 11**, left) and in a more superficial staining pattern in P6-P7 animals (**Fig. 11**, right), similar as in adult rodent cerebral cortex (Berger et al., 2007). The cortex was covered with 1% low-melting agarose and a cover slip placed on top to stabilize the tissue. Excitation light from a red LED (MRLED 625 nm, Thorlabs GmbH, Dachau, Germany) was band pass filtered (630/30 nm) and reflected towards the sample by a 650 nm dichroic mirror. The excitation light was focused onto the cortical surface with a 25 mm

Navitar video lens (Stemmer Imaging, Puchheim, Germany). Emitted fluorescence was collected via the same optical pathway but without reflection of the dichroic mirror, long pass filtered (660 nm) and focused via another 25 mm Navitar lens onto the chip of a MiCam Ultima L high speed camera (Scimedia, Costa Mesa, CA, USA). This tandem-type macroscope design (Ratzlaff and Grinvald, 1991) resulted in a 1x magnification. As the high speed camera has a detector with 100x100 pixels and a chip size of 10x10 mm^2, the field of view was 10x10 mm^2. Using a C-mount extension tube we reduced the field of view to 2.6x2.6 mm^2 and thereby reduced in addition the vignetting. Every pixel collected light from a cortical region of 26x26 μm^2. The tandem-type macroscope comprising the LED, the filter cube and the two video optics was built in the mechanical workshop of our institute. Fluorescence measurements were synchronized to electrophysiological recordings through TTL pulses.

Spontaneously ongoing activity was detected during 16 s long imaging sessions while evoked activity following whisker stimulation was imaged in 2 s long sessions, both with an unbinned whole frame sampling frequency of 500 Hz. For both set of experiments, data were not averaged.

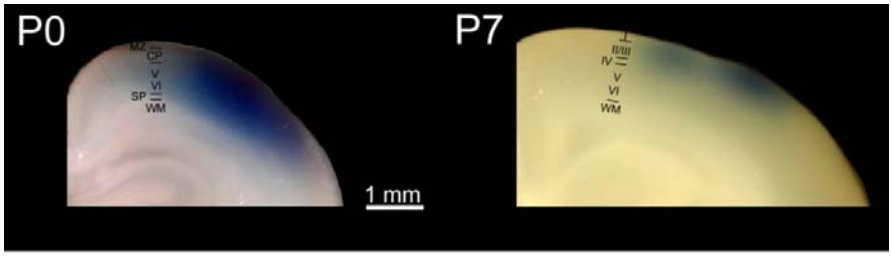

Fig. 11: Penetration of the voltage-sensitive dye RH1691 in the parietal cortex of the newborn rat. Photograph of a coronal section in a P0 rat (left) and P7 rat (right) shows the staining pattern with RH1691(blue color).

2.2.4 Evaluation of voltage sensitive dye imaging data

Images were analyzed offline using custom-made routines in MATLAB software version 7.7 (Mathworks, Natick, MA). In order to improve the signal to noise ratio, the image data were first processed using 5x5 pixel spatial binning followed by 60 Hz low pass filtering. Bleaching of fluorescence was corrected by subtraction of a best-fit double-exponential or 5^{th} degree polynomial curve (curve fitting tool in MATLAB (Mathworks). The change of fluorescence divided by the resting fluorescence ($\Delta F / F_0$) was calculated.

Evoked or spontaneous responses were defined as such if they had a maximal response with a $\Delta F / F_0$ of at least 0.2 %. To evaluate their onset, 3x3 pixels were taken around a pixel with a signal which was at least 7 times the noise (0.022 ± 0.0025 % was the baseline standard deviation). The area of the VSD image of the evoked response or the spontaneous event was defined as the half-maximal contour plot of the VSD response according to the trace with earliest responses covering 3x3 pixels (Ferezou et al., 2007). This procedure enabled us to compare the spatiotemporal properties of evoked and spontaneous activity within the same animal and between different animals (**Fig. 12**).

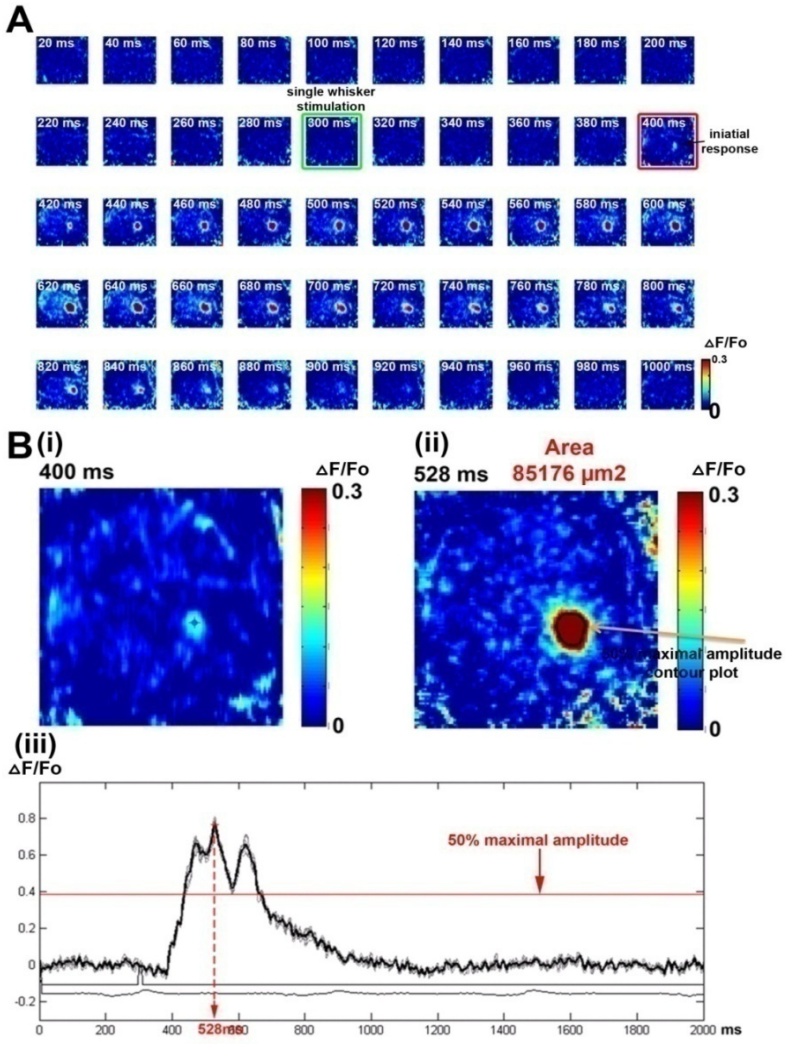

Fig. 12: The method for calculating evoked VSDI response. A: One example (from one P1 rat) displays the consecutive pictures of D2 whisker evoked response (20 ms interval). At 300ms the D2 whisker was stimulated and at 400 ms we could see the initial evoked response. The duration of the evoked response was from 400ms to 920ms. **B:** (i) The initial evoked response at 400ms. (iii) The evoked VSDI response in the position of initial evoked response in B(i). Note: The time of maximum evoked response is at 528ms and the horizontal red line represents the 50% maximal amplitude. (ii) The maximum evoked area was calculated at the time of maximum evoked response and the 50% maximal amplitude contour plot in B(iii).

2.2.5 Histology, cytochrome oxidase staining

In order to visualize the entire barrel field representing the contralateral whiskers, the barrel cortex was tangentially cut and flattened after the experiment. After 24 h of fixation in 4% paraformaldehyde, the cortex was sectioned in 100-200 µm thick sections and processed for cytochrome oxidase (CO) histochemistry according to the protocol described by Staiger and colleagues (Staiger et al., 2004). In brief, sections were rinsed in phosphate buffer, then incubated at 39°C in a solution of 0.6 mg cytochrome C, 0.5 mg DAB and 44 mg saccharose per ml (all from Sigma, Deissenhofen, Germany), with 0.3% catalase (Sigma) included. Sufficient staining was achieved after 2-7 hour of reaction. Finally, sections were intensified with 0.5% Copper(II)sulfate (Sigma) for 2-3 min, air-dried and mounted.

Both, in P0-P1 and P6-P7 the localization and dimension of several cortical barrels determined experimentally by mechanical stimulation of single whiskers in VSDI experiments (**Figs. 33A1, 2** and **33B1, 2**) was used to align the CO stainings with the barrel field map. Since P0-P1 rats do not reveal a clear barrel-like pattern using CO staining or any other histological staining pattern (Erzurumlu and Jhaveri, 1990), the predicted barrel field map in P0-P1 was constructed by shrinking the barrel maps revealed from CO stainings of P5 animals on the P0 or P1 tangential section, according to the localization and dimension determined in VSDI experiments using single whisker stimulation. To visualize the barreloids in the ventral posterior medial (VPM) nucleus of the thalamus, the brain was cut into 200 µm thick sagittal slices and processed for CO histochemistry according to the procedure described above.

2.2.6 Multi-electrode recording protocols

Two different types of multi-electrode recordings were performed. (i) After identifying the location of the arc 2 barrels using VSD response, an 8-shank 32-channel Michigan electrode (1-2 MΩ, NeuroNexus Technologies, Ann Arbor, MI) was inserted in an angle of ~35° into the barrel cortex representing the whiskers of arc 2. The recording sites were separated by 200 or 300 µm in vertical and horizontal direction (**Fig. 34A1**). In these experiments we could combine imaging and extracellular electrophysiological data acquisition and could compare the spatial extent of spindle and gamma activity recorded simultaneously with both techniques. (ii) For simultaneous recordings in the thalamus

and barrel cortex, a 4-shank 32-channel electrode (50 or 100 µm electrode spacing) was labeled with DiI (1,1'-dioctadecyl-3,3,3',3'-tetramethyl indocarbocyanine, Molecular Probes, Eugene, OR, USA) and inserted into the ventral posterior medial (VPM) nucleus of the thalamus. The DiI staining procedure allowed the reconstruction of the electrode tracks in the VPM from post-mortem CO histological sections (**Fig. 35A3**). Another 8-shank 32-channel electrode or 4-shank 16-channel electrode was inserted into the barrel cortex. Both, field potential (FP) and multi-unit activity (MUA) were recorded for 10 min to 1 h at a sampling rate of 20 kHz using a multi-channel extracellular amplifier and the MC_RACK software (Multi Channel Systems).

2.2.7 Field potential data analysis

Field potential data were imported and analyzed off-line using MATLAB (Mathworks). To detect the spindle burst events, the raw data were band-pass filtered between 5 and 80 Hz using a Butterworth 3-order filter. To detect the gamma oscillation events, the raw data were band-pass filtered between 30 and 80 Hz using a Butterworth 3-order filter. Oscillatory events were detected as FP deflections exceeding five times the baseline standard deviation. Only events lasting >100 ms and containing more than 3 cycles were considered for analysis. Time-frequency plots were calculated by transforming the FP events using Morlet continuous wavelet (Sun and Luhmann, 2007). Minimal and maximal intensities in power were normalized to values between 0 and 1 and were displayed in dark blue and red, respectively. Spikes were detected using a threshold-based detector set to a threshold of 5x the SD of the noise level via MC_RACK software. Spike datasets from all recording electrodes were imported into MATLAB for further analyses.

2.2.8 Cross- and autocorrelograms

Crosscorrelograms were calculated by the use of a spike-to-spike cross-correlation function (Perkel et al., 1967), with a 1 ms bin size:

$$C_t = \frac{N_{\text{co}}}{\sqrt{N_x * N_y}} \quad (1),$$

where N_{co} is the total number of coincident spikes in spike trains *x* and *y*. N_x and N_y are the spike numbers of spike trains *x* and *y*, respectively. C_t is cross-correlation coefficient, where *t* is a time lag between spike train *x and y*. The confidence intervals of each correlogram were estimated using a resampling (surrogate) method (10 trials). In each

surrogate, every spike was moved forward or backward by a random time interval following a Gaussian distribution (Sun et al., 2010). In the present study we used a Gaussian distribution with a mean of 0 and a SD of 50. Correlation coefficients (*C*) were considered significant if the values differed from the mean of the surrogates by >1 SD.

Autocorrelograms were calculated by the use of the same function as crosscorrelograms by making $x=y$ in equation (1).

2.2.9 Statistics

Data in the text are presented as mean ± s.e.m. Statistical analyses were performed with Systat (SPSS Inc.) using Student's t-test and Mann-Whitney-Wilcoxon test for parametric and non-parametric distribution of the data set.

3 Results

3.1 Project1

3.1.1 Neonatal somatosensory cortex expresses three distinct patterns of spontaneous oscillatory activity

We examined the activity patterns in the primary somatosensory cortex (S1) by performing long-lasting extracellular recordings of the local field potential (FP) in neonatal [postnatal day (P) 0-7] rats (n=50 pups) *in vivo* (**Fig. 13A**). Three distinct patterns of spontaneous oscillatory activity could be reliably observed in neonatal S1 cortex (**Fig. 13B, C, and Fig. 14**). As reported previously (Hanganu et al., 2006;Khazipov et al., 2004), the dominant activity pattern recorded in all investigated pups (n=50) was an intermittent network burst associated with spindle-shaped field oscillation that was defined as a spindle burst (**Figs. 13B, 13Cii, 15A**). These FP oscillations with a relative short duration (1.4 ± 1.6 s, n=918 events from 50 pups) had an average maximal amplitude of 262.4 ± 317.5 μV (n=918) and occurred at a frequency of 5.3 ± 3.4 bursts/min (n=50 pups). The dominant frequency within a spindle burst ranged in the alpha band with an average maximal frequency of 9.3 ± 4.4 Hz (n=918). However, a certain amount of theta (40.1 ± 21.9 % of relative power, n=918) and beta band activity (27.6 ± 20.1 % of relative power, n=918) also contributed to the spindle burst pattern. The spindle bursts were associated with rhythmic multiple unit discharges (MUA trace in **Fig. 15A**). To estimate the degree of synchronization between the spindle bursts and MUA, we calculated the cross-correlation by correlating the negative peak of each oscillatory cycle with the spike discharge (**Fig. 16A**). The resulting high cross-correlation of 0.48 ± 0.22 (n=10 pups) indicates a synchronization of spike discharges with the network oscillations and demonstrates the contribution of single cell firing to the generation of spindle bursts (**Fig. 16D**).

Although previous studies defined the spindle burst as the dominant activity pattern in the neonatal somatosensory and visual cortex (Hanganu et al., 2006;Khazipov et al., 2004), we identified two additional patterns of spontaneous oscillatory activity, which so far have not been described *in vivo* (for gamma activity in newborn rat hippocampus *in vitro* see (Palva et al., 2000). In 64% of the investigated pups (n=32) fast oscillations with an average frequency of 38.3 ± 7.7 Hz could be recorded (n=495 events from 32 pups) (**Figs. 13B, 13Ci, 15B**). We defined this activity pattern as gamma

oscillation, since the dominant frequency of this intermittent and short oscillatory event was in the gamma frequency range (Palva et al., 2000). Although the occurrence of gamma oscillations (5.8 ± 3.8 events/min, n=32 pups) was similar to that of spindle bursts, their duration was significantly ($p<0.001$) shorter (0.2 ± 0.2 s, n=495 events from 32 pups) and their amplitude significantly ($p<0.001$) smaller (138.6 ± 131.2 μV, n=495) than those of spindle bursts. The different frequency distribution, duration and spatio-temporal properties reinforced the conclusion that spindle bursts and gamma oscillations are two distinct patterns of neuronal activity (**Fig. 14**). Gamma oscillations were highly correlated with MUA (average cross-correlation 0.77 ± 0.17, n=10 pups) (**Fig. 16B, D**).

Beside spindle bursts and gamma oscillations, a third spontaneous activity pattern could be recorded in 20 out of 50 investigated pups (**Figs. 13B, 15C**). These oscillations were surprisingly long (21-113 s, mean 54.5 ± 20.2 s, n=51 events from 20 pups) and therefore were termed long oscillations. Despite their rare occurrence (0.04 ± 0.02 events/min, n=20 pups), long oscillations were most prominent and revealed a large amplitude of 461 ± 278.8 μV (n=51). The average maximal frequency within these oscillations was 13.6 ± 6.8 Hz (n=51). Simultaneous recordings of the FP and extracellular DC (direct current) potential demonstrated that long oscillations are not related to spreading depressions, which were experimentally induced by local application of 1 M KCl (**Fig. 17**). Long oscillations did not affect the generation or properties of spindle bursts and gamma oscillations. Both activity patterns persisted after a long oscillation with similar amplitude, occurrence, duration and frequency as before the prominent discharge (**Fig. 18**). Similar to spindle bursts and gamma oscillations, long oscillations were accompanied by MUA (**Fig. 15C, Fig. 16C**) and revealed an average cross-correlation coefficient of 0.79 ± 0.08 (n=3 pups, **Fig. 16D**).

These three activity patterns could be reliably recorded in urethane-anaesthetized as well as in non-anaesthetized rats and showed very similar properties in both experimental conditions (Table 1), indicating that these spontaneous patterns represent anesthesia-independent distinct oscillatory activities in neonatal rat S1 cortex. These patterns were further analyzed in their spatio-temporal properties, synchronization pattern and developmental profile.

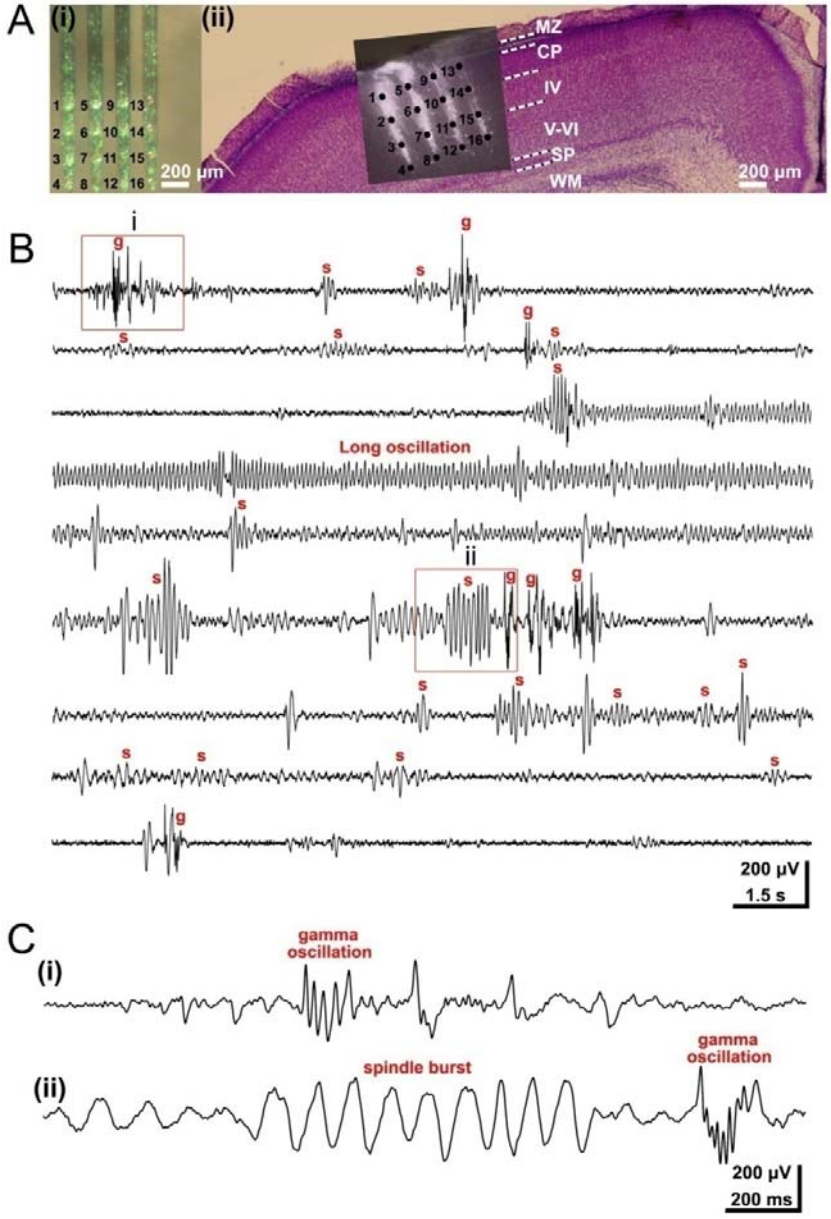

Fig. 13: Three distinct patterns of oscillatory activity in the primary somatosensory cortex (S1) of the neonatal rat in vivo. A: Multi-electrode array used for extracellular recording of the S1 network activity at different cortical depths and locations. (i) Photograph of the 4x4-channels Michigan electrode array covered with DiI crystals. The 16 recording sites are marked by red numbers. (ii) Digital photomontage reconstructing the location of the DiI-covered electrode array in S1 cortex of a Nissl-stained 200 µm thick coronal section from a P3 rat. Green dots and red numbers correspond to those in (i) and mark the 16 recoding sites in different cortical layers. **B:** Continuous recording of spontaneous activity at electrode 9 from (Aii). Several spindle bursts (marked by s), gamma oscillations (g) and one long oscillation could be recorded during this 135 s long observation period. Note the similar properties of spindle bursts and gamma oscillations before and after the long oscillation. **C:** Examples of gamma oscillations (i, ii) and spindle burst (ii) displayed at expanded time-scale and marked in by red boxes in B.

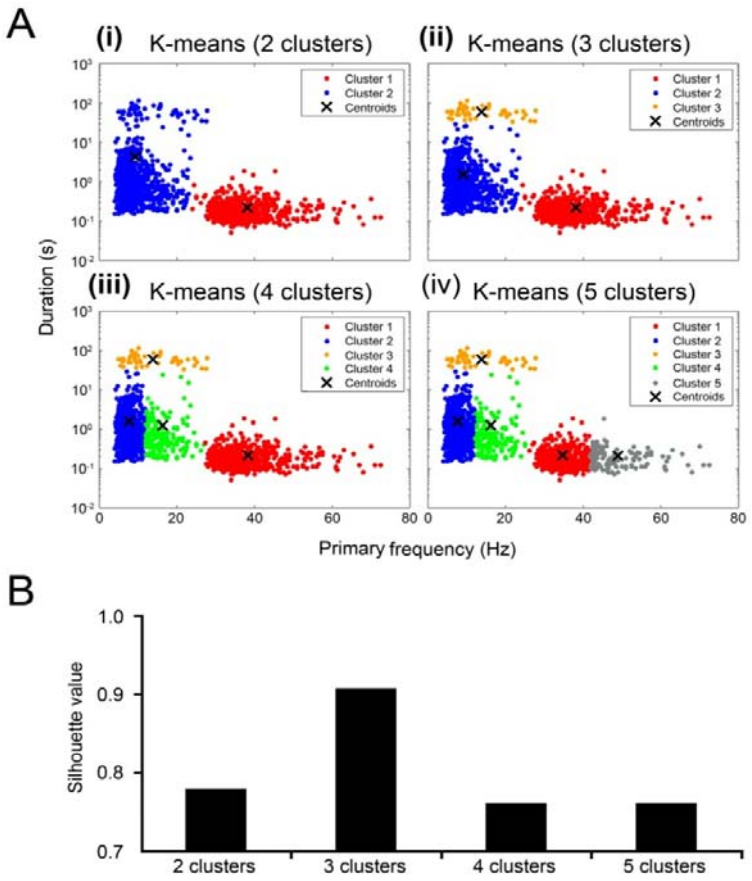

Fig. 14: Cluster analysis of the spontaneous activity patterns recorded in the barrel cortex of 50 newborn rats (n=1461 oscillatory events). The primary frequency (maximal frequency) and the duration of the oscillatory activity were used as parameters for the cluster analysis using the k-means clustering algorithm. A: Raster plots with 2, 3, 4 and 5 clusters (i to iv). B: The Silhouette validation technique was used to analyse the cluster validity. Grouping the data in 3 clusters resulted in the highest silhouette value.

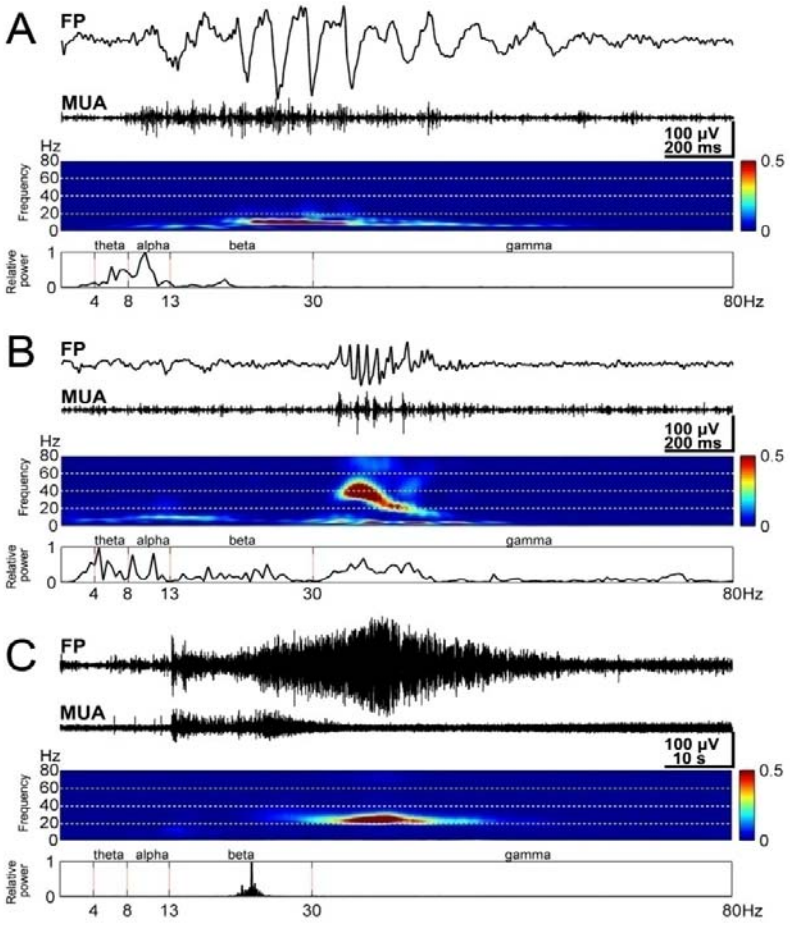

Fig. 15: Properties of spindle bursts, gamma oscillations and long oscillations. A: Characteristic spindle burst recorded in S1 cortex of a P1 rat (top) and corresponding MUA after 200 Hz highpass filtering (below). Note the correlation between spindle burst and MUA. Color-coded frequency plot shows the wavelet spectrum of the field potential recording at identical timescale. Fast Fourier transformation (FFT) of the field potential recording illustrating the relative power of the displayed spindle burst with a maximal frequency at 10 Hz (bottom). **B:** Characteristic gamma oscillation (top) recorded in the S1 cortex of a P3 rat and corresponding MUA (below). Wavelet and FFT spectrum reveal prominent gamma activity between 30 and 50 Hz. **C:** Characteristic long oscillation (top) recorded in S1 cortex of a P6 rat and corresponding MUA (below). Color-coded wavelet spectrum and FFT (bottom) of the field potential recording display a narrow peak at 23 Hz. Note strong MUA at the onset of the long oscillation and different time scale as compared to A and B.

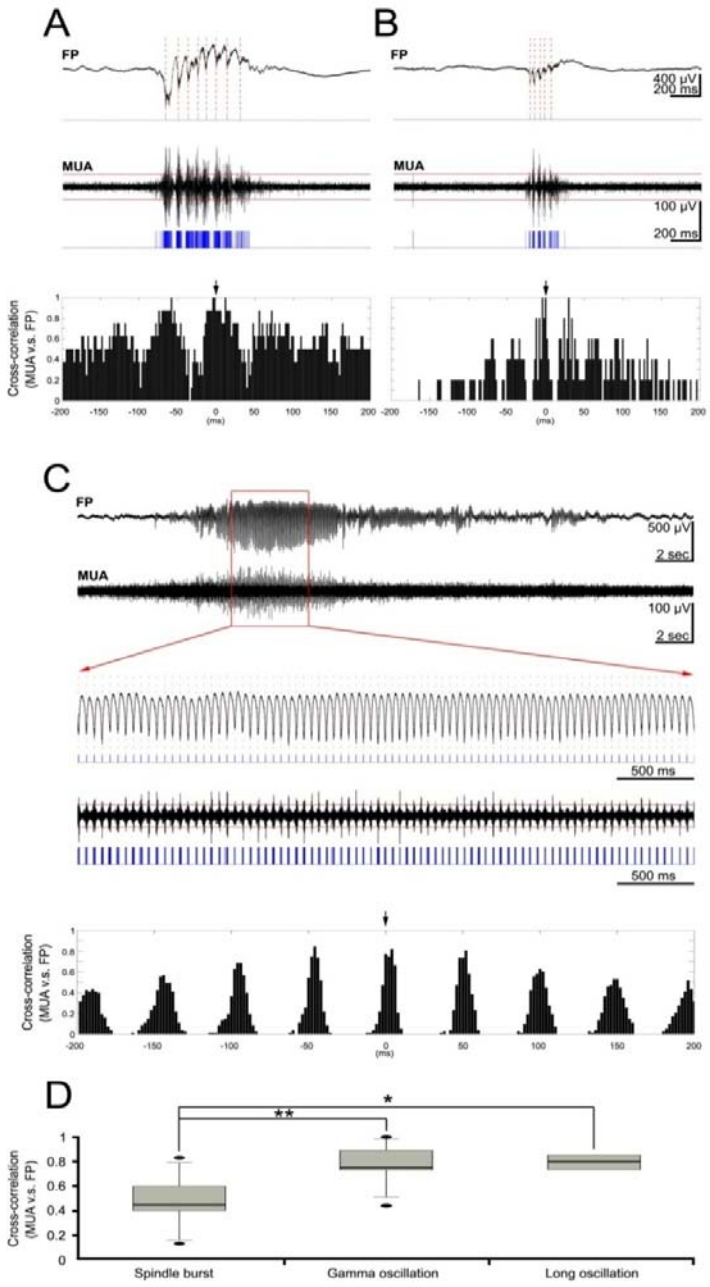

Fig. 16: Correlation of oscillatory field potentials with multiunit activity (MUA) in phase-dependent manner. A: Spindle burst field potential (upper trace) and corresponding MUA (middle trace) recorded in a P3 rat. Blue vertical lines mark single unit activity which surpasses the threshold (red horizontal lines in middle trace). Cross-correlation histogram between MUA and field potential of the spindle burst (red dotted lines) reveals close temporal relationship. **B:** Same as in A, but typical example of a gamma oscillation recorded in a P2 rat. Note closer temporal coupling between MUA and field potential when compared to the spindle activity in A. **C:** Same as in A, but example of a long oscillation recorded in a P4 rat. A 4 second period was used to calculate the cross-correlation histogram between MUA and field potential of the long oscillation. Note the precise coupling of MUA and minimum in field potential. **D:** Summary diagram illustrating as box plots the cross-correlation between MUA and field potentials as calculated from 100 spindle bursts (10 pups), 100 gamma oscillations (10 pups) and 3 long oscillations (3 pups). The sampling rate to acquire the data was 20 kHz.

	Duration (sec)			Amplitude (μV)		
	Non-anesthetized	Urethane-anesthetized		Non-anesthetized	Urethane-anesthetized	
Spindle bursts	1.22 ± 0.48 (n=10)	1.07 ± 0.57 (n=40)	n.s.	361.96 ± 385.47 (n=10)	280.4 ± 203.83 (n=40)	n.s.
Gamma oscillations	0.16 ± 0.06 (n=9)	0.15 ± 0.04 (n=14)	n.s.	177.1 ± 86.52 (n=9)	95.97 ± 55.02 (n=14)	*
Long oscillations	52.28 ± 10.47 (n=8)	61.31 ± 17.12 (n=12)	n.s.	587.81 ± 419.56 (n=8)	360.15 ± 195.95 (n=12)	n.s.

	Frequency (Hz)			Occurrence (min^{-1})		
	Non-anesthetized	Urethane-anesthetized		Non-anesthetized	Urethane-anesthetized	
Spindle bursts	9.33 ± 1.83 (n=10)	9.72 ± 2.22 (n=40)	n.s.	4.85 ± 1.71 (n=10)	5.97 ± 3.65 (n=40)	n.s.
Gamma oscillations	36.78 ± 2.28 (n=9)	37.74 ± 2.33 (n=14)	n.s.	2.44 ± 1.45 (n=9)	4.15 ± 4.35 (n=14)	*
Long oscillations	12.15 ± 6.16 (n=8)	9.51 ± 2.63 (n=12)	n.s.	0.05 ± 0.03 (n=8)	0.04 ± 0.02 (n=12)	n.s.

Table 1: Properties of spindle bursts, gamma oscillations and long oscillations recorded in non-anesthetized and urethane-anesthetized newborn rats. Note that urethane has a significant effect only on the amplitude of the gamma oscillations, whereas all other patterns and properties are similar in both experimental conditions.

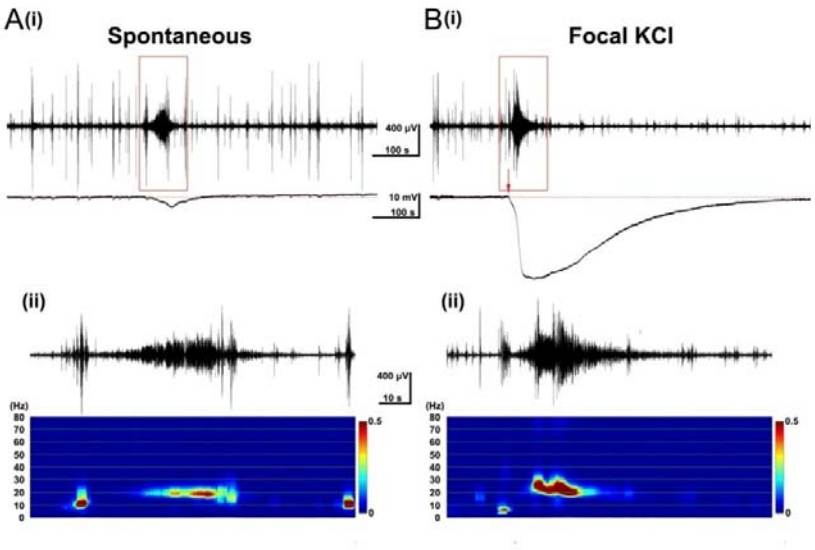

C(i)

Field potential oscillations

	Long oscillations (n=13)	KCl induced (n=4)	
Frequency (Hz)	12.7 ± 4.3	21.8 ± 4.4	*
Duration (s)	42.9 ± 12.9	36.9 ± 10.4	n.s.
Amplitude (µV)	1190.7 ± 620	953.5 ± 531.8	n.s.

(ii)

Properties of DC shift

	Long oscillations (n=13)	KCl induced SD (n=4)	
Maximum amplitude (mV)	9 ± 8.7	29.4 ± 3.5	**
Duration at 1/2 maximum amplitude (s)	40.6 ± 34	249.5 ± 43.7	**

Fig. 17: DC shifts associated with long oscillations differ from KCl-induced DC shifts. A: (i) Field potential recording with Michigan electrode (upper trace) and simultaneous extracellular DC potential recording with a glass pipette (lower trace) in the barrel cortex of a P3 rat. Note presence of numerous spindle bursts and gamma oscillations. The long oscillation (red box) is shown in (ii) at higher temporal resolution and with corresponding wavelet plot. **B:** (i) In the same P3 rat as in A a spreading depression was elicited by local application of ~100 nl 1 M KCl on the neocortical surface near the recording sites. Note characteristic large DC shift associated with the SD and suppression of spontaneous activity after the SD. Red downward arrow indicates time point of KCl application. (ii) Field potential recording during the SD and corresponding wavelet plot. **C:** Summary table illustrating the significant differences in the properties of the field potential oscillations (i) and the DC shift (ii) during spontaneous long oscillations and during KCl-induced SD.

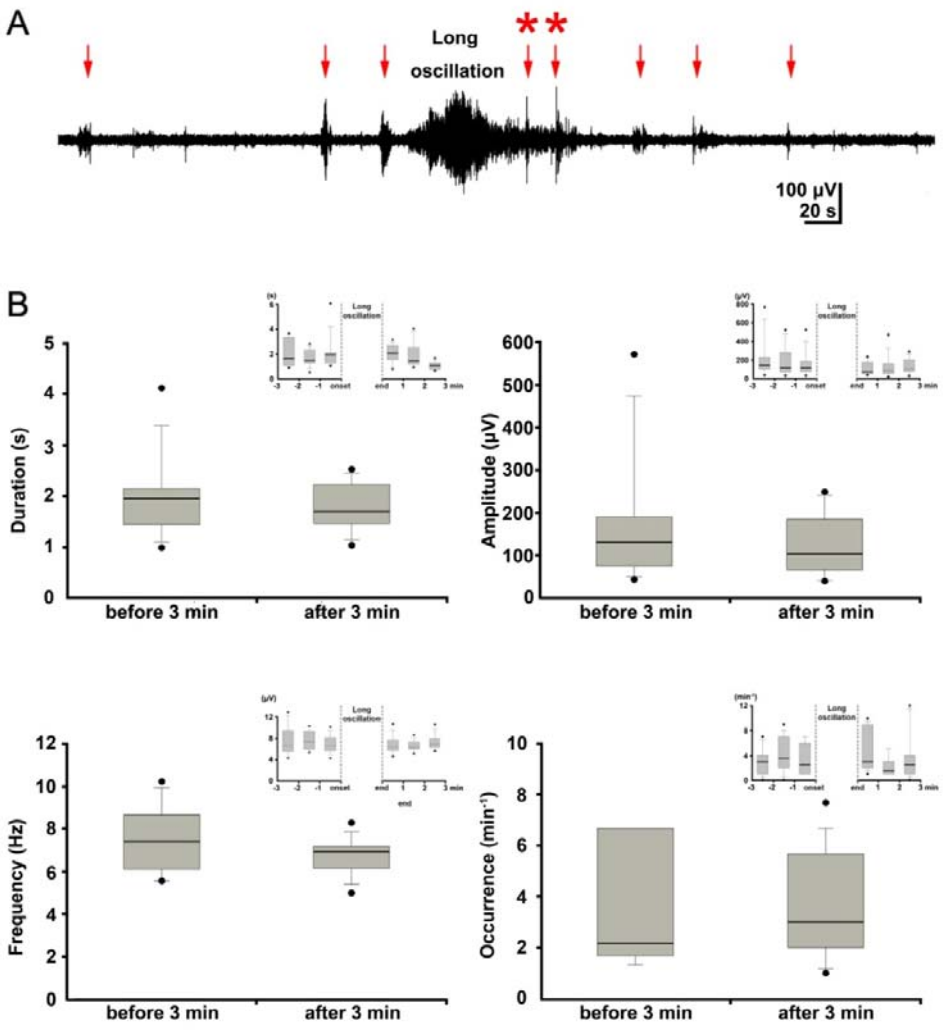

Fig. 18: Long oscillations do not impair spindle bursts discharge. A: Field potential recording of a long oscillation and several spindle bursts (red arrows) that precede and succeed the long-lasting discharge. Note the occurrence of spindle bursts (asterisk) during the long oscillation. **B:** Box plots displaying the duration (i), amplitude (ii), frequency (iii) and occurrence (iv) of spindle bursts that were quantified for 3 min before the onset and after the end of the long oscillations (n=10). There was no significant difference for these four parameters in the properties of the spindle bursts. The insert plots document the results with a 1 min temporal resolution.

3.1.2 Spindle bursts synchronize neonatal cortical activity in a column-like pattern

Spindle bursts represent the dominant spontaneous activity pattern in the S1 cortex of newborn rodents (Minlebaev et al., 2007;Khazipov et al., 2004). The spatio-temporal properties of spindle bursts were analyzed by field potential recordings in S1 cortex at multiple stereotaxic coordinates ranging from 0 to 3 mm posterior to bregma and from 1 to 4.5 mm lateral to midline (Paxinos et al., 1991). Although, spindle bursts could be recorded at all investigated 94 coordinates (50 pups), their properties were dependent on the site of recording in S1 (**Fig. 19A**). Spindle bursts recorded in the barrel field (0-2.5 mm posterior to bregma and 2.5-4.5 mm from the midline) occurred more frequently (6.2 ± 3.9 bursts/min, n=64 stereotaxic coordinates, $p<0.001$) (**Fig. 19Ai**) and had a larger amplitude (297.7 ± 271.5 μV, n=64, $p<0.05$) (**Fig. 19Aii**) and frequency within burst (9.9 ± 2.4 Hz, n=64, $p<0.01$) (**Fig. 19Aiv**), but a shorter duration (1 ± 0.6 s, n=64, $p<0.001$) (**Fig. 19Aiii**) as compared to spindle bursts recorded in S1 cortex outside of the barrel field (occurrence 3.5 ± 2.1 bursts/min, amplitude 200 ± 168.5 μV, frequency within burst 8.3 ± 1.9 Hz, duration 2.2 ± 1 s, n=30 coordinates). The different properties of spindle bursts recorded within or outside of the barrel field may reflect the unique structural and functional organization of the barrel cortex.

During the first postnatal week, spindle bursts revealed significant age-dependent alterations in their relative occurrence, amplitude and maximal frequency (**Fig. 19B**). The average occurrence of spindle bursts increased significantly ($p<0.001$) from 2.4 ± 1.6 bursts/min at P0-P1 (n=10 pups) to 6.1 ± 2 bursts/min at P6-P7 (n=12 pups) (**Fig. 19Bi**). Whereas the mean amplitude of spindle bursts also increased from 121.3 ± 85.4 μV at P0-P1 (n=157 events from 10 pups) to 442 ± 455.6 μV at P6-P7 (n=275 events from 12 pups) (**Fig. 19Bii**), their duration remained relatively constant during the first postnatal week (**Fig. 19Biii**). The average maximal frequency within spindle burst significantly ($p<0.001$) increased from 7.6 ± 2 Hz (n=157) to 10.9 ± 4.9 Hz (n=275) (**Fig. 19Biv**) and the relative power shifted from the theta toward beta-band (**Fig. 19C**). In summary, these results demonstrate that spindle bursts occur more often and increase in amplitude and frequency during the first postnatal week, corresponding to a progressive maturation of the underlying neuronal networks and mechanisms for generation.

In the majority of the recordings (92%), spindle bursts were not restricted to one channel, but rather occurred simultaneously at several neighboring recording sites of the

4x4-channel recording electrode (**Fig. 20Ai**). In order to estimate the spatio-temporal dimension of the spindle burst mediated functional coupling, the cross-correlation and coherence coefficients for all recording sites were calculated in relationship to one reference channel (**Fig. 20Aii**). In 51% of all recordings (n=663 events from 49 pups) the spindle bursts were synchronized in a column-like pattern. The average cross-correlation (0.8 ± 0.05, n=48 pups) and coherence coefficients (theta band 0.85 ± 0.06, alpha band 0.83 ± 0.05, beta band 0.82 ± 0.06, n=48 pups) of spindle bursts were significantly ($p<0.001$) higher within a 200-400 μm wide cortical column as compared to activity recorded at more remote regions (>400 μm). Only 20% of the spindle bursts (n=268 events from 38 pups) were synchronized within a horizontal column and 21% of them (n=269 events from 39 pups) appeared widely synchronized at all 16 recordings sites. The remaining 8% (n=105 events from 28 pups) appeared very localized at only one or two recording sites.

Spindle bursts were not only synchronized within one hemisphere, but surprisingly also across both hemispheres. Spontaneous activity was recorded simultaneously in both hemispheres at the same stereotaxic coordinates and depth (**Fig. 20Bi**). However, the amount of interhemispherical synchronization (**Fig. 20Bii**) was relative low (13.1 ± 9.2 %, n=204 events in 27 pups) and increased during the first postnatal week (**Fig. 20Biii**). Whereas in P0-P1 rats, only 4.7 ± 5.7 % of all recorded spindle bursts (n=9 events in 4 pups) occurred simultaneously in both hemispheres, the degree of interhemispherical synchronization progressively increased to 18.4 ± 9 % in P6-P7 rats (n=95 events in 10 pups).

Previous *in vitro* experiments in immature rat and mouse cerebral cortex demonstrated a horizontal propagation of activity over the somatosensory cortex (Garaschuk et al., 2000;Sun and Luhmann, 2007;Yuste et al., 1995;Peinado, 2001;Dupont et al., 2006). We calculated the onset delay of spindle bursts recorded at neighboring channels and could not detect a propagation of this type of spontaneous activity *in vivo*.

Our results demonstrate that non-propagating spindle bursts intra- and interhemispherically synchronize the spontaneous activity in a 200-400 μm wide column-like neocortical network.

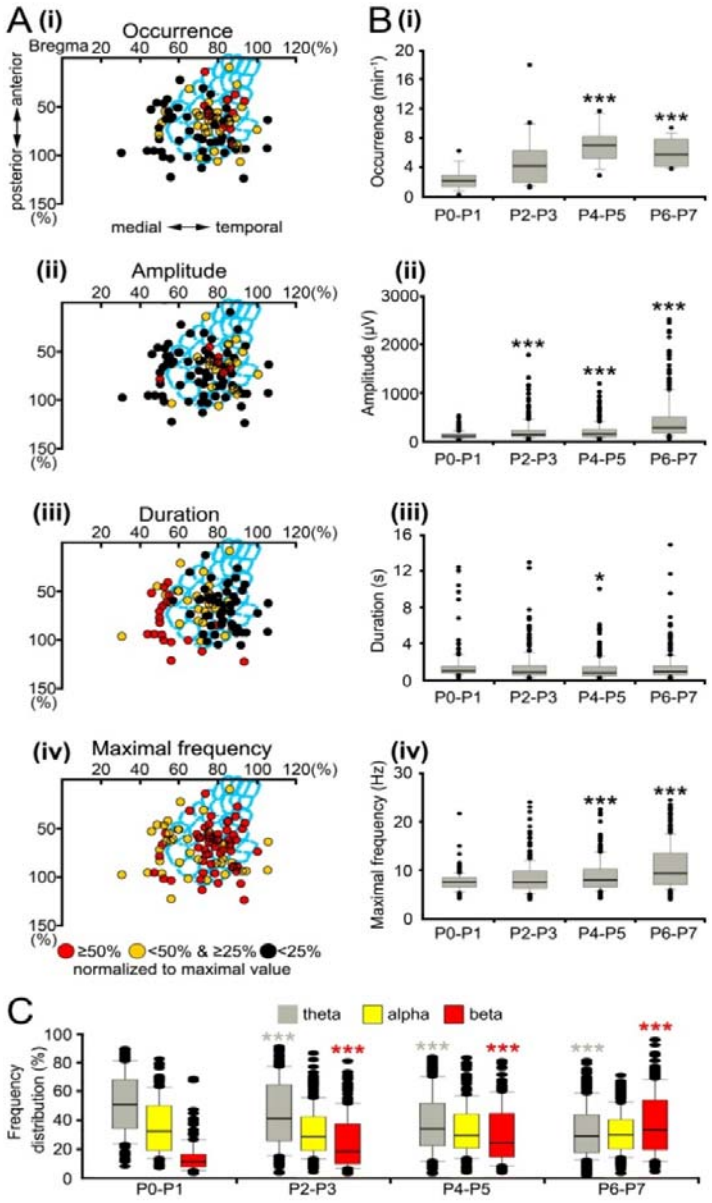

Fig. 19: Spatio-temporal properties and developmental profile of spindle burst activity in neonatal rat S1 cortex. A: Spatial distribution of spindle bursts recorded at 94 recording sites in 50 P0-P7 rats. The stereotaxic coordinates of the recording sites were determined in relationship to bregma and midline in each pup and are displayed normalized to the lateral and posterior borders (100%) of the barrel field (light-blue). The occurrence (i), amplitude (ii), duration (iii) and maximal frequency within burst (iv) of each spindle burst were normalized to the maximal value and displayed in color code. Spindle bursts recorded within the barrel field revealed a higher occurrence, larger amplitude, lower duration and higher frequency when compared to spindle bursts recorded outside the barrel field. **B:** Developmental profile of the spindle burst activity in P0 to P7 rat S1 cortex. Box plots displaying the progressive increase in the occurrence (i), amplitude (ii) and maximal frequency within burst (iv) during the first postnatal week. The average spindle burst duration reveals no major change during early development (iii). **C:** Spindle bursts gradually shift toward faster frequency bands with a relatively stable contribution of alpha activity. In B and C the values correspond to spindle bursts recorded from 10 P0-P1 pups, 16 P2-P3 pups, 12 P4-P5 pups and 12 P6-P7 pups. Data are expressed as box plots and asterisks mark significant differences in comparison to the P0-P1 group (* for $p<0.05$, ** for $p<0.01$, *** for $p<0.001$, Mann-Whitney-Wilcoxon test).

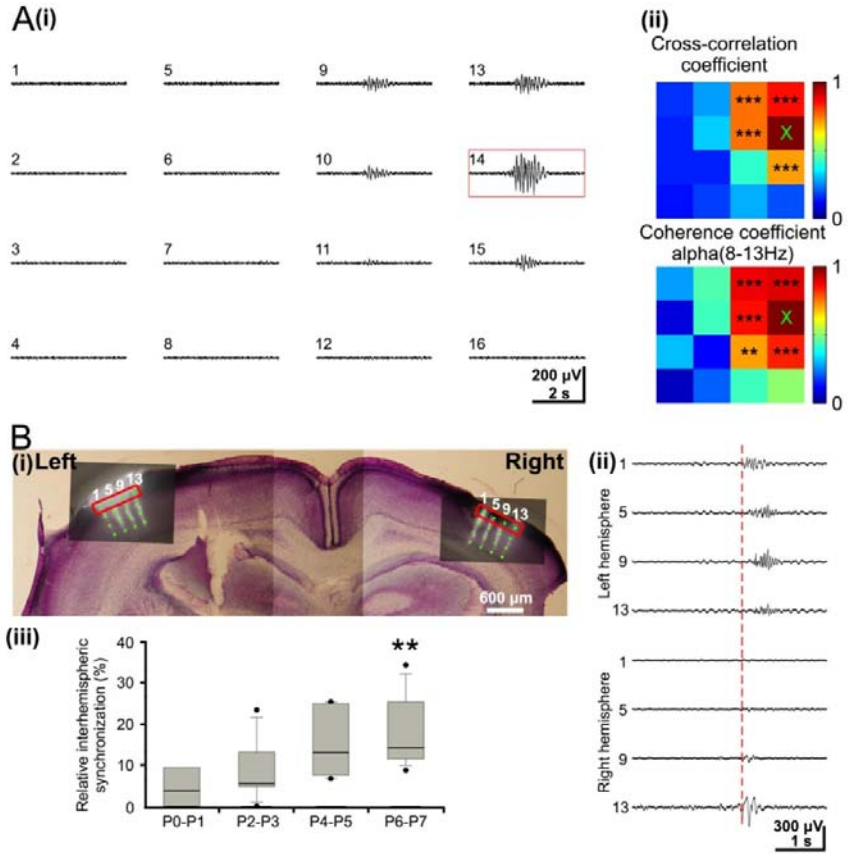

Fig. 20: Intra- and interhemispheric synchronization of spindle bursts in the neonatal rat barrel cortex. A: (i) Simultaneous field potential recordings from a P1 rat with the 4x4-channels electrode array (inter-electrode distance of 200 µm) demonstrating simultaneous spindle burst activity at multiple recording sites. (ii) Color-coded plots of maximal cross-correlation and coherence coefficients calculated for the 4x4 recordings shown in (i). Channel number 14 [red box in (i) and X in plots] was used as reference channel and the coherence was calculated for the dominant alpha frequency band. Note the columnar-like distribution of the significant cross-correlation and coherence coefficients marked by asterisks. **B:** (i) Digital photomontage of a 200 µm-thick Nissl-stained coronal slice reconstructing the position of the two DiI-covered 4x4-channels electrode arrays inserted at the same stereotaxic coordinates in both hemispheres of a P7 rat. (ii) Simultaneous field potential recordings from the upper channels of the electrode arrays [marked by red boxes in (i)]. Note synchronized spindle bursts activity at homotopic recording sites in both hemispheres (channel 1 left vs. channel 13 right hemisphere). The red dotted line marks the onset of interhemispheric spindle bursts. (iii) Age-dependent increase in interhemispheric synchronization of spindle burst activity from P0 to P7 in rat barrel cortex. Box plot displaying the relative amount of spindle bursts occurring simultaneously on both hemispheres in relationship to the total amount of spindle bursts. The displayed values were obtained in 4 P0-P1 pups, 7 P2-P3 pups, 6 P4-P5 pups and 10 P6-P7 pups.

3.1.3 Fast gamma oscillations are mainly confined to the barrel cortex where they locally synchronize developing neuronal networks

Gamma oscillations significantly differed in their spatio-temporal organization from spindle bursts (data above and **Fig. 14**). In contrast to the ubiquitary distribution of spindle bursts in the entire S1 cortex, gamma oscillations were confined to a cortical

region corresponding to the barrel field (**Fig. 21A**). Gamma oscillations could be recorded at 48 out of 64 stereotaxic coordinates located within the barrel cortex, but at only 6 out of 30 coordinates outside the barrel field. However, gamma oscillations recorded within the barrel field were relatively uniform in their occurrence (**Fig. 21Ai**), amplitude (**Fig. 21Aii**), duration (**Fig. 21Aiii**) and frequency (**Fig. 21Aiv**). Similar to spindle bursts, gamma oscillations also revealed age-dependent alterations during the first postnatal week. Their occurrence significantly ($p<0.01$) increased from 1.9 ± 1.6 oscillations/min (n=5 pups) at P0-P1 to 6.9 ± 3.4 oscillations/min (n=11 pups) at P6-P7 (**Fig. 21Bi**). Furthermore, the amplitude of gamma oscillations also significantly ($p<0.001$) increased from 95 ± 79 μV (n=43 events from 5 pups) at P0-P1 to 154.8 ± 150.2 μV (n=190 events from 11 pups) at P6-P7 (**Fig. 21Bii**). Their duration significantly ($p<0.001$) increased from 0.13 ± 0.04 s (n=43) at P0-P1 to 0.3 ± 0.2 s (n=190) at the end of the first postnatal week (**Fig. 21Biii**). In contrast, the average maximal frequency of gamma oscillations remained almost unchanged from P0 to P7 (**Fig. 21Biv**).

The cross-correlation and coherence analyses of gamma oscillations recorded with the 4x4 electrode array revealed a rather local organization and synchronization of this activity pattern in the barrel cortex. The majority of gamma oscillations (74.9% of 962 events from 32 pups) were restricted to one or two and seldom to three recording sites (**Fig. 22Ai**). The gamma activity was highly synchronized at these neighboring recording sites as illustrated in the cross-correlation plot (**Fig. 22Aii**). Synchronized gamma oscillations were restricted to a local neuronal network of about 200 μm in diameter. A small number of gamma oscillations (6.2 ± 6.9 %, n=66 events in 20 pups) revealed a synchronization between both hemispheres (**Fig. 22B**). The degree of interhemispherical synchronization increased with age from 2.6 ± 4.7 % at P0-P2 (n=6 in 5 pups) to 10.9 ± 9.2 % at P6-P7 (n=41 in 7 pups). However, these developmental changes were not significant at the $p<0.05$ level (**Fig. 22C**). Furthermore, we never observed propagation of gamma oscillations over S1.

These data indicate that local neuronal networks in the developing barrel field of S1 are highly synchronized by spontaneous oscillatory gamma activity.

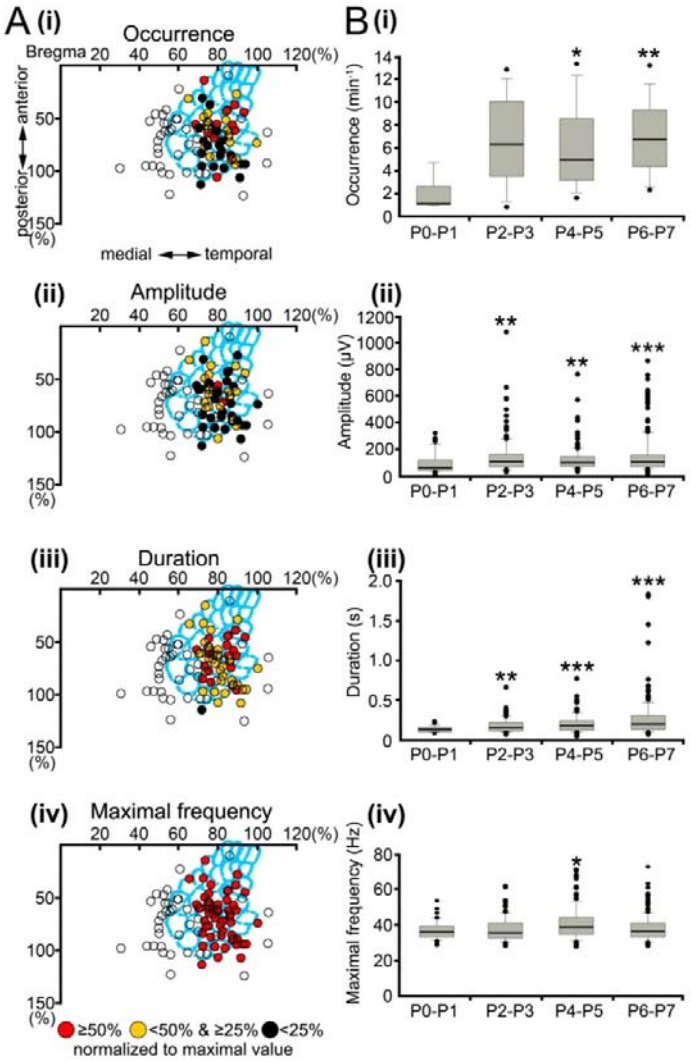

Fig. 21: Spatio-temporal properties and developmental profile of gamma oscillations. A: Spatial distribution of gamma activity recorded at 54 recording sites in 32 newborn rats. Note that gamma oscillations are mainly restricted to the cortical region corresponding to the barrel field in S1. Open circles correspond to stereotaxic coordinates where gamma oscillations could not be recorded. **B:** Developmental profile of the gamma oscillations in P0 to P7 rat S1 cortex. Box plots illustrate age-dependent alterations in the occurrence (i), amplitude (ii), duration (iii) and maximal frequency (iv) during the first postnatal week. The displayed values correspond to gamma oscillations recorded in 5 P0-P1 pups, 8 P2-P3 pups, 8 P4-P5 pups and 11 P6-P7 pups. For further details see Fig. 19.

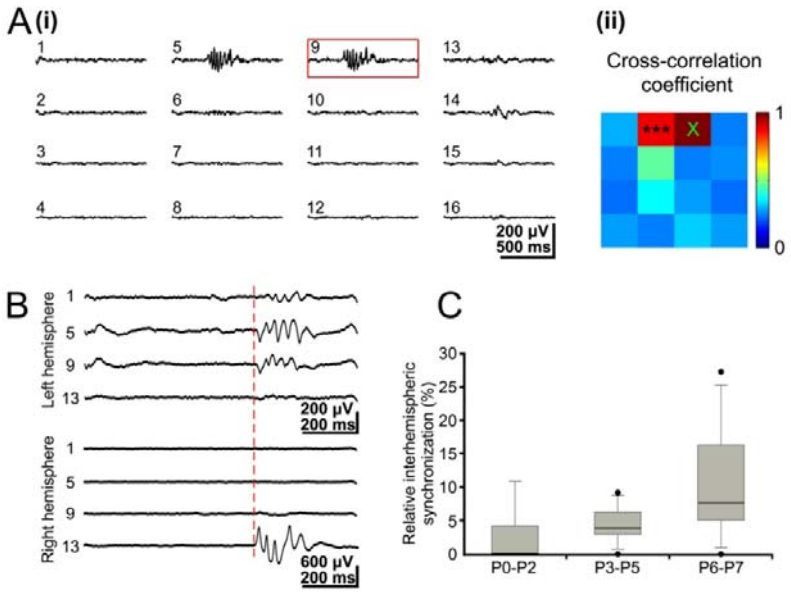

Fig. 22: Intra- and interhemispheric synchronization of gamma oscillations. A: (i) Simultaneous field potential recordings in a P3 rat somatosensory cortex showing gamma oscillations at a few recording sites. (ii) Color-coded plot of maximal cross-correlation coefficients calculated for the 16 recordings shown in (i) with channel 9 as a reference channel [red box in (i)]. Note spatial restriction of synchronized gamma activity to only 2 recording sites. **B:** Simultaneous gamma oscillations recorded at homotopic sites in left and right hemispheres in a P3 rat. The red dotted line marks the onset of synchronized interhemispheric gamma oscillations. **C:** Incidence of interhemispheric gamma synchronization during the first postnatal week. The values correspond to gamma oscillations recorded in 5 P0-P2 pups, 8 P3-P5 pups, and 7 P6-P7 pups.

3.1.4 Propagating long oscillations synchronize spontaneous activity over wide cortical regions

In contrast to spindle bursts and gamma oscillations, long oscillations propagated over wide cortical regions and thus could be recorded in the entire S1 cortex. Our data indicate that long oscillations, similar as spindle bursts, are not a specific activity pattern of the developing barrel field, but rather of the whole somatosensory or even entire cerebral cortex. Their occurrence (barrel field: 0.04 ± 0.02 oscillations/min, n=14 stereotaxic coordinates; non-barrel field: 0.05 ± 0.02 oscillations/min, n=10 stereotaxic coordinates) (**Fig. 23Ai**), amplitude (barrel field: 533.9 ± 350.6 µV, n=14; non-barrel field: 407.4 ± 311.9 µV, n=10) (**Fig. 23Aii**), duration (barrel field: 49.2 ± 13.9 s, n=14; non-barrel field: 56.4 ± 21.2 s, n=10) (**Fig. 23Aiii**) and mean maximal frequency within oscillation (barrel field: 11.8 ± 6 Hz, n=14; non-barrel field: 13 ± 6.9 Hz, n=10) (**Fig.**

23Aiv) showed no significant differences when analyzed separately for the barrel field and the remaining part of S1 cortex.

As the other spontaneous activity patterns, long oscillations also revealed significant age-dependent alterations during the first postnatal week (**Fig. 23B**). Their occurrence increased progressively ($p<0.01$) from 0.03 ± 0.015 oscillations/min (n=6 pups) at P0-P1 to 0.06 ± 0.002 oscillations/min at P6-P7 (n=4 pups) (**Fig. 23Bi**). Similarly, the maximal amplitude of long oscillations significantly ($p<0.001$) increased from 190.5 ± 142.4 µV (n=9 events from 6 pups) at P0-P1 to 586.7 ± 302.7 µV (n=16 events from 4 pups) at P6-P7 (**Fig. 23Bii**) and their frequency also increased significantly ($p<0.001$) during the first postnatal week (P0-P1: 6.5 ± 1.4 Hz, n=9; P6-P7: 21.7 ± 4.7 Hz, n=16) (**Fig. 23Biv**). Only the duration of long oscillations remained relatively constant between P0 and P7 (**Fig. 23Biii**).

Long oscillations also differed from spindle bursts and gamma oscillations in their synchronization pattern. The majority of long oscillations (76.5% of 51 events from 20 pups) occurred simultaneously at all recoding sites (**Fig. 24Ai**). The synchronization of neuronal activity over a large cortical area (~600-800 µm) was demonstrated by the high cross-correlation as well as coherence coefficients that were calculated for a large fraction of the recording channels (**Fig. 24Aii**). Long oscillations were also characterized by their propagation pattern (**Fig. 24B**). A medio-temporal spread of long oscillatory activity with an average speed of 25.1 ± 16.4 µm/s could be observed in 11 out of 39 events (28.2%) and 35.9% of the long oscillations propagated in the temporo-medial direction at 28.1 ± 10 µm/s (**Fig. 24B**). The remaining 35.9% of the long oscillations did not propagate but occurred highly synchronized at all recording sites.

These results indicate that long oscillations are a distinct propagating pattern of activity that synchronizes the developing neocortical network over large distances.

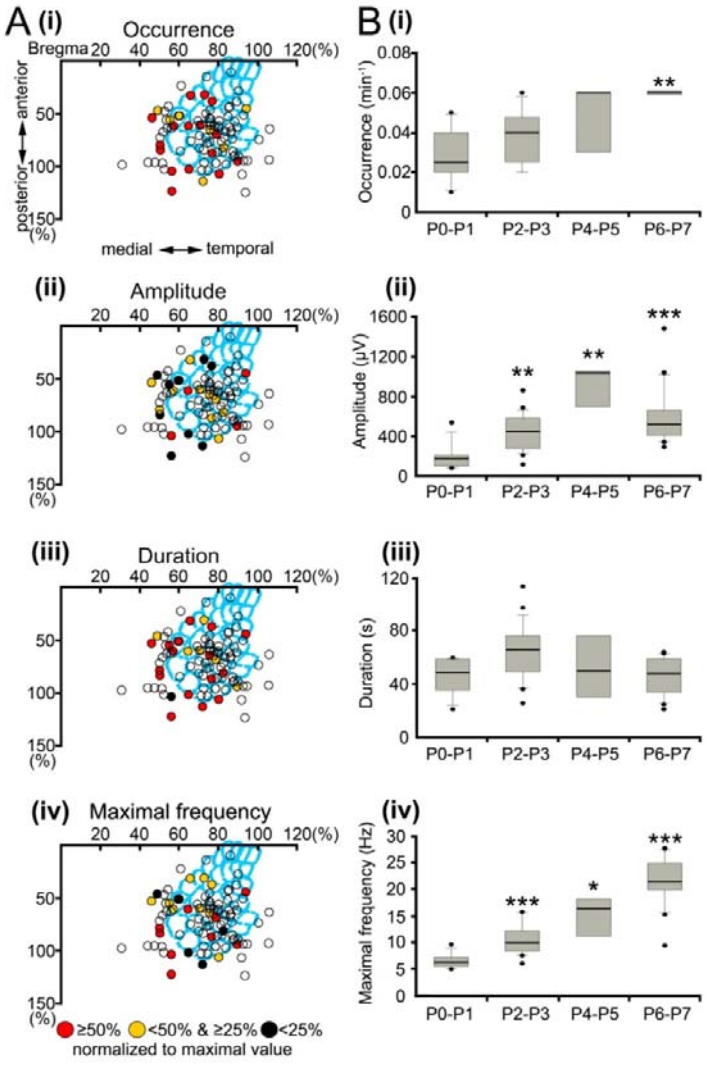

Fig. 23: Spatio-temporal properties and developmental profile of long oscillations. A: Spatial distribution of long oscillations recorded at 26 recording sites in 20 newborn rats. Note the relatively low incidence of long oscillations in the barrel field. **B:** Developmental profile of long oscillations in P0 to P7 rat S1 cortex. Box plots illustrate age-dependent alterations in the occurrence (i), amplitude (ii), duration (iii) and maximal frequency (iv) during the first postnatal week. Long oscillations reveal a significant increase in frequency during the first postnatal week. The values correspond to long oscillations recorded in 6 P0-P1 pups, 7 P2-P3 pups, 3 P4-P5 pups and 4 P6-P7 pups. For further details see Fig. 19.

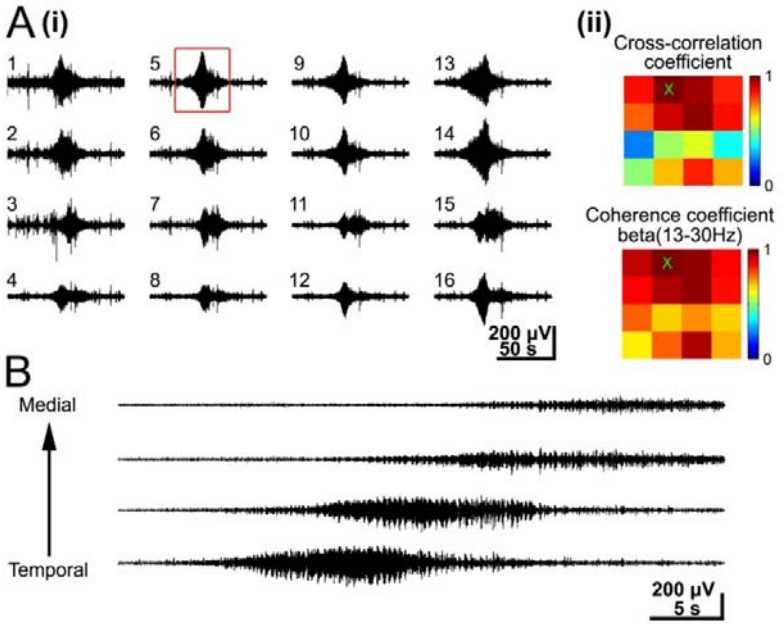

Fig. 24: Synchronization and horizontal propagation of long oscillations. A: (i) Simultaneous recordings of long oscillations in the barrel cortex of a P6 rat. Note prominent expression of long oscillations at all recording sites. (ii) Color-coded plot of maximal cross-correlation and coherence coefficients calculated for the 16 recordings shown in (i) using channel 5 [red box in (i), X in (ii)] as a reference channel. The coherence was calculated for the dominant beta frequency band. Note the wide-spread synchronization of long oscillations as indicated by the large number of recording sites with high cross-correlation and coherence coefficients. **B:** Simultaneous recordings of long oscillations at four recording sites located at the same cortical depth in the barrel field of a P6 rat.

3.1.5 All three patterns of cortical synchronized oscillations can be elicited by activation of the sensory input

Activation of the periphery has been previously reported to trigger network oscillations in the primary visual (Hanganu et al., 2006) and somatosensory cortex (Khazipov et al., 2004) of newborn rats. In order to address the question whether the three different activity patterns can be also elicited by activation of the peripheral sensory input, field potentials were recorded with the 4x4 electrode array in the barrel cortex after stimulation of all whiskers either by tactile stimulation or by electrical stimulation of the entire whisker pad (**Fig. 25Ai**). Electrical stimulation using a bipolar electrode elicited in 10 out of 10 pups in the contralateral barrel cortex a robust initial cortical response with a delay of 40.3 ± 11.2 ms and an average amplitude of 536.8 ± 435.1 µV (n=137 events in 10 pups) (**Fig. 25Aii, iii**). In contrast, stimulation of the whisker pad evoked in the ipsilateral barrel field a very small response in one rat and no response in 9 pups. In 88% of the 140 recordings the direct response in the contralateral barrel cortex was often followed by a late oscillatory component. Both, spindle bursts (**Fig. 25Aii**) as well as

gamma oscillations (**Fig. 25Aiii**) could be evoked by whisker stimulation in 87.5 ± 11.8 % (n=125 events in 10 pups) and 62.3 ± 21.4 % (n=44 events in 5 pups) of the experiments, respectively. The evoked spindle bursts started 228.4 ± 145 ms after stimulation and showed similar properties (average maximal frequency 9.9 ± 4 Hz, amplitude 670 ± 490.2 μV; n=125 in 10 pups) as the spontaneous spindle bursts. Their occurrence was strongly correlated with the MUA (mean cross-correlation coefficient 0.53 ± 0.2, n=9 pups) (**Fig. 25Aii**) and their synchronization pattern reflected the columnar organization as described for the spontaneous spindle bursts (**Fig. 25Bi**). Similar results could be obtained for the stimulus-evoked gamma oscillations. They started 410.5 ± 347.7 ms after stimulation and their average maximal frequency (38.2 ± 7.2 Hz, n=44 in 5 pups) and amplitude (557.7 ± 608.7 μV, n=44 in 5 pups) were similar to those of the spontaneous gamma events. Furthermore, the evoked gamma oscillations strongly correlated with the MUA as shown by the cross-correlation analyses (mean cross-correlation coefficient 0.77 ± 0.04, n=5 pups) and synchronized rather small local networks of about 200 μm in diameter (**Fig. 25Bii**). Beside electrical stimulation, tactile stimulation of all whiskers evoked in a very similar manner spindle bursts and gamma oscillations in 82.7 ± 19 % (n=92 from 111 trials) and 77.1 ± 21.4 % (n=55 from 71 trials) of the experiments, respectively. Although this multi whisker stimulation protocol elicited large-scale activity in the barrel cortex, the oscillatory patterns were again locally synchronized in 200-400 μm wide column-like networks (**Fig. 26**).

Although spindle bursts and gamma oscillations could be elicited by single electrical stimulation of the whisker pad, this protocol failed to evoke long oscillations in all investigated animals (n=10). However, long oscillations could be evoked by repetitive tactile stimulation of all whiskers (10 or 11 times at ~1 Hz) in 4 out of 6 pups (**Fig. 25C**). These evoked long oscillations started at 14.7 ± 10.3 s after the last tactile stimulus, lasted 52 ± 4.3 s and showed a mean amplitude of 447.7 ± 210.3 μV and an averaged maximal frequency of 17.6 ± 5.1 Hz (n=4 events in 4 pups).

The relative contribution of the sensory input to the generation of neocortical oscillatory activity patterns was also investigated by silencing the sensory periphery. A temporal peripheral deafferentiation of the whiskers was induced by injecting 2% lidocaine subcutaneously into the face just adjacent to the whisker pad as described previously (Krupa et al., 1999;Shaw and Liao, 2005). The activity persisted after lidocaine injection, but the occurrence of spindle bursts (control 10.7 ± 3.3 bursts/min,

lidocaine 4.8 ± 3.6 bursts/min, $p<0.01$, n=6 pups) and gamma oscillations (control 8.9 ± 3.3 oscillations/min, lidocaine 4 ± 2.7 oscillations/min, $p<0.05$, n=6 pups) significantly decreased in the contralateral barrel cortex (**Fig. 25D**). The amplitude of spindle bursts (control 344.1 ± 273.8 μV, n=60 events from 6 pups; lidocaine 321.6 ± 191.5 μV, n=44 events from 6 pups) and gamma oscillations (control 164.2 ± 120 μV, n=60 events from 6 pups; lidocaine 154.4 ± 81.1 μV, n=51 events from 6 pups) were not affected by the functional deafferentiation. Similarly, lidocaine did not affect the frequency of contralateral spindle bursts (control 8.4 ± 3.4 Hz, n=60, lidocaine 7.6 ± 2.6 Hz, n=44) and gamma oscillations (control 38.3 ± 7 Hz, n=60, lidocaine 38 ± 6.3 μV, n=51). Only the duration of spindle bursts decreased significantly ($p<0.05$) from 1.1 ± 1.5 s (n=60) to 0.75 ± 1.1 s (n=44) after lidocaine injection, whereas the short duration of gamma oscillations remained unchanged (control 0.23 ± 0.16 s, n=60, lidocaine 0.19 ± 0.12 s, n=51). Furthermore, the properties of spindle bursts and gamma oscillations in the ipsilateral barrel cortex remained unaffected after lidocaine injection (**Fig. 25D**). The low occurrence of long oscillations (approx. 1 per 20 min) circumvented a reliable conclusion whether functional deafferentiation affected also this activity pattern.

Summarizing, these results indicate that whisker activation can trigger both neonatal spindle bursts and gamma oscillations. The large amount of oscillatory activity persisting after functional deafferentiation indicates that the peripheral sensory input is clearly not the only mechanism to trigger these activity patterns.

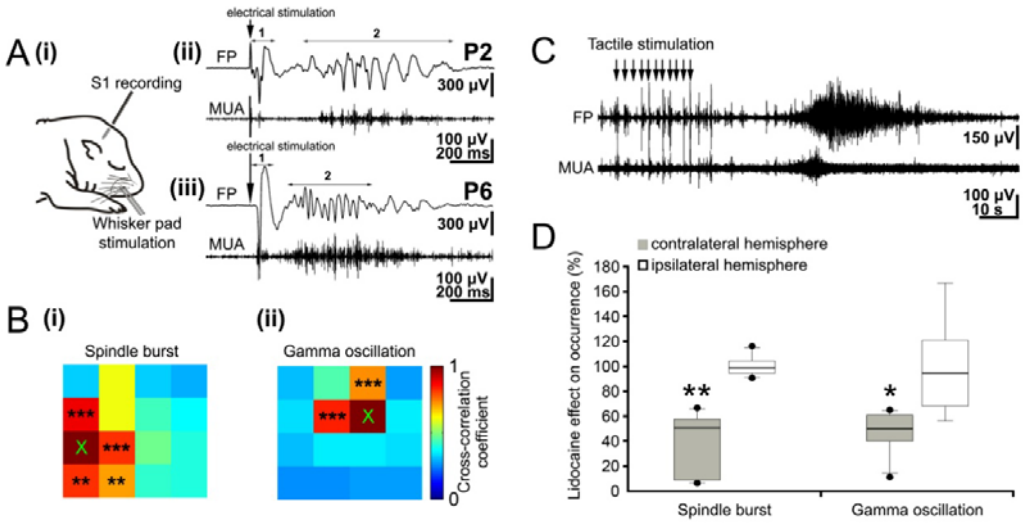

Fig. 25: Stimulation of the periphery evokes neocortical oscillatory activity patterns. A: (i) Scheme of experimental paradigm allowing electrical stimulation of the whisker pad and simultaneous recording of the field potential and MUA in the contraleral barrel cortex. (ii) Field potential (top) and MUA (below) recordings of the contralateral S1 response to a single electrical stimulus of the whisker pad in a P2 rat. The robust direct response (1) is followed by a spindle burst (2) correlated with prominent MUA. (iii) Field potential (top) and MUA (below) recordings of the contralateral S1 cortical response to electrical stimulation of the whisker pad in a P6 rat. The direct response (1) is followed by a gamma oscillation (2) correlated with MUA. **B:** Color-coded plot of maximal cross-correlation coefficients calculated for spindle bursts (i) and gamma oscillations (ii) elicited by electrical stimulation of the whisker pad. Asterisks indicate significant cross-correlation coefficients in comparison to the reference channel marked by X. **C:** Field potential (top) and MUA (below) recordings of the contralateral S1 cortical response to repetitive tactile stimulation of the whiskers (11 time at ~1 Hz) in a P6 rat. Repetitive stimulation of the sensory input elicits a robust long oscillation correlated with MUA. **D:** Effects of transient peripheral deafferentiation by injection of lidocaine into the whisker pad on spontaneous spindle bursts and gamma oscillations. Box plots display the relative occurrence of spindle bursts (left) and gamma oscillations (right) recorded in 6 pups in the contralateral (black bars) and ipsilateral (white bars) barrel cortex after lidocaine injection.

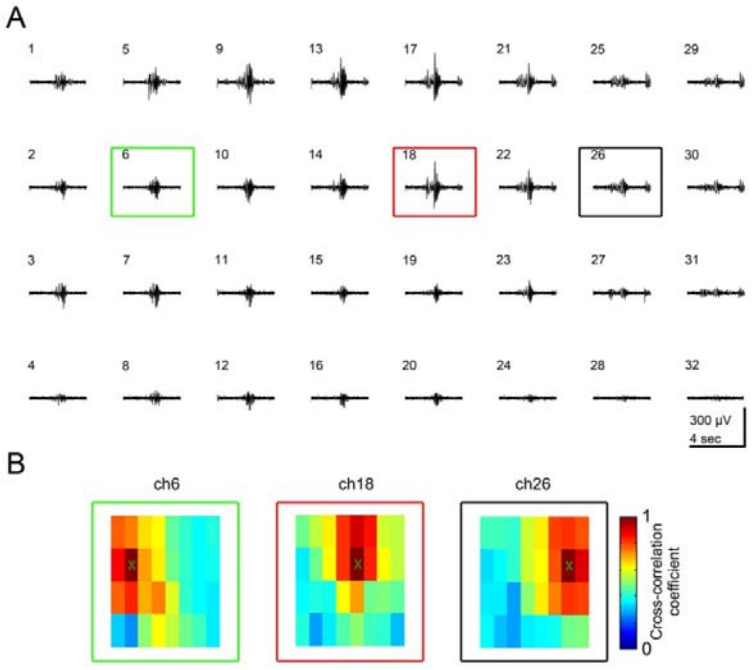

Fig. 26: Stimulation of all whiskers with a brush elicits large-scale oscillatory activity in the contralateral S1 cortex of a P7 rat. A: Simultaneous field potential recordings with an 8-shank 32-channel Michigan electrode (inter-electrode distance 200 µm). **B:** Cross-correlation plots using channel 6, 18 or 26 as reference. Note that spindle bursts activity is locally synchronized in a columnar manner of 200-400 µm in diameter.

3.1.6 Neocortical circuitry and pharmacological profile

The neocortical network underlying the spindle burst activity was studied by the use of a 1-shank 16-channel electrode covering the entire cortical depth of P0-1 pups (**Fig. 27**). Field potentials (left traces in **Fig. 27**), corresponding current source density analyses (CSD, middle traces) and averaged CSD plots (right traces) demonstrated two different depth profiles. In 61% of the 215 recorded spindle bursts, the CSD profile and the MUA revealed a clear participation of the subplate with a clear sink located in the subplate and the corresponding source in the cortical plate above (averaged CSD in **Fig. 27A**). These results support our previous *in vitro* observations that the subplate plays an important role in the generation of oscillatory network activity in the newborn rat neocortex (Dupont et al., 2006). Further support for this hypothesis comes from our analyses of the field potential recordings in the cortical plate and simultaneous recordings of the MUA in the subplate. These experiments demonstrated that the MUA in the subplate preceded the negative peaks of each oscillatory cycle in the spindle bursts on average by 13.8 ± 14.3 ms (n=128 cycles from 80 spindle bursts recorded in 6 pups) (**Fig. 30A**). These data are

also in good agreement with previous structural and functional observations in newborn rat cerebral cortex by Molnár et al., demonstrating an early innervation of the subplate by thalamocortical afferents (Molnar et al., 1998;Molnar et al., 2003). Our present report shows the contribution of the thalamic input for the generation of cortical spindle bursts. A different depth profile could be observed in the remaining spindle burst recordings. In 39% of the 215 spindle bursts, the activity was restricted to the upper cortical layers without any detectable participation of the subplate (**Fig. 27B**). These data indicate that local neuronal networks in the cortical plate and layers V/VI are also capable to generate spindle burst activity as we have previously demonstrated with the multi-electrode array technology (MEA chip) in 1000 µm thick neocortical slices from newborn mice (Sun and Luhmann, 2007). Local non-propagating spontaneous oscillations with an average frequency of 15.6 Hz and duration of 1.7 s were localized in the cortical plate and synchronized the activity in a ~200 µm wide column-like network (Sun and Luhmann, 2007).

CSD analyses were also used to study the neocortical circuitry underlying the gamma oscillations (**Fig. 28**) and the long oscillations (**Fig. 29**). In 70% of the 86 recorded gamma oscillations, the CSD profile demonstrated a sink in the subplate and the corresponding source in the cortical plate above (averaged CSD in **Fig. 28A**). In the remaining 30% of the gamma oscillations, the activity was restricted to the upper cortical layers (**Fig. 28B**). The MUA in the subplate also preceded the negative peaks of each oscillatory cycle in the gamma oscillation by 4.3 ± 4.7 ms (n=32 cycles from 19 gamma oscillations) (**Fig. 30B**), indicating that the subplate also participates in the generation of gamma oscillations in the newborn rat cerebral cortex. Finally, CSD analyses were also used to study the circuitry underlying the generation of the long oscillations (**Fig. 29**). The CSD profiles calculated from 3 long oscillations revealed in two cases a clear participation of the subplate with a clear sink located in the subplate and the corresponding source in the cortical plate above (averaged CSD in **Fig. 29A**) and in one case oscillatory activity mostly restricted to the upper cortical layers (**Fig. 29B**).

The mechanisms underlying the early network oscillations were further assessed by pharmacological manipulation of chemical and electrical synaptic transmission within S1 of the P0-P2 rat *in vivo*. We focused on the pharmacological profile of spindle bursts (**Fig. 31A**) and gamma oscillations (**Fig. 31B**), since the very rare occurrence of long oscillations precluded a reliable investigation of their pharmacological properties. Drugs

were applied on the surface of the cerebral cortex near the recording site. Control experiments with application of the vehicle (200 nl ACSF) without any drug did not cause any alterations in the spindle burst (n=17 animals) or gamma oscillation pattern (n=9), demonstrated that this application procedure by itself did not cause any changes in the neuronal network activity. In contrast, application of the NMDA receptor antagonist APV (100 μM, 200 nl) on the cortical surface caused a significant decrease in the occurrence of spindle bursts to 56.4 ± 17.8 % (n=12 pups; $p<0.001$) and of gamma oscillations to 36.1 ± 27.3 % (n=6; $p<0.01$). Blockade of gap junctional coupling by application of carbenoxolone (100 μM, 200 nl) significantly reduced the occurrence of spindle bursts to 57.5 ± 29.9 % (n=8 pups; $p<0.001$), and of gamma oscillations to 48.4 ± 17.1 % (n=6; $n<0.01$). To address the question whether a drug applied on the cortical surface actually reaches the underlying neocortical network, 2% lidocaine (200 nl) was applied in an identical manner on the surface of the cortex near the recording electrode. Spindles bursts and gamma oscillations were inhibited by lidocaine in their occurrence to 11.5 ± 10.6 % and 1.6 ± 4.6 %, respectively (**Fig. 31**), indicating that this method allows pharmacological intervention in the developing rat cerebral cortex.

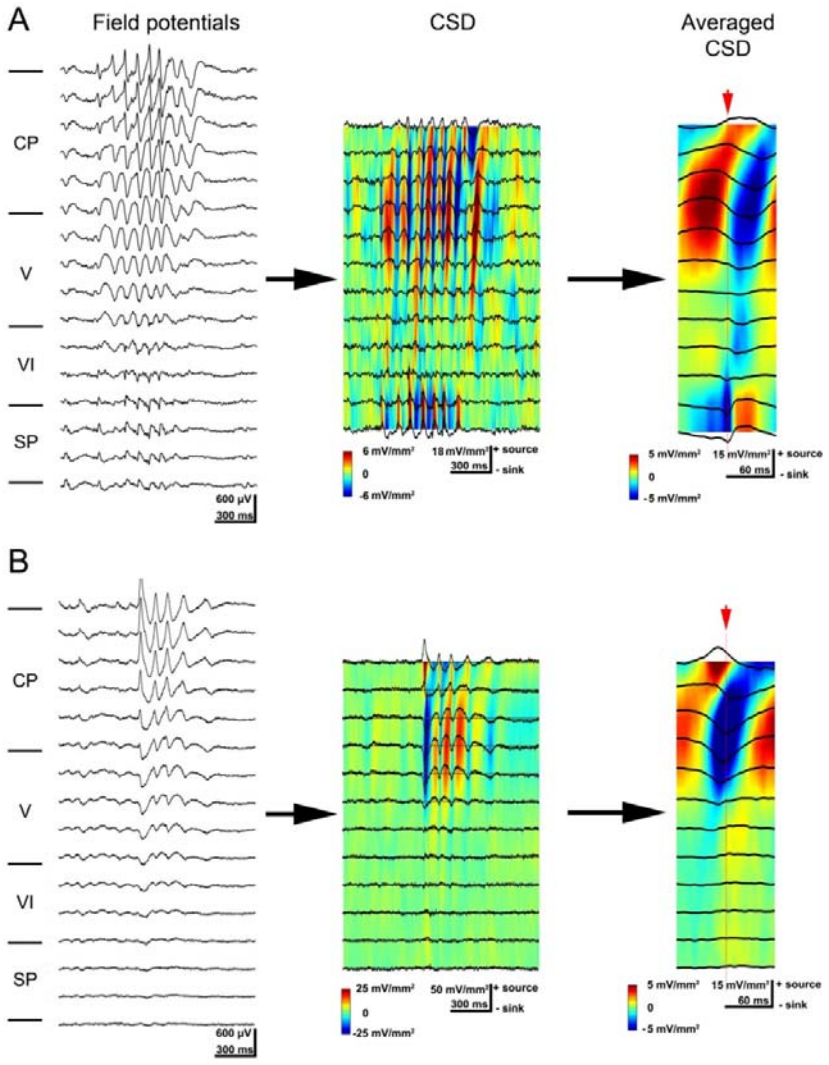

Fig. 27: Depth profile of spindle burst activity in the barrel cortex of a P0 rat. A: Simultaneous field potential recordings in the barrel cortex of a P0 rat with 16-channel one shank Michigan electrode (inter-electrode-distance 50 µm) (left traces) and corresponding CSD analysis (middle). The averaged CSD plot (right) was calculated from 54 troughs of 10 spindle bursts. Note prominent sink in subplate / layer VI and corresponding source in cortical plate. **B:** Another spindle burst recording from the same animal as in A, but with no activity and no sink in the subplate. The averaged CSD plot was calculated from 19 troughs of 5 spindle bursts.

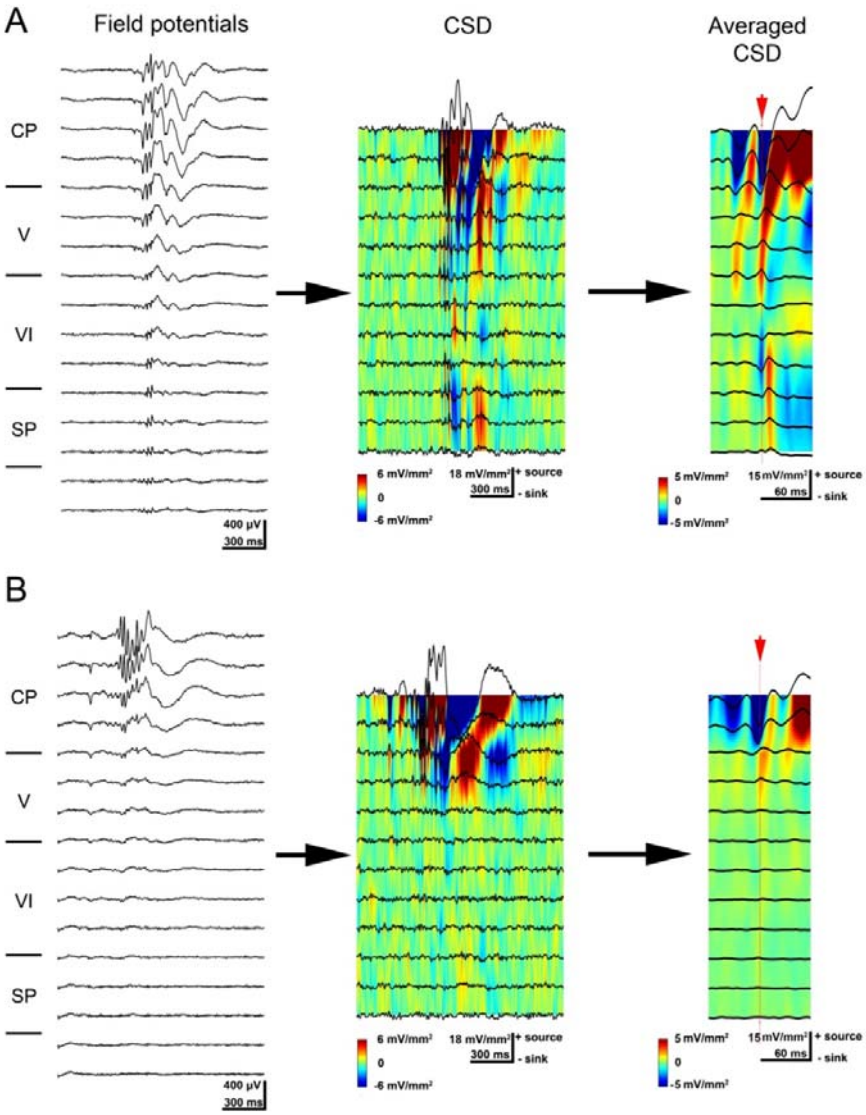

Fig. 28: Depth profile of gamma oscillation activity recorded in the barrel cortex of a P1 rat. A: Simultaneous field potential recordings (left) and corresponding CSD analysis (middle). The averaged CSD plot (right) was calculated from 27 troughs of 13 gamma oscillations. Note prominent sink in subplate / layer VI and corresponding source in cortical plate. **B:** Another gamma oscillation recorded in the same animal as in A, but with no activity and no sink in the subplate. The averaged CSD plot was calculated from 33 troughs of 9 gamma oscillations. For further details see Fig. 27.

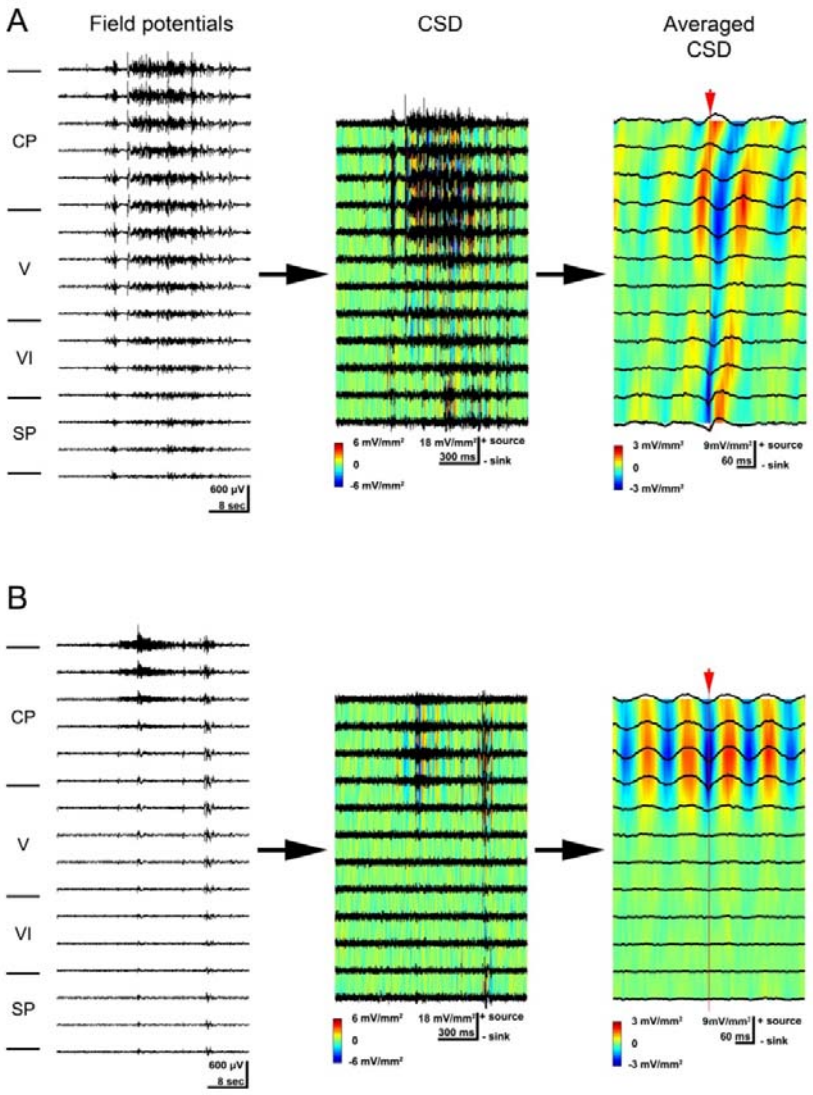

Fig. 29: Depth profile of long oscillation recorded in the barrel cortex of a P0 rat. A: Simultaneous field potential recordings (left) and corresponding CSD analysis (middle). The averaged CSD plot (right) was calculated from 43 troughs of one long oscillation. Note prominent sink in subplate / layer VI and corresponding source in cortical plate. **B:** Another long oscillation recorded in the same animal as in A, but with no activity and no sink in the subplate. The averaged CSD plot was calculated from 50 troughs of one long oscillation. For further details see Fig. 27.

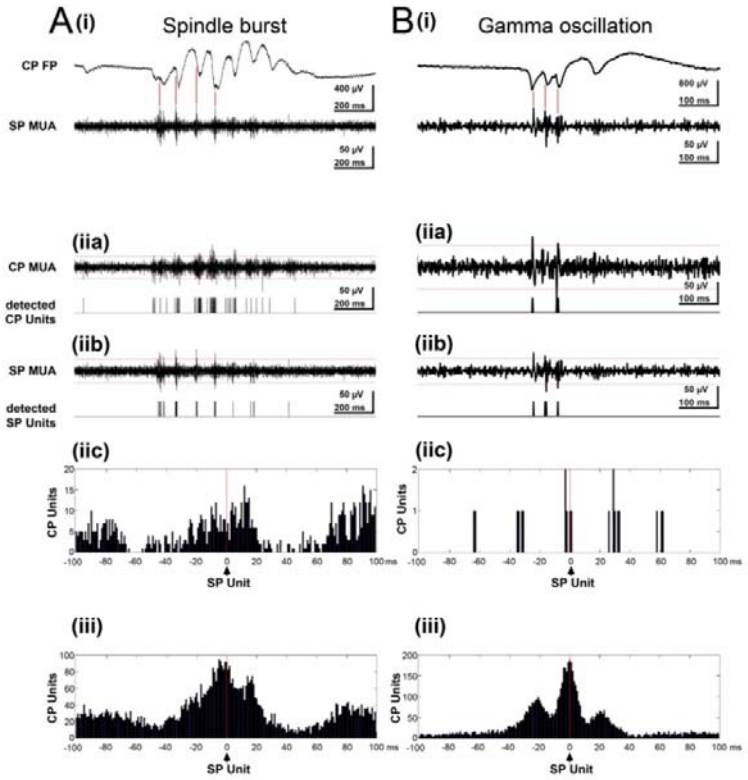

Fig. 30: MUA in subplate precedes the oscillatory activity in upper cortical layers. A: Simultaneous recording of spindle burst activity in cortical plate (upper trace) and MUA in subplate (lower trace) of a P1 rat. Red lines mark peaks of MUA in the subplate. Note that MUA precedes the troughs of the field potential oscillation. **B:** Simultaneous recording of a gamma oscillation in cortical plate (upper trace) and MUA in subplate (lower trace) of a P1 rat.

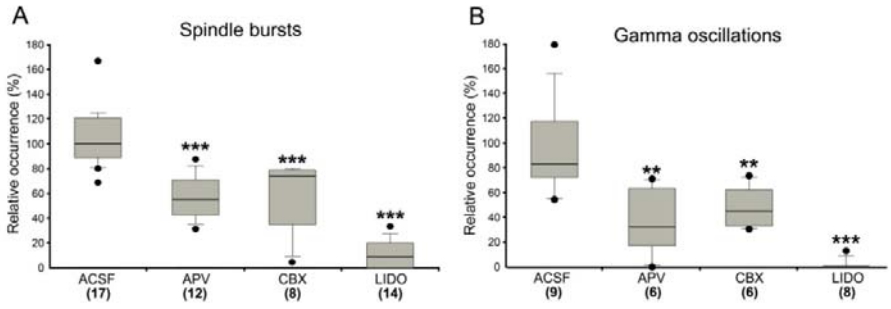

Fig. 31: Pharmacological profile of spindle bursts (A) and gamma oscillations (B) in the P0-P2 rat S1 in vivo. Control data were obtained before drug application on the cortical surface (for details see *Materials and Methods*). Recordings in ACSF without drug or in ACSF containing APV, carbenoxolone (CBX) or lidocaine (LIDO) were obtained 3 min after the beginning of ACSF or drug application. Data were normalized to the occurrence of oscillatory events during 3 min before cortical ACSF or drug application. Data are expressed as box plots and asterisks mark significant differences in comparison to the ACSF group (** for $p<0.01$, *** for $p<0.001$, Mann-Whitney-Wilcoxon test). Numbers in parentheses give number of newborn rats studied.

3.2 Project2

3.2.1 Evoked and spontaneous activity shows a columnar organization in the newborn rat barrel cortex in vivo

The cortical response to defined mechanical stimulation of a single whisker was analyzed by voltage-sensitive dye imaging (VSDI) in the barrel cortex of 39 P0-P7 rats in vivo (**Fig. 32A**). At all ages studied selective stimulation of the C2 whisker evoked in the barrel cortex of the contralateral hemisphere a reliable response, which allowed the unequivocal identification of the cortical C2 whisker representation (**Fig. 32B-D**). The cortical responses to C2 whisker stimulation revealed significant age-dependent differences in their spatial extent, onset latency and duration. In P0 rats (n=7), the evoked cortical response was highly localized and revealed an average area of 0.097 ± 0.020 mm^2. The area of the cortical response did not change significantly until P5 (n=3), when C2 whisker stimulation elicited a response of 0.197 ± 0.049 mm^2 in average size (**Fig. 32E**). In P6 animals (n=4), the maximal evoked cortical response often propagated from the initially activated barrel related column to surrounding columns, and in P7 rats (n=6) the evoked area increased dramatically to 1.786 ± 0.430 mm^2 ($p<0.01$ in comparison to the P0 age group). The onset latency of the cortical response decreased significantly ($p<0.01$) from 89.9 ± 8.6 ms at P0 to 35.3 ± 2.8 ms at P7 (**Fig. 32F**). The response duration at half-maximal amplitude varied from ~240 to ~300 ms in P0-P6 and was significantly ($p< 0.05$) shorter in P7 rats only (173 ± 26.4 ms) (**Fig. 32G**).

These results demonstrate that (i) afferent sensory stimulation elicits reliable cortical responses as early as P0, (ii) that the temporal precision of these cortical responses increases with age and (iii) that the spread of the evoked cortical response to neighboring barrel-related columns increases at the end of the first postnatal week.

Next we studied with VSDI the spatio-temporal properties of spontaneous cortical activity *in vivo* and compared P0-P1 rats with P6-P7 animals, since these age groups showed the most significant differences in the evoked cortical activity patterns. In P0-P1 rats, spontaneous events occurred every 4.9 ± 1.7 s, revealed an average duration at half-maximal amplitude of 247.6 ± 6.4 ms and covered a cortical area of 0.135 ± 0.007 mm^2 (n= 317 events recorded in 5 P0-P1 rats), demonstrating that spontaneous events reveal very similar properties as the whisker evoked activity. When these spontaneous events were superimposed on the predicted barrel field map of each individual animal, it became

evident that (i) 76% of all spontaneous events (241 of 317 events recorded in 5 P0-P1 rats) were located in the barrel field and (ii) that the large majority of these spontaneous events were restricted to a small cortical region of 200 to 400 μm in diameter, which resembled in its localization and dimension a single whisker-defined barrel (**Fig. 33A1-4**). Since discrete cortical barrels cannot be demonstrated with histological or immunocytochemical methods before P3 (Erzurumlu and Jhaveri, 1990), we refer to these early neuronal networks as functional pre-barrel related columns or pre-columns. In P0-P1 rats (n=14), 70-80% of the spontaneous events were localized in 1 or 2 pre-barrel related columns and about 20% in 3 to 6 pre-columns (**Fig. 33A4-6, C**). In this age group the spontaneous activity only rarely covered an area of >6 pre-barrel related columns. In P6-P7 rats, spontaneous events (n=462 in 15 animals) occurred every 2.6 ± 0.2 s ($p<0.05$ versus P0-P1), revealed an average duration at half-maximal amplitude of 184 ± 6.6 s ($p<0.001$) and 77% of the them were located in the barrel field (**Fig. 33B1-3**). As in P0-P1 rats, ~70% of the spontaneous events recorded in P6-P7 animals covered only 1 or 2 barrel related columns (**Fig. 33B4**). About 20% of the events were localized in 3-6 columns and ~10% in more than 6 barrel related columns (**Fig. 33B5-6, C**).

These results demonstrate that (i) in the newborn rat barrel cortex spontaneous events are predominantly restricted to single pre-barrel related columns, (ii) that these spontaneous events have similar properties as evoked cortical responses, and (iii) that at the end of the first postnatal week spontaneous activity may spread from the initially activated pre-barrel related column to numerous neighbouring columns.

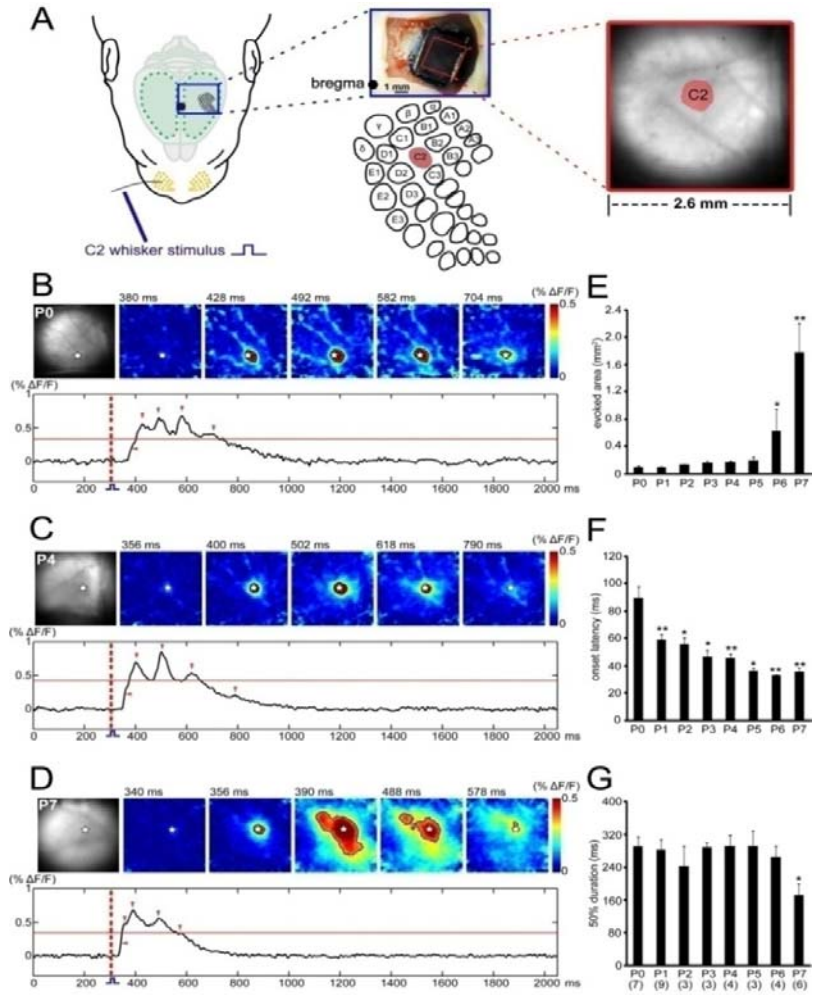

Fig. 32: Properties of whisker evoked responses in the barrel cortex of newborn rats using voltage-sensitive dye imaging (VSDI) in vivo. A: Schematic illustration of experimental set-up for selective mechanical stimulation of the C2 whisker (left) and simultaneous VSDI in the barrel cortex. Photograph of somatosensory cortex stained with the voltage-sensitive dye RH1691 (upper middle), schematic illustration of the barrel field map with localization of the C2 barrel (lower middle) and microscopic picture of the cortical surface with the evoked response in the C2 barrel-related column after mechanical stimulation of the C2 whisker (right). Black dot indicates bregma position. **B-D:** VSDI in the barrel cortex of a P0 (B), P4 (C) and P7 (D) rat following C2 whisker stimulation at time point 300 ms (red dotted line). The localization of the C2 whisker representation in the barrel cortex and five successive poststimulus VSDI responses are shown in the upper rows. White stars show the center of the C2 whisker evoked response. Lower rows show 2 s long optical recordings in which the time points of the five successive frames are marked by red arrow heads. Red horizontal line indicates half maximal response amplitude. Note large area of the response in the P7 rat at 390 and 488 ms as compared to the smaller responses in the P0 and P4 rat, where the activity is restricted to the C2 barrel. **E-G:** Average area (E), onset latency (F) and duration at half maximal amplitude (G) of the C2 evoked VSDI response in P0 to P7 rats. Number of animals are given in parentheses in G. In this and the subsequent figures data are expressed as mean ± s.e.m. Statistical significant differences (Mann-Whitney-Wilcoxon test) versus the P0 age group are indicated by * ($p<0.05$) and ** ($p<0.01$).

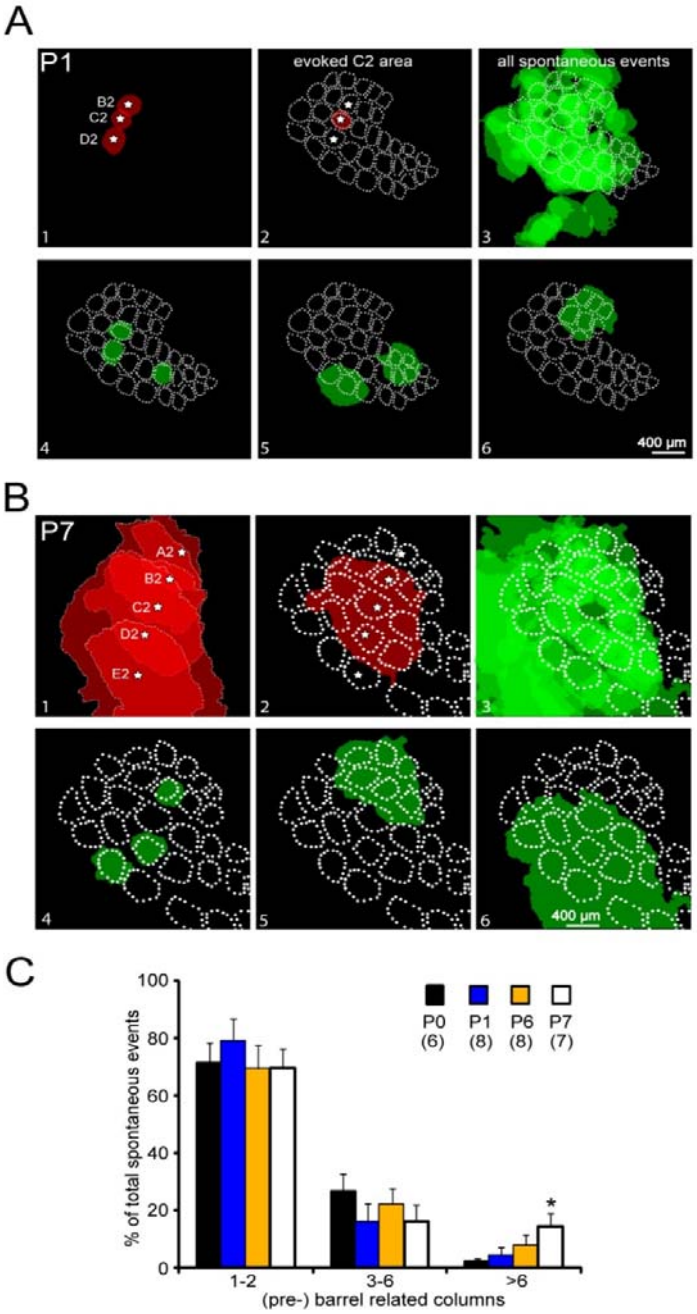

Fig. 33: Developmental differences in the pattern of spontaneous and stimulus evoked activity determined with VSDI in the barrel cortex of newborn rats. A, B: Spontaneous and whisker evoked activity recorded in the somatosensory cortex of one P1 **(A)** and one P7 **(B)** rat. Panel 1 shows the cortical representation of 3 or 5 whiskers of arc 2 as determined by selective mechanical stimulation of a single whisker. White star marks the center of each activated barrel. Panel 2 illustrates the response to C2 whisker stimulation in the map of the whole barrel field. Barrel field map was generated on the basis of a cytochrome oxidase stained horizontal section and superimposed according to the evoked responses (for details see Methods). In panel 3 all spontaneous events (n=75 in A and n=71 in B) recorded in this P1 or P7 rat are superimposed on the barrel field map. Single spontaneous events localized in a single (pre-)barrel related column (panel 4) or in more than one (pre-)column (panel 5 and 6) are shown. **C:** Percentage distribution of spontaneous events, which are restricted to 1-2, 3-6 or >6 (pre-)barrel related columns. Number of animals in each age group are given in parentheses. Statistical significant differences (Mann-Whitney-Wilcoxon test) versus the P0 age group are indicated by * ($p<0.05$).

3.2.2 Correlation Gamma oscillations mediate the activation of cortical pre-columns

In order to characterize in more detail the mechanisms underlying the evoked and spontaneous optical activity patterns, we performed simultaneous VSDI and multi-electrode extracellular recordings *in vivo* (**Fig. 34A1**). After identification of the cortical C2 barrel by selective mechanical stimulation of the C2 whisker and simultaneous VSDI, an 8-shank 32-channel electrode was inserted at an angle of ~35° into the cortex at the site of the C2 barrel (**Fig. 34A2 left**). In good agreement with the VSDI response, the electrophysiological response to C2 whisker stimulation also consisted of a rather localized activity (**Fig. 34A2 right**). When all eight shank recording electrodes (S1 to S8) were positioned in an appropriate manner, the stimulus-evoked electrophysiological responses depicted the topographic cortical representation of five single arc 2 whiskers A2 to E2 (**Fig. 34A3**). These experiments also demonstrated a close correlation of the field potential responses with the VSDI responses in their location and spatial extent.

Previous electrophysiological studies in newborn rat barrel cortex demonstrated two main types of spontaneous and stimulus-evoked activity patterns: (i) spindle bursts with a duration of 1-2 s and frequency of ~10 Hz and (ii) gamma oscillations of 150-300 ms in duration and 30-40 Hz in frequency (Yang et al., 2009;Minlebaev et al., 2007). Our VSDI and simultaneous multi-channel extracellular recordings demonstrate that both types of electrophysiological activity patterns contribute to the optical activity (**Fig. 34B**). Gamma oscillations correlated with the rising phase of the optical signal, indicating that the initial response was dominated by gamma activity and that gamma oscillations play an important role in synchronizing the pre-columnar network. Although in a small number of experiments (n=7 out of 65 events recorded in 13 P0-P1 rats) pure gamma oscillations could be observed, in most cases the gamma oscillation was followed by a spindle burst (n=56). Only 2 out of 65 events recorded in P0-P1 rats were pure spindle bursts without gamma oscillation. When the peak-to-peak amplitude of the evoked response was plotted against the distance between the recording electrode and the center of the VSDI identified barrel, it became evident that gamma oscillations in P0-P1 rats are spatially confined to ~200 μm, whereas spindle bursts cover a larger distance of 300-400 μm in diameter (upper panels in **Fig. 34C**). In agreement with our previous VSDI data, the spatial extent of the electrophysiological responses became larger with increasing age (lower panels in **Fig. 34C**).

These results demonstrate that (i) gamma oscillations and spindle bursts are the electrophysiological activity patterns underlying the VSDI signals and (ii) that gamma oscillations in P0-P1 rats synchronize a pre-barrel related column of ~200 µm in diameter.

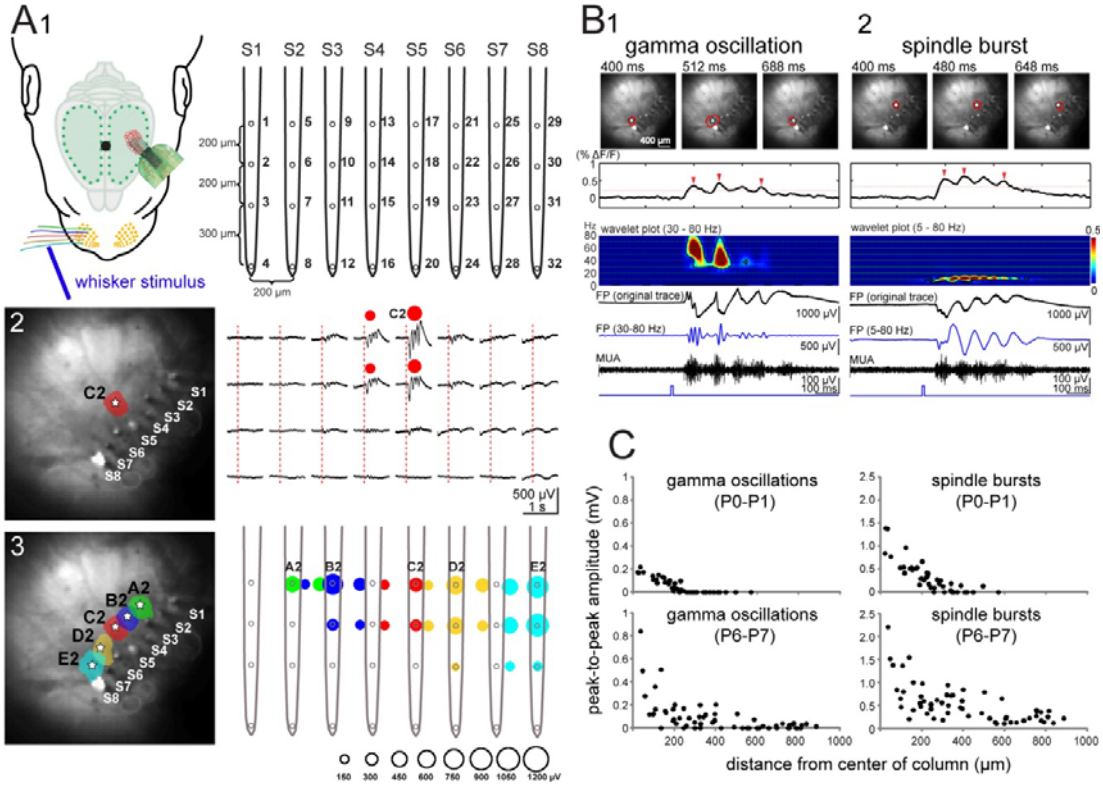

Fig. 34: Simultaneous VSDI and multi-channel extracellular recordings in newborn rat barrel cortex. **A1:** Schematic illustration of experimental set-up combining selective single whisker stimulation, VSDI and 32-channel recordings using an 8-shank electrode (S1 to S8) with inter-electrode distances of 200 µm. **A2:** Mechanical stimulation of the C2 whisker in a P1 rat elicits a local VSDI (left) and electrophysiological (right) response in the C2 barrel. **A3:** Colour-coded localisation of the evoked cortical VSDI (left) and electrophysiological (right) responses to stimulation of single whiskers in arc 2. The peak-to-peak amplitude of the electrophysiological response corresponds to the size of the colour-coded circle as shown below the graph. **B:** Simultaneous VSDI (upper 2 rows) and electrophysiological recordings (lower 3 rows) of evoked cortical gamma oscillatory (1) and spindle burst (2) responses to E2 (1) and B2 (2) single whisker mechanical stimulation. Three successive poststimulus VSDI responses are shown as red circles in the upper row. Second row shows 1 s long optical recording in which the time points of the three successive frames are marked by red arrow heads. The third row shows the wavelet plot calculated from different filter ranges at 30-80 Hz in (1) and 5-80 Hz in (2). **C:** Relationship between peak-to-peak amplitude and distance from (pre-)barrel related column for evoked gamma oscillations (left, n=44) and spindle bursts (right, n=59) in P0-P1 (upper panels) and P6-P7 rats (lower panels).

3.2.3 Thalamic activity drives cortical pre-columns

In order to study the role of the thalamus in the generation of stimulus-evoked cortical responses we performed simultaneous multi-channel extracellular recordings in the ventral posterior medial (VPM) nucleus of the thalamus and in the barrel cortex (**Fig. 35A1, 3**). First we characterized the functional properties of the thalamocortical projection in the newborn rat *in vivo* by studying stimulus-evoked responses in the VPM and barrel cortex. In simultaneous recordings from in total 960 thalamic and 560 neocortical recording sites from 22 animals we found only 15 functional thalamocortical connections upon mechanical single whisker stimulation (**Fig. 35A2**). This very low connectivity rate can be explained by the fact that in contrast to the cortical VSDI the thalamic multi-electrode recording does not allow a priori an identification of the whisker representation. Since thalamic nuclei do not represent a physical dipole (as the cortex), field potential recordings can not reveal a local network activity. The analyses of the multi-unit activity (MUA) showed that both the thalamic and the cortical response consisted of an early component followed by a late response (**Fig. 35A4**). In P0-P1 rats, the early thalamic response had a stimulus-to-onset latency of 40.7 ± 2.3 ms, a duration of 72.8 ± 7.6 ms and was followed by a late response of 2.3 ± 0.6 s in duration (n=7 connections in 5 animals, **Fig. 35B,** left filled bars). In P6-P7 animals, the early thalamic response was significantly faster ($p<0.01$, 28.5 ± 2.4 ms), had a duration of 37 ± 7.4 ms and was followed by a long late response of 3.5 ± 0.6 s in duration (n= 8 connections in 4 animals; **Fig. 35B,** left open bars). The properties of the cortical responses showed similar age-dependent differences. In P0-P1 rats, the early cortical response had an onset latency of 62.7 ± 4.4 ms, a duration of 79 ± 7.7 ms and was followed by a late response of 1 ± 0.1 s in duration (n=7 connections in 4 animals, **Fig. 35B,** right filled bars). In P6-P7 animals, the early cortical response was significantly faster ($p<0.001$, 37.4 ± 2.1 ms), had a duration of 41.3 ± 5.2 ms and was followed by a significantly ($p<0.01$) longer late response of 3.3 ± 0.5 s in duration (n= 8 connections in 4 animals; **Fig. 35B,** right open bars). These data demonstrate a significant ($p<0.01$) speedup of the thalamocortical information transfer from 22 ± 3.5 ms at P0-P1 to 8.9 ± 1.1 ms at P6-P7.

As already described above, in both age groups the early cortical response was generally characterized by gamma activity, which followed the early thalamic response (**Fig. 35C1, D1**). The transfer of sensory information from the thalamus to the barrel cortex functions surprisingly reliable already in P0-P1 rats showing no failures (see single

trial dot histograms in **Fig. 35C2**). During further development this reliable connection becomes faster (**Fig. 35D2**). These age-dependent modifications in the thalamocortical transfer function of stimulus-evoked sensory activity can be also detected in the auto- and crosscorrelograms of whisker-evoked responses recorded in a P0 and P6 rat (**Fig. 35C3, D3**). The autocorrelogram of the early cortical response in the P0 rat shows an apparent peak at approximately ±20 ms illustrating the synchronization of this early stimulus-evoked response in the gamma frequency (~50 Hz) (upper right panel in **Fig. 35C3**). The crosscorrelogram of the early thalamocortical response reveals a broad peak between +15 and +40 ms documenting the variability of this connection (lower right panel in **Fig. 35C3**). This crosscorrelogram also shows a small peak at approximately -35 ms, suggesting a corticothalamic feedback loop functioning already at P0. The thalamocortical connection becomes more precise in the P6 rat as documented in the crosscorrelogram of the thalamocortical responses (lower right panel in **Fig. 35D3**). Here, the crosscorrelogram reveals a relatively narrow peak at approximately +15 ms and a smaller peak at about -20 ms, suggesting a reliable thalamocortical connection and weak corticothalamic feedback loop.

Our data demonstrate that (i) the thalamocortical projection reliably transfers the sensory information from the whisker to the barrel cortex as early as P0-P1, and (ii) that the thalamocortical synaptic connection becomes faster and more precise during the first postnatal week.

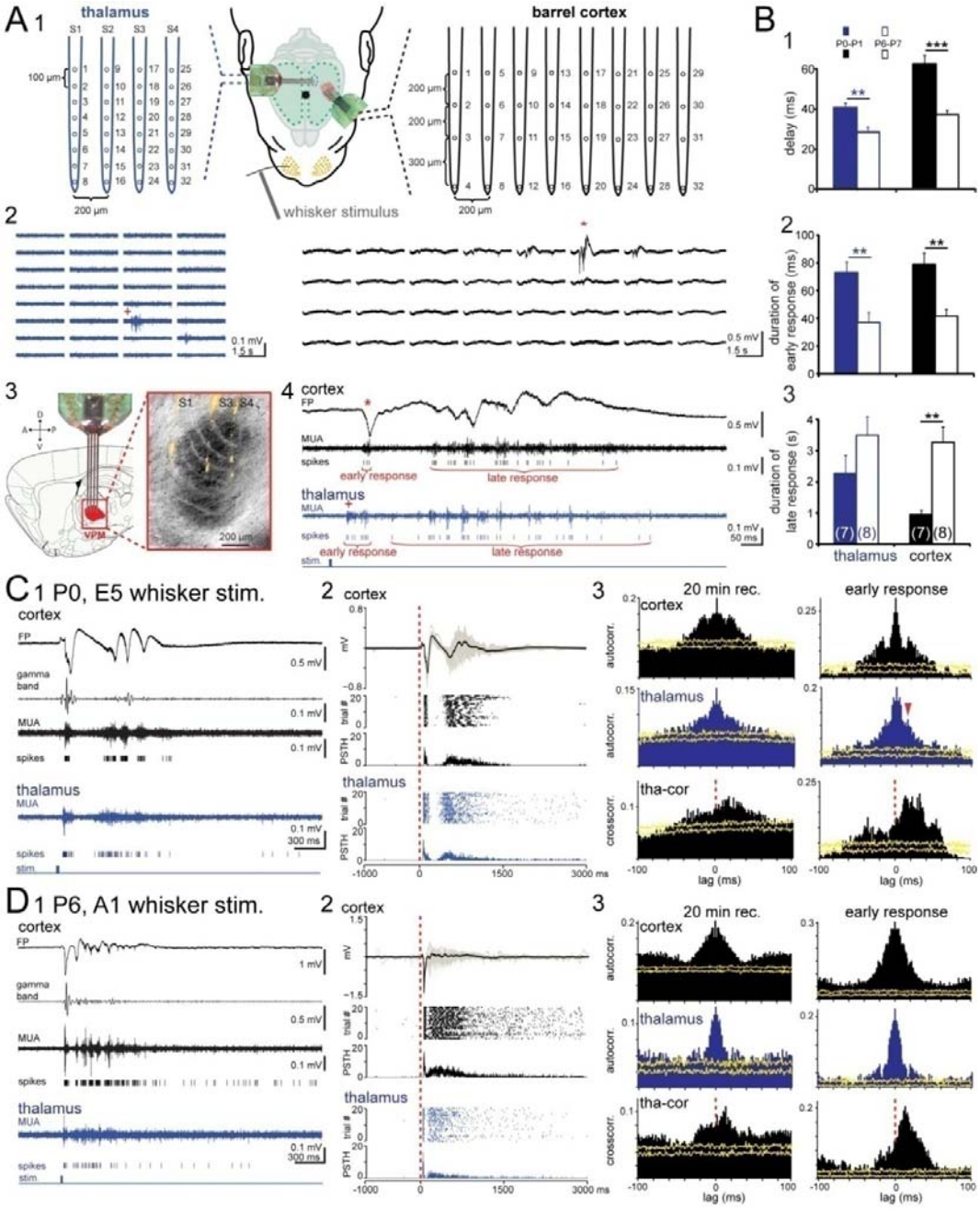

Fig. 35: Simultaneous electrophysiological recordings of whisker evoked responses in thalamus and barrel cortex. A1: Schematic illustration of experimental set-up with a 4-shank 32-channel electrode located in the thalamus (blue) and an 8-shank 32-channel electrode in the cortex (black). **A2:** Representative simultaneous recordings of thalamic (left in blue) and cortical responses (right in black) to single whisker stimulation. Note spatial restriction of the responses both in the thalamus and cortex. **A3:** Schematic illustration of a sagittal brain section showing the location of the recording electrodes in the VPM thalamus (left). Photograph from same animal as in (2) showing three DiI-stained electrode tracks in a section stained for cytochrome oxidase (right). **A4:** Response in thalamus (red cross) and cortex (red asterisk) at higher temporal resolution (cf. marks in 2). Both, the thalamic and the cortical response consist of an early and a late response. **B:** Age-dependent differences in the onset delay of the evoked response (1), the duration of the early response (2) and the late response (3) in the thalamus (left in blue) and cortex (right in black). Data were obtained from 7 thalamo-cortical connections in 5 P0-P1 rats (filled bars) and 8 thalamo-cortical connections in 4 P6-P7 animals (open bars). **C1:** Simultaneous recordings of thalamic and

cortical responses to E5 single whisker stimulation in a P0 rat. Gamma band activity was obtained by band-pass filtering (30-80 Hz) of the field potential response. **C2:** Average (black line) and superimposed 20 single (shaded area) cortical field potential responses (upper panel) and cortical (black) and thalamic (blue) post-stimulus time histograms (PSTH) of 20 succeeding whisker stimulations every 60 s. C3, Autocorrelogram of cortical (upper) and thalamic responses (middle), and crosscorrelograms (lower) calculated from the recordings in the P0 rat. Left panels show correlograms calculated from 20 min continuous recording and right panels show correlograms of early reponses only. Yellow lines indicate 95% of confidence intervals. **D:** Same as in C, but recordings were obtained in a P6 rat following stimulation of the A1 whisker. Note narrow autocorrelograms and shorter lag in crosscorrelograms in the P6 as compared to the P0 rat.

3.2.4 Self-organization of cortical pre-columns by thalamic and intracortical activity

Next we addressed the question whether spontaneous activity recorded in the barrel cortex is triggered from the sensory periphery and transmitted via the thalamus or whether cortical activity can be also generated independently from the thalamus by intracortical mechanisms. In all of the 15 simultaneous recordings with a functional thalamocortical connection we observed spontaneous activity (cf. **Fig. 35A1, 3**). Very similar to the stimulus-evoked responses (**Fig. 34B**) and in agreement with our previous findings (Yang et al., 2009), spontaneous activity in the barrel cortex consisted of gamma oscillations followed by spindle bursts. Cortical field potential activity was accompanied by spike activity in the thalamus and barrel cortex (**Fig. 36A2, B2**). In P0-P1 rats, 93% of the recorded spontaneous cortical events (n=172) were accompanied by thalamic activity. At this age, the gamma-related thalamic and cortical activities had a duration of 339.6 ± 127.3 ms and 352.1 ± 131.5 ms, respectively (both, n=4 connections in 3 animals). In P6-P7 animals, 97% of the recorded spontaneous cortical events (n=213) were accompanied by thalamic activity and the spontaneous events were significantly longer ($p<0.05$) in the thalamus and cortex (2.5 ± 0.6 s and 2.1 ± 0.7 s, respectively; n=5 connections in 3 animals). Similar to the evoked activity patterns, the thalamocortical transfer of spontaneous events also became significantly ($p<0.05$) faster from 34 ± 4.3 ms at P0-P1 to 9.8 ± 1.5 ms at P6-P7. When for analyses the thalamic activity was aligned with the onset of spontaneous cortical gamma activity (**Fig. 36A3, 36B3**), the thalamocortical transfer function of spontaneous activity in P0-P1 rats (lower panels in **Fig. 36A4**) revealed a similar broad scatter in the delay as for the evoked responses. With development this scatter again became narrower in P6-P7 rats (lower panels in **Fig. 36B4**).

These data demonstrate that spontaneous activity generated in the thalamus or in the sensory periphery trigger gamma oscillations in functional pre-columns.

Next we studied the role of the sensory periphery in the generation of spontaneous cortical gamma oscillations and spindle bursts by video analysis of the whisker movement and simultaneous multi-channel extracellular recordings in barrel cortex. Mechanical stimulation of a single whisker reliably elicited a cortical response in the corresponding barrel consisting of an early and spatially confined gamma activity followed by spindle burst activity (**Figs. 34B1, 35C1, 37A1**). A similar activity pattern could be observed in the cortical barrel when the rat performed a spontaneous whisker movement without mechanical stimulation and without touching of an object (**Fig. 37A2**), suggesting that a motor-sensory signal from the periphery is sufficient to trigger the local cortical gamma activity combined with spindle bursts. Finally, local gamma oscillations followed by spindle bursts can be also recorded in (pre-)barrel related columns without any movement of the corresponding whisker (**Figs. 37A3**), indicating that the cortical gamma activity can be also generated by intrathalamic and / or intracortical mechanisms. In P0-P1 rats, 79% of the spontaneous events (93 of 118 events recorded in 4 P0-P1 rats) were triggered by spontaneous whisker movements, indicating that at this early age the sensory periphery plays an important role in driving local columnar network activity. In P6-P7 rats, only 49% of the spontaneous events (62 of 126 events recorded in 6 P6-P7 rats) were triggered by spontaneous whisker movement, suggesting that thalamic and/or intracortical mechanisms become more important in the generation of spontaneous cortical activity. The cortical activity patterns evoked by these three different stimulation paradigms differed in their amplitude and duration, but not in their frequency. Stimulus evoked responses are larger than spontaneous events with or without whisker movement, but this difference was significant ($p<0.01$) in the P6-P7 age group only (**Fig. 37B1, C1**). Furthermore, in both age groups the duration of cortical activity evoked by spontaneous whisker movement is longer than that of the stimulus evoked response and spontaneous activity without whisker movement (**Figs. 37B2, C2**).

These data demonstrate that cortical gamma oscillations forming early functional pre-columns can be generated spontaneously without mechanical stimulation, active sensing or movement of the whiskers. Therefore, this activity pattern may play an important role in the functional self-organization of the cortical columnar architecture at earliest ages and before the formation of a structural correlate of a cortical column.

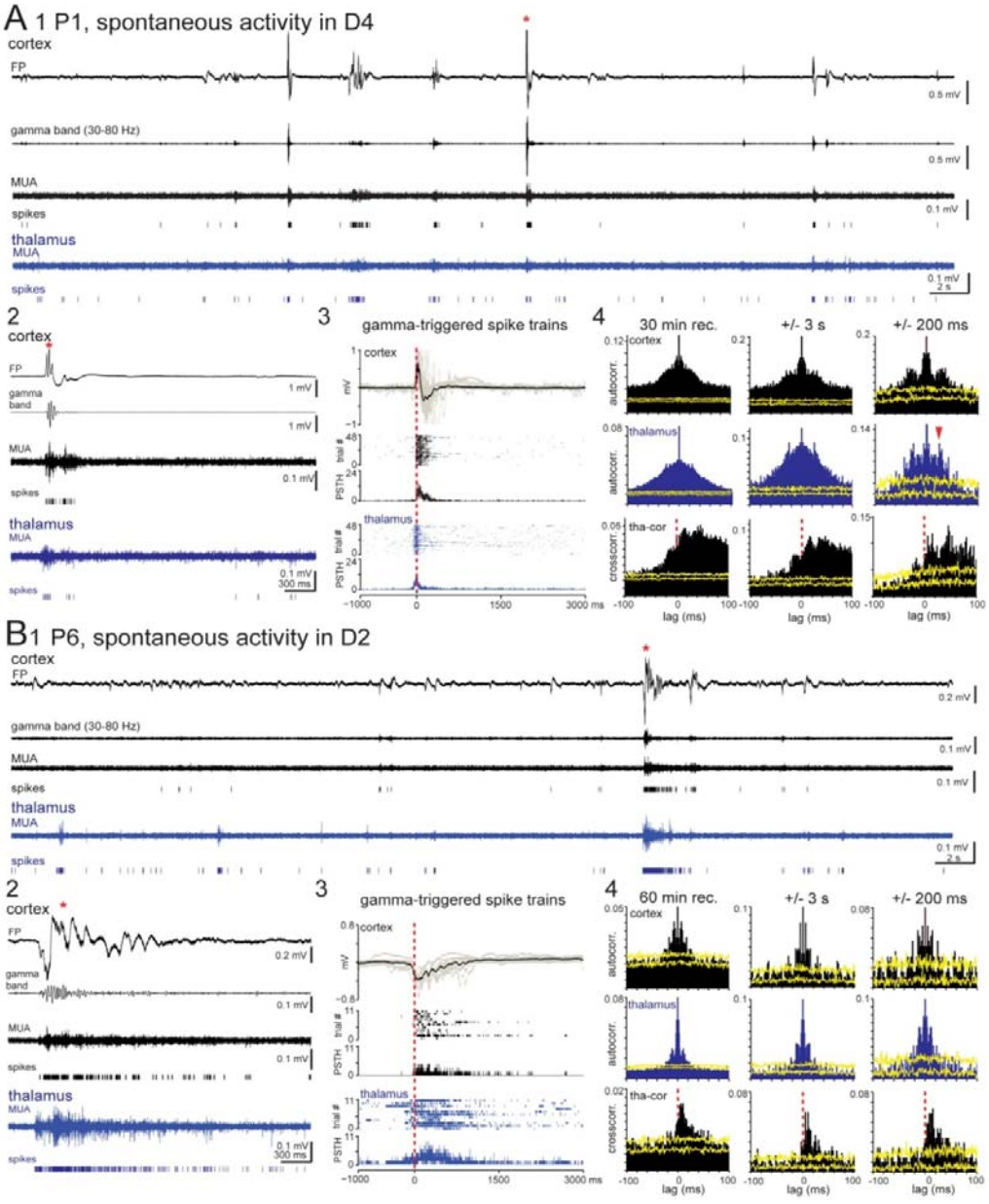

Fig. 36: Spontaneous events in the thalamocortical system of newborn rats are initiated in the thalamus. A1: Continuous 60 s simultaneous recording of spontaneous activity in the cortex (upper black traces) and thalamus (lower blue traces). **A2:** Spontaneous activity in cortex and thalamus at higher temporal resolution (cf. asterisk in A1). **A3:** Average (black line) and superimposed 48 single (shaded area) spontaneous cortical field potential recordings, which were triggered to the spontaneous gamma oscillations (upper panel). Below, cortical (black) and thalamic (blue) PSTHs of 40 spontaneous gamma-triggered spike trains. **A4:** Autocorrelogram of spontaneous cortical (upper) and thalamic activity (middle), and crosscorrelograms (lower) calculated from the recordings in the P1 rat. Left panels show correlograms calculated from 30 min continuous recording, middle panels illustrate correlograms of gamma-triggered activity within an interval of ±3 s around gamma onset and right panels show correlograms of gamma-triggered activity within a ±200 ms interval. **B:** Same as in A, but spontaneous thalamic and cortical activity was recorded in a P6 rat for 60 min. Note narrow autocorrelograms and shorter lag in crosscorrelograms in the P6 as compared to the P1 rat.

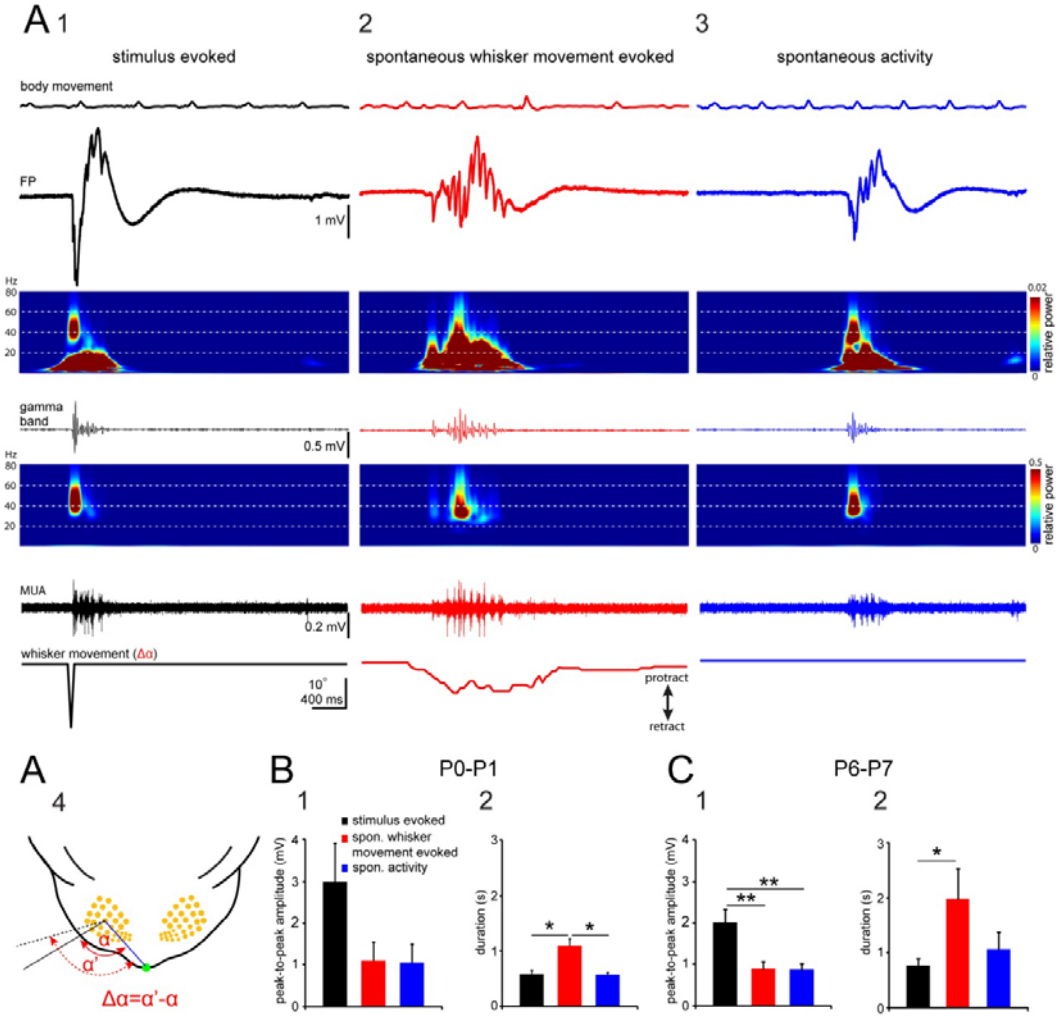

Fig. 37: Electrophysiological recordings in the cortical C2 whisker representation during mechanical single whisker stimulation (left), spontaneous whisker movement (middle) and without any whisker movement (right). A: Cortical activity following selective stimulation of the C2 whisker (1), during spontaneous movement of the C2 whisker (2), and when the C2 whisker is not moved (3). Third row shows corresponding wavelet plot (5-80Hz filtered to prevent the strong effect of delta wave). Upper traces show the registration of the body movement. Note large amplitude of the stimulus evoked gamma response (1) as compared to the spontaneous activity (2, 3). Traces below shows filtered gamma band (30-80 Hz) traces, corresponding wavelet plots, corresponding multiunit activity and recording of whisker movement. (4) Schematic illustration of the method to calculate the angle of whisker movement. **B, C:** Average maximal peak-to-peak amplitude (1) and duration (2) of evoked and spontaneous cortical activity patterns in P0-P1 rats (B, n=4) and P6-P7 rats (C, n=6).

4 Discussion

4.1 Project1

Coordinated network activity is a hallmark of developing neuronal networks in a variety of species including humans (for review (Torborg and Feller, 2005;Vanhatalo and Kaila, 2006;Khazipov and Luhmann, 2006). In project1 we investigated the properties and mechanisms of coordinated activity patterns in the primary somatosensory cortex (S1) of the newborn rat *in vivo* using multi-electrode recording techniques. We demonstrate for the first time that (i) the neonatal rat S1 generates under *in vivo* conditions three distinct oscillatory activity patterns; (ii) these activity patterns synchronize spatially and temporally distinct neuronal networks; (iii) spatially confined synchronized activity may contribute to the refinement of function-related architecture of the developing barrel field; (iv) the subplate, gap junctional coupling and NMDA receptor mediated synaptic transmission are involved in the generation of these early oscillatory activity patterns *in vivo*. I project2 we used VSDI combined the multi-electrode recording techniques to investigate the evoked and spontaneous activity in the whole barrel cortex.

Spindle bursts

Spindle bursts of 1 to 2 s in duration and ~10 Hz in frequency occur approximately every 10 s. They have been previously observed in the somatosensory cortex (Minlebaev et al., 2007;Khazipov et al., 2004) and visual cortex (Hanganu et al., 2006) represent the dominant pattern of neocortical activity in the newborn rat *in vivo*. This activity resembles in many aspects the so-called delta-brush oscillations recorded with EEG in preterm human neonates of 29-31 weeks of postconceptional age (Vecchierini et al., 2007;Milh et al., 2007) (for recent review of EEG activity in preterm and neonatal babies see (Vanhatalo and Kaila, 2006). Khazipov et al. (Khazipov et al., 2004) demonstrated in newborn rat somatosensory cortex that spindle bursts are spatially confined and selectively triggered in a somatotopic manner by spontaneous movements via sensory feedback signals. Our results are not only in good agreement with these previous observations, but document the specific contribution of this activity pattern in the synchronization of a column-like neocortical network. Similar local network oscillations have been previously observed in the *in vitro* preparation of the intact cerebral cortex of the newborn rodent following activation of muscarinic or metabotropic

glutamate receptors (Dupont et al., 2006;Wagner and Luhmann, 2006). However, under these conditions and with bath application of selective agonists to trigger the network oscillations, the activity propagates over large cortical regions (Kilb and Luhmann, 2003;Calderon et al., 2005;Peinado, 2000). Direct activation of the cholinergic basal forebrain *in vivo* facilitated the generation of spindle bursts (Hanganu et al., 2007), but the activity did not propagate.

Beside intracortical network mechanisms and neuromodulatory subcortical inputs, the main trigger for spindle bursts in rodents as well as for delta brushes in human babies comes from the sensory periphery (Khazipov et al., 2004;Minlebaev et al., 2007;Milh et al., 2007;Hanganu et al., 2006). We demonstrate that electrical stimulation of the whisker pad as well as tactile activation of the whiskers elicited spatially confined spindle bursts in the contralateral barrel cortex. The spatial organization and precise synchronization of neonatal spindle bursts indicate that this early activity pattern may serve as a template for the development of cortical barrels. A small number of spindle bursts were synchronized between both hemispheres and the degree of synchronization increased significantly during the first postnatal week. This interhemispheric synchronization is most likely mediated by callosal connections, which are innervating the subplate as early as P0 (Ivy and Killackey, 1981). It has been demonstrated that early neuronal activity is necessary for the normal development and maintenance of these callosal projections (Wang et al., 2007) and that the corpus callosum may modulate functionally inhibitory interactions between homotopic regions of the newborn rodent somatosensory cortex (Marcano-Reik and Blumberg, 2008).

Gamma oscillations

Gamma oscillations have been previously demonstrated in the newborn rat hippocampus *in vitro* (Palva et al., 2000) and with EEG techniques in the cerebral cortex of 8 months old infants (Csibra et al., 2000). Here we describe *in vivo* gamma oscillations in the cerebral cortex of the newborn rodent, which in ontogenetic comparison resembles the prenatal state of the human cerebral cortex (Romijn et al., 1991). Gamma oscillations in the newborn rat somatosensory cortex revealed a frequency of 30-40 Hz, duration of 150-300 ms and occurred every 10-30 s. Spontaneous as well as evoked spatially confined gamma oscillations were restricted to the barrel field demonstrating the

existence of a functional whisker representations at a time when the thalamocortical projection to layer IV and layer IV itself is not even present. Since in rodents the subplate is already innervated by the thalamic input at late embryonic stages (Molnar et al., 2003;Schlaggar and O'Leary, 1994;Higashi et al., 2002), this periphery-driven gamma activity can be transferred to the developing cortex only via the subplate. We have previously suggested that the subplate does not only operate as a transient passive relay station between the thalamus and the developing cerebral cortex, but rather as an active element amplifying the incoming neuronal activity and converting it into local synchronized oscillations (Dupont et al., 2006). Here we show that the subplate is involved in the generation of oscillatory activity *in vivo*.

Propagating long oscillations

Whereas spontaneous and stimulus-evoked spindle bursts and gamma oscillations did not propagate and both patterns synchronized a local neuronal network, the long oscillations propagated over large cortical regions and synchronized in the 10-20 Hz frequency range the activity over 600-800 μm. An activity pattern lasting up to 83 s have been previously recorded with EEG in premature infants from 24-27 weeks of gestation (Vecchierini et al., 2007). From all activity patterns observed in the newborn rat cerebral cortex, the long oscillations revealed the largest amplitude (250-750 μV) and longest duration (>40 s). However, this activity pattern occurred only every ~20 min. In a previous report, we describe a similar spontaneous oscillatory pattern with a faster propagation velocity in newborn mouse somatosensory cortical slices *in vitro* (Fig. 5 in (Sun and Luhmann, 2007). Moreover, long-lasting propagating activity has been described as prominent calcium wave activity in the neonatal mouse cortex *in vivo* (Adelsberger et al., 2005). We have recently shown that transient activation of muscarinic receptors on subplate neurons elicits a long-lasting oscillatory activity in the newborn rat somatosensory cortex (Hanganu et al., 2009). This large-scale propagating activity pattern may interact with the non-propagating local spindle bursts and gamma oscillations in an activity-depending manner, thereby promoting the formation of early neuronal ensembles. Interestingly subplate neurons show a pronounced facilitation upon intracortical stimulation in the 10-40 Hz frequency range (Hirsch and Luhmann, 2008). Propagating long oscillations activate the developing cortex including the subplate in this frequency range and may boost the periphery-driven input.

Physiological and pathophysiological relevance

The topographic development of the thalamocortical connections and the maturation of cortical columns depends on guidance molecules and electrical activity (Molnar et al., 2003;Price et al., 2006;Lopez-Bendito and Molnar, 2003). An increasing number of experimental evidence indicates that both processes interact and that transcription factors and patterned neuronal activity are both important for the formation of early connections and local neuronal networks (Nicol et al., 2007;Torborg and Feller, 2005;Dunn et al., 2006;Pfeiffenberger et al., 2006;Hanson and Landmesser, 2004). Not only spontaneous neuronal activity (Huberman et al., 2006), but at a later developmental stage also sensory activity is required for the formation and remodeling of topographic connections (Hooks and Chen, 2006). Our report characterizes in detail the spontaneous and evoked activity patterns of the newborn rat S1 *in vivo* and demonstrates the columnar-like organization and precise synchronization of these early activity patterns. Spindle bursts synchronize a neuronal network of 200-400 µm in diameter and gamma oscillations are spatially confined to about 200 µm in the barrel field. These spatial dimensions correlate well with the diameter of a barrel in the somatosensory cortex of a neonatal rat (Schlaggar and O'Leary, 1994). Our data suggest that functional barrel-related columns already exist at the day of birth. Waters et al. (Waters et al., 1990) suggested that an intrinsic template for the organization of cortical patterns may already exist during late embryonic development. If the thalamocortical input influences the cortical patterning at that early developmental stage, the subplate as a transient recipient zone for thalamocortical afferents must play an important role in this process (Kostovic and Judas, 2002;Allendoerfer and Shatz, 1994). Local electrical stimulation of the subplate *in vitro* elicits a gap junction mediated oscillatory activity which synchronizes a columnar network of 100-150 µm in diameter (Dupont et al., 2006). The sensitivity of spindle bursts and gamma oscillations to carbenoxolone supports the role of gap junctional coupling for the generation of oscillatory activity *in vivo*. Additionally, the MUA and CSD profiles reinforce the role of the subplate in the generation of early activity patterns. The subplate may act as an amplifier which transmits the oscillatory activity to the overlying cortical plate (Hanganu et al., 2009). In the subplate and developing cortical plate, neurons are coupled via gap junctions and form early functional columnar networks (Yuste et al., 1992). This early columnar arrangement may originate from the gap junctional coupling between radial glial cells and migrating neurons (Elias

and Kriegstein, 2008;Elias et al., 2007), as initially suggested by Rakic in the "radial unit hypothesis" (Rakic, 1988).

Disturbances of neuronal network activity during early ontogenesis may interfere with developmental programs and may cause long-term alterations in cortical microcircuitry (Le Van et al., 2006;Penn and Shatz, 1999). The formation of cortical columns may be disturbed leading to cognitive dysfunction (Levitt et al., 2004). Since the subplate plays a central role in early cortical development, structural and / or functional changes in the subplate and disturbances of early cortical activity patterns have been correlated with certain neurological deficits, such as epilepsy, schizophrenia or autism (Le Van et al., 2006;McQuillen and Ferriero, 2005;Bunney and Bunney, 2000;Bunney et al., 1997). Experimental and clinical evidence indicate that EEG measurements in preterm infants may be of central importance to monitor cortical activity and to detect pathophysiological alterations at earliest developmental stages (Vanhatalo and Kaila, 2006).

4.2 Project2

We have shown that the cerebral cortex reveals a functional and topographic columnar organization already during earliest stages of development. Although the graded expression of several transcription factors set the rudimentary topography of thalamocortical connectivity, thereby specifying cortical areas and creating crude cortical maps (Lopez-Bendito and Molnar, 2003), our data indicate that self-generated activity arising from the sensory periphery and transmitted via the thalamus to the developing cortex may play an important role in the early formation of columnar networks.

In the barrel cortex of newborn rats spontaneous and stimulus-evoked gamma oscillations synchronize local neuronal networks (pre-barrel related columns*)* even before all cortical layers have been formed. During the first two postnatal days, about 80% of the spontaneous cortical oscillatory activity is triggered by spontaneous whisker movements, indicating that the sensory periphery can drive cortical columnar networks already during early stages of corticogenesis. In the visual cortex of slightly older rats (P10-P11, before eye opening), 87% of the spontaneous cortical activity is generated by the retina (Colonnese and Khazipov, 2010), indicating that different sensory systems

reveal similar network mechanisms to drive early cortical networks although with a different developmental profile (Colonnese et al., 2010).

We show that spontaneous and evoked cortical activity patterns correlate with local thalamic activity, indicating a precise topographic organization of the whisker-thalamus-barrel cortex pathway already in newborn rats. At this age the thalamocortical input forms a functional synaptic connection with the subplate (Hanganu et al., 2002;Friauf et al., 1990), which serves as a transient relay and hub station in the developing cerebral cortex (Kanold and Luhmann, 2010). It has been previously shown in cat visual cortex that the subplate plays a pivotal role in the formation of ocular dominance and orientation columns (Kanold et al., 2003;Ghosh and Shatz, 1992) and in newborn rat somatosensory cortex the subplate is involved in the generation of local cortical gamma oscillations and spindle bursts (Yang et al., 2009). Here we demonstrate in P0-P1 rats that spontaneous whisker movements trigger cortical activity patterns, thereby constructing a functional topographic network of self-organized cortical pre-columns. Our data are in good agreement with previous observations by Khazipov et al. (Khazipov et al., 2004) demonstrating in somatosensory cortex of newborn rats in vivo that spatially confined spindle bursts are selectively triggered in a somatotopic manner by spontaneous muscle twitches.

A surprisingly early segregation of ocular dominance columns, as the first component of modular circuitry to emerge in visual cortex, has also been described in ferrets and cats before the thalamocortical afferents innervate layer IV (Crowley and Katz, 2000). During this early developmental period total removal of retinal activity by enucleation does not disrupt the formation of ocular dominance columns (Crowley and Katz, 1999), suggesting that intrinsic molecular cues or spontaneous thalamic and / or intracortical activity remaining after enucleation could generate sufficient correlated information to drive the cortical columnar network (Crowley and Katz, 2002). Spontaneous correlated neuronal activity has been recorded in the lateral geniculate nucleus of awake behaving ferrets before eye opening (Weliky and Katz, 1999), indicating that the thalamus can drive the initial patterning of neocortical circuits in the absence of retinal drive. Our intrathalamic recordings of spontaneous neuronal activity support this hypothesis.

Finally, the neonatal cerebral cortex also has the intrinsic capacity to generate local columnar activity patterns even without thalamocortical synaptic input. Under in

vitro conditions, optical imaging and multi-electrode recordings in somatosensory cortical slices and intact cortex preparations have revealed functional columnar units and subplate-driven local oscillatory networks in newborn rodents (Yuste et al., 1992;Dupont et al., 2006;Sun and Luhmann, 2007). In vivo multi-electrode extracellular recordings in developing ferret area 17 revealed an intrinsic patchy organization of patterned correlated activity at horizontal distances of ~1 mm, independent of thalamic input activity (Chiu and Weliky, 2001), and these patches correlated with early ocular dominance columns before eye opening (Chiu and Weliky, 2002).

Our observations in P0-P1 rats show that cortical pre-columns can be activated by sensory inputs, by spontaneous whisker deflections and by spontaneous thalamic activity, which emphasize the important functions of sensory, motor-sensory and spontaneous activity patterns for the formation of functional neuronal circuits. We suggest that the convergence of these three different mechanisms supports an adequate maturation of the somatosensory system even in the absence of sensory stimuli, while it also allows a functional adaptation of developing circuits to the demands set by the sensory environment.

5 Summary

Coordinated patterns of electrical activity are important for the early development of sensory systems. The spatiotemporal dynamics of these early activity patterns and the role of the peripheral sensory input for their generation are essentially unknown.

In project1, we performed extracellular multielectrode recordings in the somatosensory cortex of postnatal day 0 to 7 rats *in vivo* and observed three distinct patterns of synchronized oscillatory activity. (1) Spontaneous and periphery-driven spindle bursts of 1–2 s in duration and ~10 Hz in frequency occurred approximately every 10 s. (2) Spontaneous and sensory-driven gamma oscillations of 150–300 ms duration and 30–40 Hz in frequency occurred every 10–30 s. (3) Long oscillations appeared only every ~20 min and revealed the largest amplitude (250–750 μV) and longest duration (>40 s). These three distinct patterns of early oscillatory activity differently synchronized the neonatal cortical network. Whereas spindle bursts and gamma oscillations did not propagate and synchronized a local neuronal network of 200–400 μm in diameter, long oscillations propagated with 25–30 μm/s and synchronized 600 800 μm large ensembles. All three activity patterns were triggered by sensory activation. Single electrical stimulation of the whisker pad or tactile whisker activation elicited neocortical spindle bursts and gamma activity. Long oscillations could be only evoked by repetitive sensory stimulation. The neonatal oscillatory patterns *in vivo* depended on NMDAreceptor-mediated synaptic transmission and gap junctional coupling. Whereas spindle bursts and gamma oscillations may represent an early functional columnar-like pattern, long oscillations may serve as a propagating activation signal consolidating these immature neuronal networks.

In project2, Using voltage-sensitive dye imaging and simultaneous multi-channel extracellular recordings in the barrel cortex and somatosensory thalamus of newborn rats *in vivo*, we found that spontaneous and whisker stimulation induced activity patterns were restricted to functional cortical columns already at the day of birth. Spontaneous and stimulus evoked cortical activity consisted of gamma oscillations followed by spindle bursts. Spontaneous events were mainly generated in the thalamus or by spontaneous whisker movements. Our findings indicate that during early developmental stages cortical networks self-organize in ontogenetic columns via spontaneous gamma oscillations triggered by the thalamus or sensory periphery.

Reference List

1. Adelsberger H, Garaschuk O, Konnerth A (2005) Cortical calcium waves in resting newborn mice. Nat Neurosci 8: 988-990.

2. Allendoerfer KL, Shatz CJ (1994) The subplate, a transient neocortical structure: its role in the development of connections between thalamus and cortex. Annu Rev Neurosci 17: 185-218.

3. Andersen SL (2003) Trajectories of brain development: point of vulnerability or window of opportunity? Neurosci Biobehav Rev 27: 3-18.

4. Andre M, Lamblin MD, d'Allest AM, Curzi-Dascalova L, Moussalli-Salefranque F, The SN, Vecchierini-Blineau MF, Wallois F, Walls-Esquivel E, Plouin P (2010) Electroencephalography in premature and full-term infants. Developmental features and glossary. Neurophysiol Clin 40: 59-124.

5. Aronoff R, Petersen CC (2008) Layer, column and cell-type specific genetic manipulation in mouse barrel cortex. Front Neurosci 2: 64-71.

6. Berger T, Borgdorff A, Crochet S, Neubauer FB, Lefort S, Fauvet B, Ferezou I, Carleton A, Luscher HR, Petersen CC (2007) Combined voltage and calcium epifluorescence imaging in vitro and in vivo reveals subthreshold and suprathreshold dynamics of mouse barrel cortex. J Neurophysiol 97: 3751-3762.

7. Brecht M, Fee MS, Garaschuk O, Helmchen F, Margrie TW, Svoboda K, Osten P (2004) Novel approaches to monitor and manipulate single neurons in vivo. J Neurosci 24: 9223-9227.

8. Bunney BG, Potkin SG, Bunney WE (1997) Neuropathological studies of brain tissue in schizophrenia. J Psychiatr Res 31: 159-173.

9. Bunney WE, Bunney BG (2000) Evidence for a compromised dorsolateral prefrontal cortical parallel circuit in schizophrenia. Brain Res Brain Res Rev 31: 138-146.

10. Calderon DP, Leverkova N, Peinado A (2005) Gq/11-induced and spontaneous waves of coordinated network activation in developing frontal cortex. J Neurosci 25: 1737-1749.

11. Catalano SM, Robertson RT, Killackey HP (1996) Individual axon morphology and thalamocortical topography in developing rat somatosensory cortex. J Comp Neurol 367: 36-53.

12. Chiu C, Weliky M (2002) Relationship of correlated spontaneous activity to functional ocular dominance columns in the developing visual cortex. Neuron 35: 1123-1134.

13. Clancy B, Finlay BL, Darlington RB, Anand KJ (2007) Extrapolating brain development from experimental species to humans. Neurotoxicology 28: 931-937.

14. Colonnese MT, Kaminska A, Minlebaev M, Milh M, Bloem B, Lescure S, Moriette G, Chiron C, Ben Ari Y, Khazipov R (2010) A conserved switch in sensory processing prepares developing neocortex for vision. Neuron 67: 480-498.

15. Colonnese MT, Khazipov R (2010) "Slow activity transients" in infant rat visual cortex: a spreading synchronous oscillation patterned by retinal waves. J Neurosci 30: 4325-4337.

16. Crowley JC, Katz LC (1999) Development of ocular dominance columns in the absence of retinal input. Nat Neurosci 2: 1125-1130.

17. Crowley JC, Katz LC (2000) Early development of ocular dominance columns. Science 290: 1321-1324.

18. Crowley JC, Katz LC (2002) Ocular dominance development revisited. Curr Opin Neurobiol 12: 104-109.

19. Csibra G, Davis G, Spratling MW, Johnson MH (2000) Gamma oscillations and object processing in the infant brain. Science 290: 1582-1585.

20. Dekaban AS (1978) Changes in brain weights during the span of human life: relation of brain weights to body heights and body weights. Ann Neurol 4: 345-356.

21. Diamond ME, von Heimendahl M, Arabzadeh E (2008a) Whisker-mediated texture discrimination. PLoS Biol 6: e220.

22. Diamond ME, von Heimendahl M, Knutsen PM, Kleinfeld D, Ahissar E (2008b) 'Where' and 'what' in the whisker sensorimotor system. Nat Rev Neurosci 9: 601-612.

23. Dunn TA, Wang CT, Colicos MA, Zaccolo M, DiPilato LM, Zhang J, Tsien RY, Feller MB (2006) Imaging of cAMP levels and protein kinase A activity reveals that retinal waves drive oscillations in second-messenger cascades. J Neurosci 26: 12807-12815.

24. Dupont E, Hanganu IL, Kilb W, Hirsch S, Luhmann HJ (2006) Rapid developmental switch in the mechanisms driving early cortical columnar networks. Nature 439: 79-83.

25. Elias LA, Kriegstein AR (2008) Gap junctions: multifaceted regulators of embryonic cortical development. Trends Neurosci 31: 243-250.

26. Elias LA, Wang DD, Kriegstein AR (2007) Gap junction adhesion is necessary for radial migration in the neocortex. Nature 448: 901-907.

27. Erzurumlu RS, Jhaveri S (1990) Thalamic axons confer a blueprint of the sensory periphery onto the developing rat somatosensory cortex. Brain Res Dev Brain Res 56: 229-234.

28. Feldman DE, Brecht M (2005) Map plasticity in somatosensory cortex. Science 310: 810-815.

29. Feldmeyer D, Lubke J, Sakmann B (2006) Efficacy and connectivity of intracolumnar pairs of layer 2/3 pyramidal cells in the barrel cortex of juvenile rats. J Physiol 575: 583-602.

30. Ferezou I, Haiss F, Gentet LJ, Aronoff R, Weber B, Petersen CC (2007) Spatiotemporal dynamics of cortical sensorimotor integration in behaving mice. Neuron 56: 907-923.

31. Freeman JA, Nicholson C (1975) Experimental optimization of current source-density technique for anuran cerebellum. J Neurophysiol 38: 369-382.

32. Friauf E, McConnell SK, Shatz CJ (1990) Functional synaptic circuits in the subplate during fetal and early postnatal development of cat visual cortex. J Neurosci 10: 2601-2613.

33. Garaschuk O, Linn J, Eilers J, Konnerth A (2000) Large-scale oscillatory calcium waves in the immature cortex. Nat Neurosci 3: 452-459.

34. Ghosh A, Shatz CJ (1992) Involvement of subplate neurons in the formation of ocular dominance columns. Science 255: 1441-1443.

35. Hanganu IL, Ben Ari Y, Khazipov R (2006) Retinal waves trigger spindle bursts in the neonatal rat visual cortex. J Neurosci 26: 6728-6736.

36. Hanganu IL, Kilb W, Luhmann HJ (2002) Functional synaptic projections onto subplate neurons in neonatal rat somatosensory cortex. J Neurosci 22: 7165-7176.

37. Hanganu IL, Okabe A, Lessmann V, Luhmann HJ (2009) Cellular mechanisms of subplate-driven and cholinergic input-dependent network activity in the neonatal rat somatosensory cortex. Cereb Cortex 19: 89-105.

38. Hanganu IL, Staiger JF, Ben Ari Y, Khazipov R (2007) Cholinergic modulation of spindle bursts in the neonatal rat visual cortex in vivo. J Neurosci 27: 5694-5705.

39. Hanson MG, Landmesser LT (2004) Normal patterns of spontaneous activity are required for correct motor axon guidance and the expression of specific guidance molecules. Neuron 43: 687-701.

40. Higashi S, Molnar Z, Kurotani T, Toyama K (2002) Prenatal development of neural excitation in rat thalamocortical projections studied by optical recording. Neuroscience 115: 1231-1246.

41. Hirsch S, Luhmann HJ (2008) Pathway-specificity in N-methyl-D-aspartate receptor-mediated synaptic inputs onto subplate neurons. Neuroscience 153: 1092-1102.

42. Hooks BM, Chen C (2006) Distinct roles for spontaneous and visual activity in remodeling of the retinogeniculate synapse. Neuron 52: 281-291.

43. Huberman AD, Speer CM, Chapman B (2006) Spontaneous retinal activity mediates development of ocular dominance columns and binocular receptive fields in v1. Neuron 52: 247-254.

44. Huttenlocher PR (1979) Synaptic density in human frontal cortex - developmental changes and effects of aging. Brain Res 163: 195-205.

45. Ivy GO, Killackey HP (1981) The ontogeny of the distribution of callosal projection neurons in the rat parietal cortex. J Comp Neurol 195: 367-389.

46. Jerbi K, Lachaux JP, N'Diaye K, Pantazis D, Leahy RM, Garnero L, Baillet S (2007) Coherent neural representation of hand speed in humans revealed by MEG imaging. Proc Natl Acad Sci U S A 104: 7676-7681.

47. Kanold PO, Kara P, Reid RC, Shatz CJ (2003) Role of subplate neurons in functional maturation of visual cortical columns. Science 301: 521-525.

48. Kanold PO, Luhmann HJ (2010) The subplate and early cortical circuits. Annu Rev Neurosci 33: 23-48.

49. Katz LC, Shatz CJ (1996) Synaptic activity and the construction of cortical circuits. Science 274: 1133-1138.

50. Khazipov R, Luhmann HJ (2006) Early patterns of electrical activity in the developing cerebral cortex of humans and rodents. Trends Neurosci 29: 414-418.

51. Khazipov R, Sirota A, Leinekugel X, Holmes GL, Ben Ari Y, Buzsaki G (2004) Early motor activity drives spindle bursts in the developing somatosensory cortex. Nature 432: 758-761.

52. Kilb W, Luhmann HJ (2003) Carbachol-induced network oscillations in the intact cerebral cortex of the newborn rat. Cereb Cortex 13: 409-421.

53. Kostovic I, Judas M (2002) The Role of the Subplate Zone in the Structural Plasticity of the Developing Human Cerebral Cortex. Neuroembryology 1: 145-153.

54. Krupa DJ, Brisben AJ, Nicolelis MA (2001) A multi-channel whisker stimulator for producing spatiotemporally complex tactile stimuli. J Neurosci Methods 104: 199-208.

55. Krupa DJ, Ghazanfar AA, Nicolelis MA (1999) Immediate thalamic sensory plasticity depends on corticothalamic feedback. Proc Natl Acad Sci U S A 96: 8200-8205.

56. Le Van QM, Khalilov I, Ben Ari Y (2006) The dark side of high-frequency oscillations in the developing brain. Trends Neurosci 29: 419-427.

57. Levitt P, Eagleson KL, Powell EM (2004) Regulation of neocortical interneuron development and the implications for neurodevelopmental disorders. Trends Neurosci 27: 400-406.

58. Lopez-Bendito G, Molnar Z (2003) Thalamocortical development: how are we going to get there? Nat Rev Neurosci 4: 276-289.

59. Lu H, Hartmann MJ, Bower JM (2005) Correlations between purkinje cell single-unit activity and simultaneously recorded field potentials in the immediately underlying granule cell layer. J Neurophysiol 94: 1849-1860.

60. Lubke J, Feldmeyer D (2007) Excitatory signal flow and connectivity in a cortical column: focus on barrel cortex. Brain Struct Funct 212: 3-17.

61. Marcano-Reik AJ, Blumberg MS (2008) The corpus callosum modulates spindle-burst activity within homotopic regions of somatosensory cortex in newborn rats. Eur J Neurosci 28: 1457-1466.

62. McQuillen PS, Ferriero DM (2005) Perinatal subplate neuron injury: implications for cortical development and plasticity. Brain Pathol 15: 250-260.

63. Milh M, Kaminska A, Huon C, Lapillonne A, Ben Ari Y, Khazipov R (2007) Rapid cortical oscillations and early motor activity in premature human neonate. Cereb Cortex 17: 1582-1594.

64. Minlebaev M, Ben Ari Y, Khazipov R (2007) Network mechanisms of spindle-burst oscillations in the neonatal rat barrel cortex in vivo. J Neurophysiol 97: 692-700.

65. Minlebaev M, Ben Ari Y, Khazipov R (2009) NMDA receptors pattern early activity in the developing barrel cortex in vivo. Cereb Cortex 19: 688-696.

66. Molnar Z, Adams R, Blakemore C (1998) Mechanisms underlying the early establishment of thalamocortical connections in the rat. J Neurosci 18: 5723-5745.

67. Molnar Z, Kurotani T, Higashi S, Yamamoto N, Toyama K (2003) Development of functional thalamocortical synapses studied with current source-density analysis in whole forebrain slices in the rat. Brain Res Bull 60: 355-371.

68. Nicol X, Voyatzis S, Muzerelle A, Narboux-Neme N, Sudhof TC, Miles R, Gaspar P (2007) cAMP oscillations and retinal activity are permissive for ephrin

signaling during the establishment of the retinotopic map. Nat Neurosci 10: 340-347.

69. Nishioka Y (1995) The origin of common laboratory mice. Genome 38: 1-7.

70. Palva JM, Lamsa K, Lauri SE, Rauvala H, Kaila K, Taira T (2000) Fast network oscillations in the newborn rat hippocampus in vitro. J Neurosci 20: 1170-1178.

71. Paxinos G, Törk I, Tecott LH, Valentino KL (1991) Atlas of the developing rat brain. San Diego: Academic Press.

72. Peinado A (2000) Traveling slow waves of neural activity: a novel form of network activity in developing neocortex. J Neurosci 20: RC54.

73. Peinado A (2001) Immature neocortical neurons exist as extensive syncitial networks linked by dendrodendritic electrical connections. J Neurophysiol 85: 620-629.

74. Penn AA, Shatz CJ (1999) Brain waves and brain wiring: the role of endogenous and sensory-driven neural activity in development. Pediatr Res 45: 447-458.

75. Perkel DH, Gerstein GL, Moore GP (1967) Neuronal spike trains and stochastic point processes. II. Simultaneous spike trains. Biophys J 7: 419-440.

76. Petersen CC (2007) The functional organization of the barrel cortex. Neuron 56: 339-355.

77. Pfeiffenberger C, Yamada J, Feldheim DA (2006) Ephrin-As and patterned retinal activity act together in the development of topographic maps in the primary visual system. J Neurosci 26: 12873-12884.

78. Price DJ, Kennedy H, Dehay C, Zhou L, Mercier M, Jossin Y, Goffinet AM, Tissir F, Blakey D, Molnar Z (2006) The development of cortical connections. Eur J Neurosci 23: 910-920.

79. Rakic P (1988) Specification of cerebral cortical areas. Science 241: 170-176.

80. Ratzlaff EH, Grinvald A (1991) A tandem-lens epifluorescence macroscope: hundred-fold brightness advantage for wide-field imaging. J Neurosci Methods 36: 127-137.

81. Romijn HJ, Hofman MA, Gramsbergen A (1991) At what age is the developing cerebral cortex of the rat comparable to that of the full-term newborn human baby? Early Hum Dev 26: 61-67.

82. Ronan R.O'Rahilly (2006) The embryonic human brain : An atlas of developmental stages (3rd Ed.).

83. Rousseeuw PJ (1987) Silhouettes - a graphical aid to the interpretation and validation of cluster-analysis.

84. Sampaio RC, Truwit CL (2001) Myelination in the developing brain. In:Handbook of developmental cognitive neuroscience (Nelson CA, Luciana M, eds).

85. Schlaggar BL, O'Leary DD (1994) Early development of the somatotopic map and barrel patterning in rat somatosensory cortex. J Comp Neurol 346: 80-96.

86. Schubert D, Kotter R, Luhmann HJ, Staiger JF (2006) Morphology, electrophysiology and functional input connectivity of pyramidal neurons characterizes a genuine layer va in the primary somatosensory cortex. Cereb Cortex 16: 223-236.

87. Schubert D, Kotter R, Staiger JF (2007) Mapping functional connectivity in barrel-related columns reveals layer- and cell type-specific microcircuits. Brain Struct Funct 212: 107-119.

88. Shaw FZ, Liao YF (2005) Relation between activities of the cortex and vibrissae muscles during high-voltage rhythmic spike discharges in rats. J Neurophysiol 93: 2435-2448.

89. Spitzer NC (2006) Electrical activity in early neuronal development. Nature 444: 707-712.

90. Staiger JF, Flagmeyer I, Schubert D, Zilles K, Kotter R, Luhmann HJ (2004) Functional diversity of layer IV spiny neurons in rat somatosensory cortex: quantitative morphology of electrophysiologically characterized and biocytin labeled cells. Cereb Cortex 14: 690-701.

91. Sun JJ, Kilb W, Luhmann HJ (2010) Self-organization of repetitive spike patterns in developing neuronal networks in vitro. Eur J Neurosci 32: 1289-1299.

92. Sun JJ, Luhmann HJ (2007) Spatio-temporal dynamics of oscillatory network activity in the neonatal mouse cerebral cortex. Eur J Neurosci 26: 1995-2004.

93. Tharp BR (1990) Electrophysiological brain maturation in premature infants: an historical perspective. J Clin Neurophysiol 7: 302-314.

94. Torborg CL, Feller MB (2005) Spontaneous patterned retinal activity and the refinement of retinal projections. Prog Neurobiol 76: 213-235.

95. Torres F, Anderson C (1985) The normal EEG of the human newborn. J Clin Neurophysiol 2: 89-103.

96. Vanhatalo S, Kaila K (2006) Development of neonatal EEG activity: from phenomenology to physiology. Semin Fetal Neonatal Med 11: 471-478.

97. Vecchierini MF, Andre M, d'Allest AM (2007) Normal EEG of premature infants born between 24 and 30 weeks gestational age: terminology, definitions and maturation aspects. Neurophysiol Clin 37: 311-323.

98. Wagner J, Luhmann HJ (2006) Activation of metabotropic glutamate receptors induces propagating network oscillations in the intact cerebral cortex of the newborn mouse. Neuropharmacology 51: 848-857.

99. Wang CL, Zhang L, Zhou Y, Zhou J, Yang XJ, Duan SM, Xiong ZQ, Ding YQ (2007) Activity-dependent development of callosal projections in the somatosensory cortex. J Neurosci 27: 11334-11342.

100. Waters RS, McCandlish CA, Cooper NG (1990) Early development of SI cortical barrel subfield representation of forelimb in normal and deafferented neonatal rat as delineated by peroxidase conjugated lectin, peanut agglutinin (PNA). Exp Brain Res 81: 234-240.

101. Weliky M, Katz LC (1999) Correlational structure of spontaneous neuronal activity in the developing lateral geniculate nucleus in vivo. Science 285: 599-604.

102. Welker C (1976) Receptive fields of barrels in the somatosensory neocortex of the rat. J Comp Neurol 166: 173-189.

103. Woolsey TA, Van der LH (1970) The structural organization of layer IV in the somatosensory region (SI) of mouse cerebral cortex. The description of a cortical field composed of discrete cytoarchitectonic units. Brain Res 17: 205-242.

104. Yang JW, Hanganu-Opatz IL, Sun JJ, Luhmann HJ (2009) Three patterns of oscillatory activity differentially synchronize developing neocortical networks in vivo. J Neurosci 29: 9011-9025.

105. Yuste R, Nelson DA, Rubin WW, Katz LC (1995) Neuronal domains in developing neocortex: mechanisms of coactivation. Neuron 14: 7-17.

106. Yuste R, Peinado A, Katz LC (1992) Neuronal domains in developing neocortex. Science 257: 665-669.

Acknowledgments

Thanks to my supervisor, for giving me the opportunity to work in his lab.

It is a pleasure to thank the many people who made this thesis possible.